TU/e EINDHOVEN UNIVERSITY OF TECHNOLOGY

Characterization of (co)polymers by MALDI-TOF-MS

Citation for published version (APA):
Staal, B. B. P. (2005). *Characterization of (co)polymers by MALDI-TOF-MS*. [Phd Thesis 1 (Research TU/e / Graduation TU/e), Chemical Engineering and Chemistry]. Technische Universiteit Eindhoven. https://doi.org/10.6100/IR583506

DOI:
10.6100/IR583506

Document status and date:
Published: 01/01/2005

Document Version:
Publisher's PDF, also known as Version of Record (includes final page, issue and volume numbers)

Please check the document version of this publication:

• A submitted manuscript is the version of the article upon submission and before peer-review. There can be important differences between the submitted version and the official published version of record. People interested in the research are advised to contact the author for the final version of the publication, or visit the DOI to the publisher's website.
• The final author version and the galley proof are versions of the publication after peer review.
• The final published version features the final layout of the paper including the volume, issue and page numbers.

Link to publication

General rights
Copyright and moral rights for the publications made accessible in the public portal are retained by the authors and/or other copyright owners and it is a condition of accessing publications that users recognise and abide by the legal requirements associated with these rights.

• Users may download and print one copy of any publication from the public portal for the purpose of private study or research.
• You may not further distribute the material or use it for any profit-making activity or commercial gain
• You may freely distribute the URL identifying the publication in the public portal.

If the publication is distributed under the terms of Article 25fa of the Dutch Copyright Act, indicated by the "Taverne" license above, please follow below link for the End User Agreement:

www.tue.nl/taverne

Take down policy
If you believe that this document breaches copyright please contact us at:

openaccess@tue.nl

providing details and we will investigate your claim.

Download date: 16. Nov. 2023

Characterization of (co)polymers by MALDI-TOF-MS

Bastiaan Staal

Cover: The enclosure of a (co)polymer MALDI-TOF-MS spectrum into the polymer characteristics can be seen as a challenging jigsaw. The colored spot on the front cover represents a gradient copolymer fingerprint as described in chapter 6. The figure at the back side represents the coupling between SEC-MALDI visualized as a SEC chromatogram which is connected to a MALDI spectrum.

Characterization of (co)polymers by MALDI-TOF-MS

PROEFSCHRIFT

ter verkrijging van de graad van doctor aan de
Technische Universiteit Eindhoven, op gezag van de
Rector Magnificus, prof.dr. R.A. van Santen, voor een
commissie aangewezen door het College voor
Promoties in het openbaar te verdedigen
op dinsdag 18 januari 2005 om 16.00 uur

door

Bastiaan Bram Pieter Staal

geboren te Hoogerheide

Dit proefschrift is goedgekeurd door de promotoren:

prof.dr. A.M. van Herk
en
prof.dr.ir. P.J. Schoenmakers

CIP-DATA LIBRARY TECHNISCHE UNIVERSITEIT EINDHOVEN

Staal, Bastiaan B.P.

Characterization of (co)polymers by MALDI-TOF-MS / door Bastiaan Bram Pieter Staal. – Eindhoven : Technische Universiteit Eindhoven, 2005.
Proefschrift. - ISBN 90-386-2826-9
NUR 913
Subject headings: polymer and copolymer characterization; fingerprints / mass spectrometry; MALDI-TOF / size exclusion chromatography; SEC / discriminant analysis / molecular weight distribution / light scattering / viscosity
Trefwoorden: polymeer- en copolymeerkarakterisatie; vingerafdruk / massaspectroscopie; MALDI-TOF / exclusiechromatografie; SEC / discriminatie-analyse / molmassaverdeling / lichtverstrooiing / viscositeit

© 2004, Bastiaan Staal

Printed by Printpartners Ipskamp te Endschede

An electronic copy of this thesis is avaiable from the site of the Eindhoven University Library in PDF format (http://w3.tue.nl/nl/diensten/bib).

Opgedragen aan mijn ouders

Table of contents

1 General introduction 11
1.1 Introduction 11
1.2 Outline of this thesis. 12

2 Matrix Assisted Laser Desorption/Ionization Time of Flight Mass Spectrometry (MALDI-TOF-MS) 15
2.1 Introduction 15
2.2 Basic principles 15
2.2.1 Transfer of polymer molecules into the gas phase 16
2.2.2 Separation of the polymer molecules 17
2.2.3 Variations in flight time 19
2.2.4 Detection of the ions 21
2.3 Experimental parameters 21
2.3.1 Instrument settings 22
2.4 Data analysis 23
2.5 Molar-mass distribution 26

3 Absolute molar-mass distributions 31
3.1 Introduction 31
3.2 Size-Exclusion Chromatography (SEC) 32
3.2.1 Experimental 34
3.3 Calibration methods in SEC 34
Conventional calibration 35
Universal calibration 36
Static light scattering 39
Calibration of detector constants 40
3.4 Band broadening in SEC 42
3.5 Results 43
Error analysis 47
3.6 Conclusions 49

4 The relationship between the MMD from MALDI and from SEC 59
4.1 Introduction 59
4.2 Experimental 60
4.3 Results and discussion 61
4.3.1 The relationship between the MMD from MALDI and from SEC 61
4.4 SEC and MALDI-TOF-MS 62
4.5 Conclusions 68

5 MALDI of homopolymers 75
5.1 Introduction 75
5.2 Definitions 75
5.2.1 Determination of numbers of repeat units and end-group masses 75
5.2.2 End-group Correlation Function (ECF) 77
5.2.3 Auto-Correlation Function (ACF) 80
5.2.4 Conclusion 81
5.3 End-group analysis with MALDI-TOF-MS to reveal the initiator functionality 82
5.3.1 Introduction 82
5.3.2 The use of the ECF function 92
5.4 Copolymerizations of polyketones 94
5.4.1 Results and discussion 96

6 MALDI of copolymers 107
6.1 Introduction 107
6.2 Copolymer analysis 107
6.2.1 Copolymer topologies 108
6.2.2 Copolymer structure 109
6.2.3 Peak-shape differences 110
6.2.4 Overlapping isotopes 110
6.2.5 Isotope broadening 114
6.3 Copolymer fingerprints 114
6.3.1 Isotope overlap and isotope interference 114
6.3.2 Calculation of Δnr_A and Δnr_B for isotope overlap 116
6.3.3 Calculation of Δnr_A and Δnr_B for isotope interference 120
6.3.4 Estimating the chemical composition. 122
6.4 characteristics of copolymer fingerprints 125
6.4.1 Block copolymers 125
6.4.2 Random copolymers 126
6.5 End-group analysis 131
6.6 Determining types of topology 132
6.7 Polystyrene-co-isoprene 134
6.8 Polystyrene-gradient-butadiene 139
6.8.1 Experimental section 139
6.8.2 MALDI-TOF-MS Analysis 139
6.9 Conclusions 142

7 Outlook and development 149

Glossary of Symbols and Abbreviations 151
Summary 154
Samenvatting 156
Scientific papers 158
Acknowledgements 159
Curriculum vitae 160

Chapter 1

General introduction

1.1 *Introduction*

The molecular characterization of polymeric material is a key step in elucidating the relationship between polymer properties, morphology, and chemical structure. The challenge for polymer chemists is to control and alter the polymerization conditions to obtain polymers with well-defined molecular structures and desired properties. The research into and development of synthetic polymers during the last century has led to new classes of polymers. The new types of synthetic polymers, with tailor-made properties and often complex structures, e.g. gradient copolymer, require better characterization techniques such as coupled ("hyphenated") systems. Traditionally characterization involves molar-mass analysis, repeat-unit or sequence analysis, end-group analysis, and purity examination. The techniques used, such as light scattering, viscometry, NMR and FTIR provide a wealth of information, albeit this information is only an average over the entire molar-mass distribution. Size exclusion chromatography does characterize molar-mass distributions, but it is a technique with many imperfections (see chapter 3). Mass spectrometry is an attractive alternative for the molecular characterization of polymeric material. Due to its high sensitivity and accuracy, a single measurement reveals nearly as much (and often more accurate) information as most of the traditional characterization techniques together.

During the past decade, mass spectrometry has revolutionized the characterization of synthetic polymers[1]. With the introduction of matrix-assisted-laser-desorption ionization time-of-flight mass spectrometry (MALDI-TOF-MS), it has become possible to bring intact polymers in the gas phase predominately singly charged, *i.e.* without degrading the polymer molecule. This so-called soft ionization technique offers the possibility to obtain structural information on polymer chains as a

function of its molar mass, i.e. repeat units, end-group masses, copolymer compositions and some aspects of the polymer topology (see chapter 6) as well the overall molar mass distribution (MMD).

Mass spectrometry has many advantages over other polymer-characterization techniques, because it measures the mass over charge ratio of ions, allowing individual polymer chains to be studied. Mass spectrometry also has its limitations. For example, quantification is only possible to a limited extent. Moreover, mass discrimination is a known phenomenon. Although various authors[2-9] have shown that accurate molar-mass distributions can be obtained for polymers with a low polydispersity index (PDI<1.2 is a reasonable indication), for samples with a higher polydispersity, both underestimation and overestimation of the high-molar-mass fractions have been reported[10,11].

The complexity of the obtained spectra and the difficulty of interpretation, especially for copolymer systems, is another issue with requires attention.
In this thesis MALDI-TOF-MS was extensively used to characterize (co)polymer systems in terms of absolute molar masses, end groups, and the chain construction (number(s) of repeat units used to construct a polymer chain). The chain construction provides direct information of the polymer topology (block, random or gradient). Methods to elucidate polymer topology are often time consuming, whereas MALDI is an accurate and fast characterization method. Special attention was devoted to the development of new mathematical techniques to extract the embedded information from complex spectra. Software was written to identify and characterize spectra exhaustively.

1.2 *Outline of this thesis*

MALDI-TOF-MS is an absolute method for molar-mass determination. However, as mentioned before, mass discrimination affects the experimentally determined MMD. An alternative method to determine the MMD is Size-Exclusion Chromatography (SEC). Chapter 3 describes different calibration methods to obtain the molar mass distribution from SEC. Chapter 4 focuses on the proper conversion of the MALDI-TOF-MS signal to a “SEC-like” signal and on the validation of the conversion method. The second part of chapter 4 describes a quantitative study of mass discrimination, by comparing molar-mass distributions of a broad mixture of polystyrenes obtained by SEC and MALDI.
Chapter 5 deals with the development of new mathematical techniques for end-group analysis and homopolymer analysis. The end-group-correlation function (ECF) rapidly reveals all possible end groups present in the sample. The accuracy of the obtained end-group masses is not always sufficient to decide between end groups of nearly the same mass. An expanded ECF method was developed to exploit the maximum accuracy of a MALDI measurement. A recently published

method, the autocorrelation function (ACF), can be used to obtain the repeat-mass units and a possible identification of the polymer[12].

In chapter 6 the more-challenging complex copolymer spectra are discussed. The numerous possible combinations in which monomers are manifested in polymeric chains are beyond the limits of one simple algorithm to extract all embedded characteristics of the copolymer from a mass spectrum such as end groups, block-length distributions, chemical composition and the copolymer topology. The methods, described in chapter 6, require an absolute minimum of prior knowledge about the polymer sample. The relative abundance of the peaks in a spectrum is different for each topology, which makes it possible to distinguish between, for example, a gradient and block copolymer. Therefore one should not look at each peak individually, but at the coherence of all peaks within the entire molar-mass distribution. The analysis of dozens of peaks is laborious and calls for appropriate software. The methods described in chapter 6 form the basis of the software developed in-house. With this software a full Molar-Mass-Chemical-Composition Distribution (MMCCD), the polymer architecture, and the individual block-length distributions (i.e. the length distributions of the *A* and *B* blocks) can be obtained from only one simple MALDI-TOF-MS measurement. In the final chapter the status of MALDI-TOF-MS and future developments are discussed.

Reference List

1. Hanton, S. D. *Chem. Rev.* **2001,** *101*, 527-569.

2. Byrd, M. H. C.; McEwen, C. N. *Anal. Chem.* **2000,** *72*, 4568-4576.

3. Lehrle, R. S.; Sarson, D. S. *Polym. Degrad. Stab.* **1996,** *51*, 197-204.

4. Tang, X.; Dreifuss, P. A.; Vertes, A. *Rapid Commun. Mass Spectrom.* **1995,** *9*, 1141-1147.

5. Belu, A. M.; DeSimone, J. M.; Linton, R. W.; Lange, G. W.; Friedman, R. M. *J. Am. Soc. Mass Spectrom.* **1996,** *7*, 11-24.

6. Schriemer, D. C.; Li, L. *Anal. Chem.* **1997,** *69*, 4176-4183.

7. Shimada, K.; Lusenkova, M. A.; Sato, K.; Saito, T.; Matsuyama, S.; Nakahara, H.; Kinugasa, S. *Rapid Commun. Mass Spectrom.* **2001,** *15*, 277-282.

8. Rashidzadeh, H.; Guo, B. *Anal. Chem.* **1998,** *70*, 131-135.

9. Axelsson, J.; Scrivener, E.; Haddleton, D. M.; Derrick, P. J. *Macromolecules* **1996,** *29*, 8857-8882.

10. McEwen, C. N.; Jackson, C.; Larsen, B. S. *Int. J. Mass Spectrom. Ion Phys* **1997,** *160*, 387-394.

11. Hanton, S. D.; Clark, P. A.; Owens, K. G. *J. Am. Soc. Mass Spectrom.* **1999,** *10*, 104-111.

12. Wallace, W. E.; Guttman, C. M.; Antonucci, J. M. *J. Am. Soc. Mass Spectrom.* **1999,** (10), 224-230.

Chapter 2

Matrix Assisted Laser Desorption/Ionization Time of Flight Mass Spectrometry (MALDI-TOF-MS)

2.1 *Introduction*

Traditionally, mass-spectrometry techniques based on magnetic and electrical fields, time-of-flight, ion trap and ion cyclotron resonance, are the most commonly used techniques to separate ions by their mass over charge ratio. Until recently, the most common ionization technique was electron ionization. This technique is based on the electron irradiation of vaporized sample molecules, resulting in ionized molecules and fragments. Since polymers are not volatile and fragmentation of ionized polymers should be avoided, this technique is not suitable to obtain structural information of complex mixtures of polymer molecules, with for example, a molar-mass distribution (MMD). A more appropriate choice would be a mass spectrometry technique that place charged polymer molecules in the gas phase without degrading the polymer sample.

In the last decade, soft ionization techniques such as matrix assisted laser desorption/ionization (MALDI) and electrospray ionization (ESI) have enabled the introduction of intact high-molar-mass polymers into the gas phase. The work described in this thesis is focused on MALDI. MALDI is predominantly used for all but not the (very) nonpolar synthetic polymers , whereas ESI is generally used for polar polymers. Note that for MALDI, synthetic polymers only form a small part of the application field. A simple literature search on MALDI returns numerous articles on proteins and other biopolymers, and only a few on synthetic polymers.

2.2 *Basic principles*

MALDI mass spectrometry may be regarded as a three-step process. The first step concerns the production of charged gas-phase species from the original polymer molecules. This step involves

the transfer of the solid material into the gas phase and its ionization. The second step involves the separation of the ionized polymers according to mass or, more correctly, according to mass over charge ratio (*m/z*). The last step involves the detection of the ions.
According to the IUPAC, the mass of molecular ion obtained by mass spectrometry is expressed in *amu*, being the unified atomic mass unit based on the convention that the mass of the isotope $_{12}C$ equals 12 amu exactly.
The MALDI three-step process will be described in more detail in the next sections.

2.2.1 Transfer of polymer molecules into the gas phase

The MALDI process is the ablation of the polymer molecules dispersed in a matrix of small organic-molecules, most commonly organic acids. In a typical MALDI experiment the polymer molecules, the matrix, and optionally the salt of an organic acid are deposited together on a target plate. A short ultraviolet or infrared laser pulse is fired at the deposited sample on the target. The role of the matrix can be seen as mediator for energy absorption of the laser. The highly ultraviolet absorbing matrix transfers the laser energy efficient and guards the polymer molecules from excessive amounts of energy. The laser energy excites the matrix molecules, causing the matrix to vaporize and decompose into what is called a supersonic phase transformation[1]. As a result of this phase transformation a plume of matrix species and polymer species is spread into the gas phase. In general, ions or exited species are formed by the removal or addition of an electron giving a radical cation $M^{+\bullet}$ or anion $M^{-\bullet}$, respectively, or by the addition of other charged species:

$$A + e^{-\bullet} \rightarrow A^{+\bullet} + 2e^{-}$$

or with a lower probability:

$$A + e^{-} \rightarrow A^{-\bullet}$$
$$A + e^{-} \rightarrow A^{*} + e^{-}$$
$$A + X^{+} \rightarrow [AX]^{+}$$

Where X corresponds to proton, Na-, K- or Ag- etc. atom, A denotes the molecular species to be ionized, e^{-} an electron and * indicates an exited species.
Besides the polymer molecules, matrix molecules and cations, also clusters of polymer molecules, matrix molecules, and cations have been detected in the plume[2-4]. Clusters of the polymer molecules, can typically be seen at molar masses exceeding 10,000 amu.

Synthetic polymers are not easy to charge (negative or positive), unless they contain labile protons, as for example in the case of polyacrylic acid. The majority of the synthetic polymers requires the addition of a salt to the polymer-matrix mixture for effective adduction of ions to the polymer. For rather polar polymers alkali-metal ions are normally used. Ions such as Na^+ and K^+ are often present as impurities originating from the glassware or solvent used in the sample preparation, or are simply present as impurity in the matrix material. For nonpolar polymers that contain double bonds, an organic salt with Ag^+ or Cu^{2+} is added.

Irrespective of the normally stable charged state of the metal ion, MALDI produces only single charged polymeric species in the gas phase[5]. This behavior is still not completely understood. Although the ionization mechanism is not completely understood, it was thought to be a straightforward explanation that laser generated ions are formed by the direct multiphoton ionization of a matrix molecule leading to a matrix radical cation. However, the ionization potentials for matrix molecules in crystals or matrix aggregates are still not know. Moreover, other experiments revealed that the potential energies are rather far too high to result in direct multiphoton ionization. More details about the possible ionization steps has been given by Zenobi and Knochenmuss[6]. The theory of Karas and Kruger[7] claimed that the ionization process may be understood as initial formation of clusters between matrix, analyte (and salt ions) which brake down to singly charged species.

2.2.2 Separation of the polymer molecules

After the polymer molecules are transferred to the gas phase as an ion, the ionized polymers are separated on the basis of mass over charge ratio (m/z). For MALDI, the most common mass-separation technique is Time-of-Flight (TOF). Other mass separation techniques, such as quadrupole-filter, Fourier-Transform Mass Spectroscopy (FTMS) and Ion Trap Spectroscopy (ITS) can be used as well but are currently limited to masses up to m/z 4,000 and 20,000 respectively[8,9]. In a TOF analyzer a high voltage (typically 25 kV over a distance of a few millimeters) accelerates the ions from the MALDI plume. After the acceleration, the ions enter into an evacuated tube of typically one meter long, the so-called drift tube. The obtained velocity is given by the simple equation:

$$ze\Delta V = \frac{m v^2}{2} \qquad \textbf{(2.1)}$$

Where ΔV is the electric potential difference applied to accelerate the ion with charge $z \cdot e$, m the mass of the charged (polymer) molecules, and v the velocity. Since the drift tube is long compared to the acceleration region, v can be expressed as:

$$v = \frac{L}{t - t_0} \qquad \textbf{(2.2)}$$

Where L is the length of the drift tube, t_0 is the time when the ablating laser pulse hits the target, and *t* is the total flight time of the ions. Substitution of (2.2) into (2.1) yields:

$$\frac{m}{z} = e\Delta V \frac{2(t - t_0)^2}{L^2} \text{ or } \frac{m}{z} = C(t - t_0)^2 \qquad \textbf{(2.3)}$$

Where *C* is a constant. This general calibration equation relates the mass-to-charge with the flight time of the ions. Small corrections to this equation have been published elsewhere[10,11].

Nowadays, instruments are equipped with different operation modes, the linear mode and the reflector mode (Figure 2-1 and Figure 2-2).

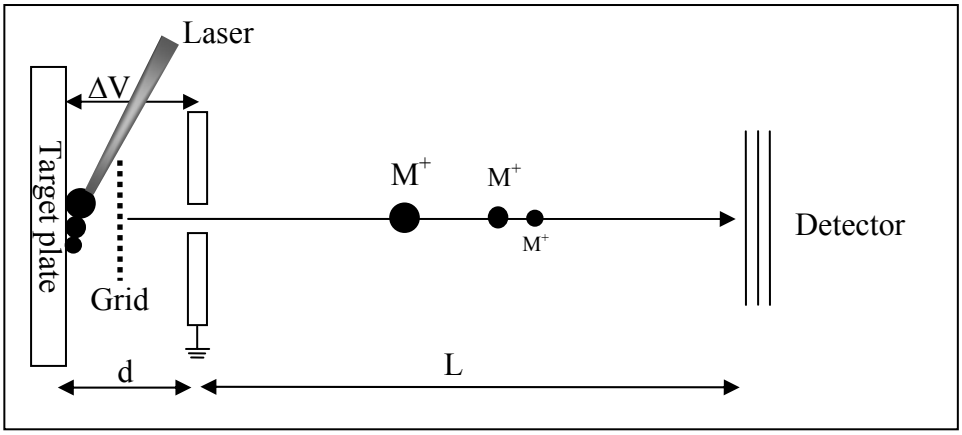

Figure 2-1 Scheme of the linear mode. The polymer molecules mixture deposited on the target plate is irradiated with a laser pulse. After the laser ablation of the polymer molecules into the gas phase and acceleration over a distance *d*, the ions enter the drift tube with a length *L*. At the end of the drift tube the ions are detected by a detector.

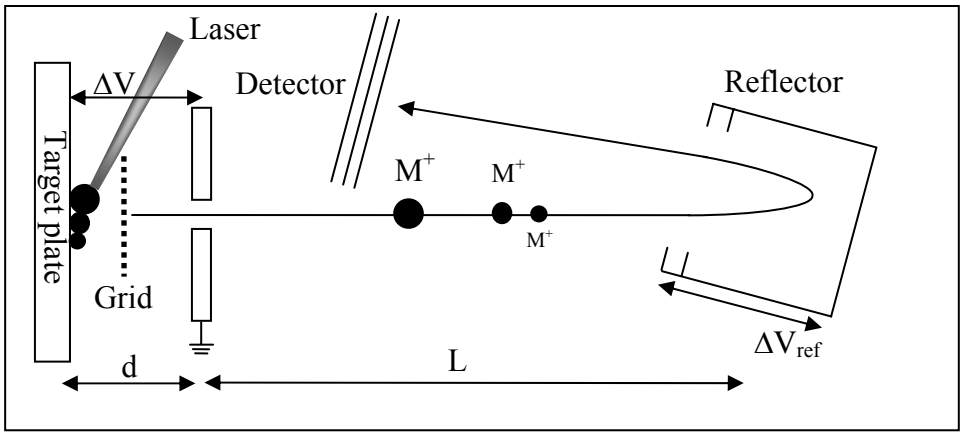

Figure 2-2 Scheme of the reflector mode. In contrast to the linear mode, ions are reflected at the end of the drift tube. An electrostatic-energy mirror provides a cascade of retarding fields in a direction opposite to the acceleration field. After reflection the ions hit the detector.

The main difference between the linear and the reflector mode is the electrical mirror which reflects the ions. Ions of a given mass and velocity will penetrate into the field of the reflector to a different content. Fast ions penetrate deeper into the field and, hence, take a longer time to be reflected. The longer flight time will enhance the resolution.

The mass resolution in a time-of-flight system is given by[11]

$$\frac{\Delta m}{m} = \frac{2\Delta t}{t} \qquad \textbf{(2.4)}$$

Where Δm is the mass difference across a peak at full-width-half-height (FWHH), m the mass, t the flight time and Δt the time difference across a peak at FWHH.

According to Equation (2.3), Δm is proportional to $\Delta t / L$. A longer flight tube will decrease the value of Δm and increase the resolution.

2.2.3 Variations in flight time

Variations in flight times, due to the initial-velocity distribution, finite sample-deposition height and instability of the polymer molecules, are explained in Figure 2-3.

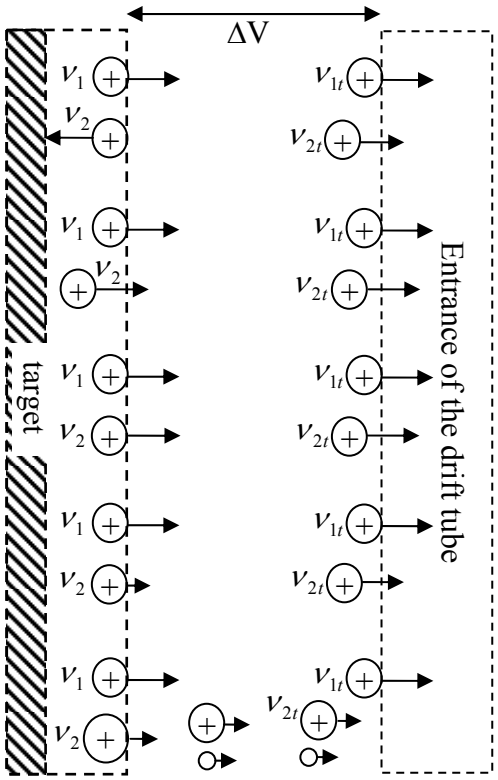

Two ions of the same mass, the same, but opposite-initial velocities and the same initial kinetic energy.
$v_1 = -v_2$, $v_{1t} > v_{2t}$, $t_1(0) = t_2(0)$

Two ions of the same mass, the same initial velocity, and the same kinetic energy, but originated at different locations (thickness differences of the deposited sample) on the target. $v_1 = v_2$, $v_{1t} > v_{2t}$, $t_1(0) = t_2(0)$

Two ions of the same mass, the same initial velocity, and the same kinetic energy, but ionized at different times during the laser ablation of the matrix. $v_1 = v_2$, $v_{1t} = v_{2t}$, $t_1(0) \neq t_2(0)$

Two ions of the same mass, a different initial velocity, and a different initial kinetic energy.
$v_1 \neq v_2$, $v_{1t} > v_{2t}$, $t_1(0) = t_2(0)$

One of the ions fragments in such a way that two of the remaining ions have the same mass. Initial kinetic energy is the same.
$v_1 \neq v_2$, $v_{1t} > v_{2t}$, $t_1(0) = t_2(0)$

Figure 2-3 Illustration of the variations in flight time due to the different events at the onset of the ionization process.

The last situation in Figure 2-3 is an example of fragmentation. Fragmentation that takes place during the ablation by the laser or during the acceleration is called *early* fragmentation[12], prompt fragmentation[13].

An effective way to reduce the energy spread of the ions is delayed extraction. A second plate, called grid (Figure 2-1 and Figure 2-2), placed a few millimeters from the target, is charged for a brief time, keeping the plume trapped after the laser ablation. After the grid voltage is suddenly switched to zero, potential ions with large initial-velocity vectors pointed towards the entrance of the drift tube will experience a lower potential difference than ions with a small initial-velocity vector. In other words, at the moment the grid voltage drops to zero, ions close to the target plate will experience the maximum potential difference, resulting in a high velocity. Ions located further away from the target surface will experience a lower potential difference, resulting in a lower velocity. In this way ions with the same mass, but different velocities, will reach the detector at the same time. This correction is dependent on molar mass and can only be applied across a certain molar mass range.

The phenomenon that molecules fragment in the drift tube after acceleration is called *late* fragmentation. Late fragmentation has no effect on the kinetic energy of the ions in the linear mode and the ions will reach the detector at the correct time. However, in the reflector mode these ions

are re-accelerated with the mass of the charged fragment and will reach the detector at the incorrect times. *Late* fragmentation[12] or also called post-scource decay can be used to perform MS-MS experiments to obtain molecular information. Unfortunately this technique is strongly dependent of the stability of the polymer in the gas phase and not frequently used due to much better alternatives to perform MS-MS experiments, e.g. quadrupole-filter and collision induced MALDI.

2.2.4 Detection of the ions

The MultiChannel Plate (MCP) is the most common detector used for polymers. The MCP consists of an assembly of lead and glass capillaries, coated on the inside with electron-emissive materials, and fused together. The capillaries are biased by a high voltage. Ions strike the inside wall, creating secondary electrons which amplifies each ion-impact signal. The secondary electrons are measured by photo multiplication. MCP detectors tend to saturate easily and may also be less sensitive for high-molar-mass molecules, since the ion-to-electron conversion is dependent on the impact velocity[14,15].

2.3 *Experimental parameters*

The methods for sample preparation described in literature are numerous and seem to have a somewhat alchemistic touch. However, only two processes in sample preparation dominate the quality of spectra: the co-crystallization and the homogeneous mixing of matrix and sample. As a rule of thumb, the polarity of the matrix and the polymer should be similar, so that both are soluble in a common solvent. In this way the intimate mixing of matrix, polymer molecules, and salt will result in the best co-mixing of the deposited solid mixture.

The most commonly used methods for sample preparation are hand-spotting and sample spraying. The hand-spotted or dry-droplet method uses a pipette to deposit 0.3-2 µL of the matrix, polymer molecules, and salt solution on the target. The solvent will evaporate and matrix crystals are usually obtained. The main disadvantage of the hand-spotting method is the large signal variation across the target plate. A more homogeneous co-crystallization of the matrix and sample is obtained by electrospray deposition or by air-spray deposition. The majority of the work in this thesis is done by the hand-spotted method.

In this work, one matrix is used extensively: trans-2-[3-(4-tert-Butylphenyl)-2-methyl-2-propenylidene]malononitrile (DCTB)[a]. Besides the low threshold for the laser energy, this matrix

[a] This matrix is now commercially available. The synthesis of the matrix DCTB used in this thesis is described elsewhere[16]

has a low crystallization rate. After the sample mixture has been deposited, the solvent quickly vaporizes and one can follow, by simply looking at the target, the crystal growth. This crystallization process takes typically 5 seconds up to one minute. Practical experience has learned that the best spectra are obtained if the crystal growth can be observed. Loss or complete absence of the MALDI signal arose when the sample concentrations are too high (no crystal growth could be seen) or when matrix concentrations were too low. In all experiments performed in this thesis the matrix concentration was kept at 40 mg/mL in the matrix solution.

It is at least remarkable that, compared to other matrices, DCTB gave the best results for the majority of the investigated polymers, as will be discussed in more detail in Chapter 4. This is somewhat in contradiction with the above-mentioned matching of polarity between polymer and matrix.

A review of MALDI of synthetic polymers containing an extensive reference list of polymers and the appropriate matrices is given by Nielen[17]. Nowadays, internet provides online databases to find the reported matrices, polymers and used salts[18]. Note that many matrices are highly selective in their performance, which underlines the importance of reliable databases. Salt concentrations should be kept low to prevent cluster formation. For polystyrene even clusters of the form Matrix-Ag-Polymer and Matrix-Ag-Ag-Polymer have been reported[4].

2.3.1 Instrument settings

As discussed before, the instrument can be operated in the linear and in the reflector mode. Important other parameters are grid voltage, extraction-delay time, laser intensity and low-mass gate. The low-mass gate is used to prevent low-mass ions from entering and saturating the detector. The extraction-delay time needs to be adjusted for higher masses to obtain the best performance. Typical values in the reflector mode are 150-500 ns while in the linear mode values up to 1500 ns were found to give the best performance. Note that these values depend on the instrument geometry and are apparatus specific. Unfortunately, the extraction-delay time depends on the grid-voltage setting and is best determined experimentally during the measurement. In the linear mode the best values were found for grid voltages of 92-94% of the applied voltage, depending of the mass (higher mass, higher grid voltage). In the reflector mode this value was kept at 70%. Changing the grid voltage in the reflector mode, for different mass ranges, does not lead to improved resolutions. The fronting and tailing of peaks is related to the extraction-delay times. A too short delay time causes tailing, whereas a too long delay time results in fronting. Ringing indicates the observed dissymmetry at the high-mass end of a well-resolved isotope-peak due to electronic settings of the detector. During all experiments an accelerating voltage of 25 kV and a laser pulse frequency of

20Hz were applied. The laser used is most commonly a 337nm wavelength nitrogen laser. The laser energy per unit area is adjustable. Under normal conditions, the laser energy is adjusted to the minimum intensity to avoid fragmentation. Low laser energy results in a low initial velocity and a narrow initial-velocity distribution within the plume[7]. A narrow initial-velocity distribution minimizes the variations in flight time.

2.4 *Data analysis*

The mass-axis calibration is normally performed by using a (bio)polymer with known end groups. In case of a protein, only one signal is obtained. Using a synthetic polymer allows calibration of the entire mass range at once. To obtain the best calibration, the same matrix is used at a position, on the target, close (or the same) to the calibration spot. A position far away from the calibration position is more often biased due to imperfections of the target-surface flatness.

More challenging is the calibration of the signal axis, as this axis may be in error due to a variety of reasons[19]. Moments of the molar-mass distribution as determined by MALDI-TOF-MS are often lower than those determined via classical methods.[15,20-23] This is generally attributed to mass discrimination. Mass discrimination could originate from: (1) Desorption difference. The fact that desorption of low-molar-mass species is more promoted than that of high molar mass species. No evidence for this effect has been provided so far. (2) Detector saturation, due to the slow charge-up recovery of the MCP detectors[15,24,25]. (3) The way the ions are detected. For high-molar-mass species the ion-to-ion conversion is diminished due to the decrease of the ion impact velocity[14,15]. (4) The data handling such as raw data transformation and baseline corrections.
Mass discrimination as given by the first three items can be diminished using samples with narrow molar mass distributions. To prevent mass discrimination as given by the fourth item will be discussed in the following text.

Improper transformation of the raw data signal, *e.g.* conversion of the time domain to the mass domain, leads to erroneous molar-mass distributions. Furthermore, baselines drawn in MALDI TOF-MS require a multi-point line which could lead to errors.

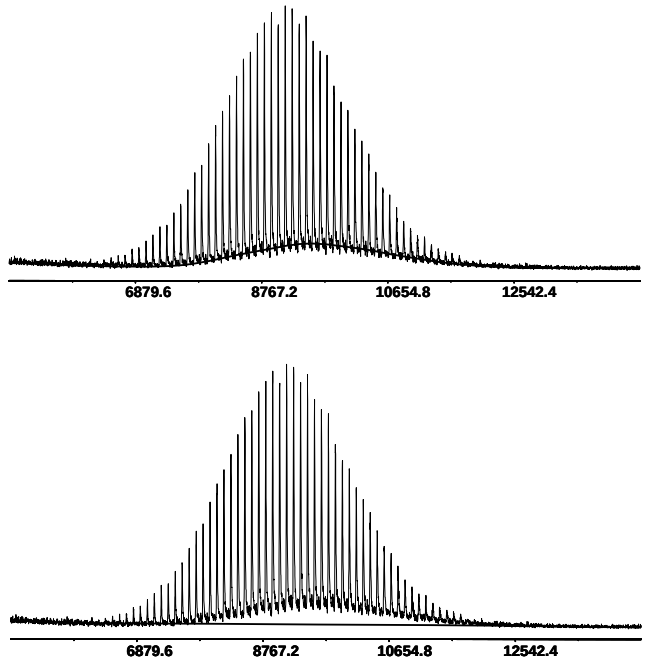

Figure 2-4 Two different methods for drawing a baseline, the valley-to-valley and the continuous-decay baseline. The valley-to-valley approach searches for the minimum value between two consecutive peaks. The decay baseline describes a monotonously decaying function based on the parts of the spectrum where no peaks are present.

Typical MALDI spectra are depicted in Figure 2-4. Two types of baselines can be drawn.

1. The valley-to-valley baseline, where the minimum value between two consecutive peaks is used.
2. A monotonously decaying baseline, based on parts of the spectrum where no peaks are seen.

It is hardly possible to distinguish which baseline method provides the best numbers for the calculation of the average moments (calculation of $\overline{M}_n$, $\overline{M}_w$, and $\overline{M}_z$ as described in paragraph 3.3) since the moments determined by classical methods are not accurate enough. To be able to distinguish between the two baseline methods a system with an internal reference is needed. For this purpose a block copolymer was synthesized containing a fixed block-length distribution for the first block which could be used as reference. During polymerization of the second block, different samples were drawn. The projection of block-length distributions of the first block, at different time intervals should be identical. The use of anionic polymerization techniques allowed us to keep the molar mass distributions narrow and, hence, mass discrimination was suppressed. Chapter 6 describes a method to extract the individual block-length distributions from the two different blocks of a (block) copolymer MALDI spectrum.

The effect of the chosen baseline method on the experimentally determined block-length distributions is shown in Figure 2-5. Both graphs do show the block-length distributions of the first

block, obtained from different samples drawn during the synthesis of the second block. For completeness the homopolymer of the starting block is included. Although the block length of the first block is fixed, a slight change in block length maximum is observed. The spectra in the upper graph were corrected with the monotonously-decaying-function method. The spectra in the bottom graph are corrected with the valley-to-valley baseline method. A significant improvement has been realized in the overlaid distributions. All peaks display the maximum intensity at the same chain length. The valley-to-valley baseline method shows the best performance and will be used in this thesis for baseline corrections. Unfortunately, this method can only work if all peaks of interest are well separated. As soon as peaks start to overlap, the entire baseline rises. As a rule of thumb, masses below 25,000 amu can be corrected with the valley-to-valley method. Masses exceeding 25,000 amu must be corrected by fitting a monotonously decaying function. Note that molar masses exceeding 25,000 amu are generally not sensitive to the baseline settings.

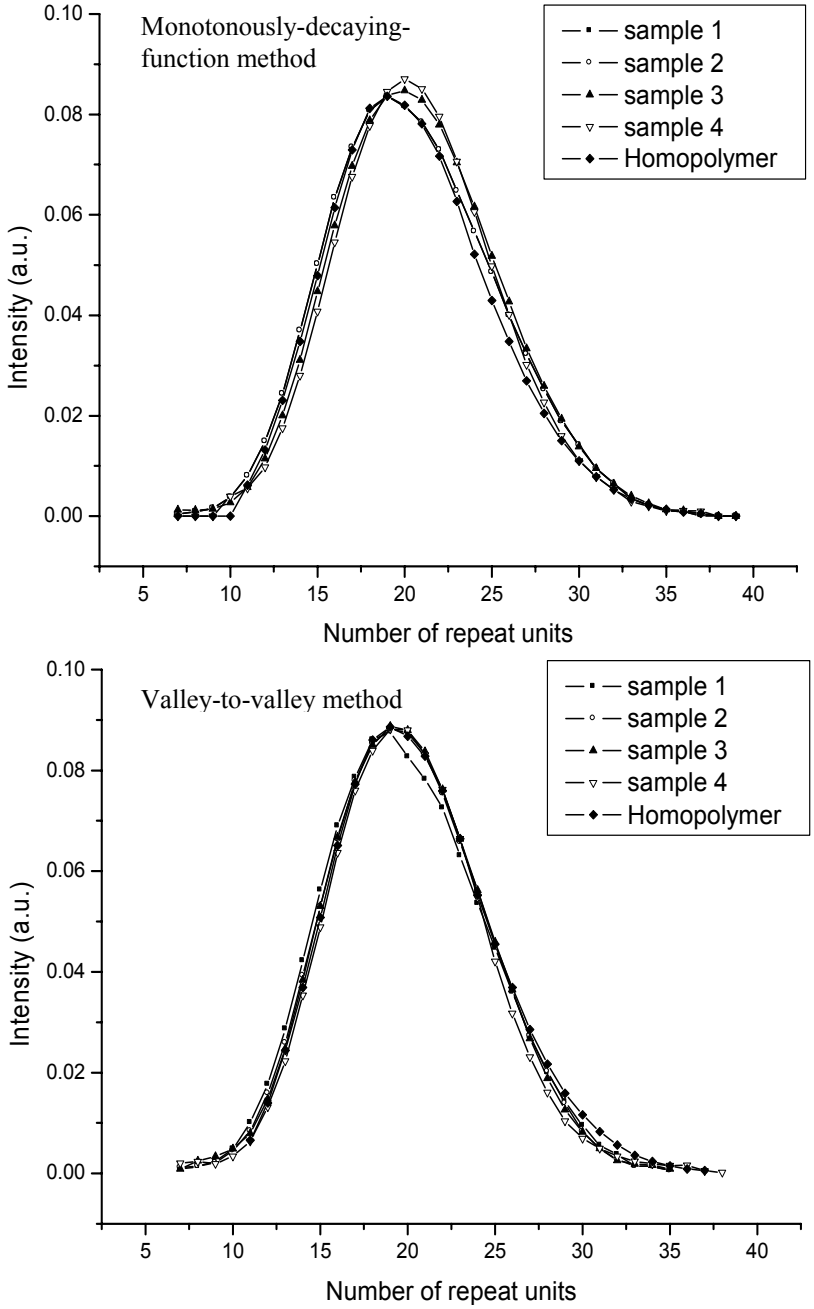

Figure 2-5 Observed block length distributions of the same spectra, but with different baseline-corrections methods.

2.5 *Molar-mass distribution*

The MCP detector counts the number of ions that hit the detector plate. The intensity in MALDI reflects the total number of counted ions of a given mass. Therefore, MALDI measures the *number* molar-mass distribution *nMMD*. The transformation of the MALDI signal from the time domain to the mass domain is different for each instrument[26]. The instrument used in this thesis records all data in the time domain and converts the data directly to the mass domain using equation 2.3. This is not completely correct. The area of a time interval $t + dt$ represents a certain number of species with a given singly charged mass $m + dm$. Whether the integration takes place in the time domain or mass domain, the number of species remains the same. The area A can be written as:

$$A = \int I(t)dt = \int I(t)\frac{dt}{dm}dm = \int I(m)dm \quad \textbf{(2.5)}$$

Where $I(t) \neq I(m)$. $I(t)$ is data acquired in the time domain and $I(m)$ is data acquired in the mass domain. Since our instrument measures the data in the time domain, but presents the data in the mass domain, the correction factor of $\frac{dt}{dm}$ is needed to correctly integrate the observed area under a peak and to obtain $I(m)$. The relation between time and mass is given by equation 2.3. Solving equation 2.3 for *t* and only using the positive root:

$$t = t_0 + \frac{\sqrt{m}}{\sqrt{Cz}} \quad \textbf{(2.6)}$$

The value $\frac{dt}{dm}$ is given by:

$$\frac{dt}{dm} = \frac{1}{2\sqrt{m} \cdot \sqrt{Cz}} \quad \textbf{(2.7)}$$

The relationship between $I(t)$ and $I(m)$ is given by:

$$I(m) = \frac{I(t)}{2\sqrt{m} \cdot \sqrt{Cz}} \quad \textbf{(2.8)}$$

In this way the observed intensity is corrected and displayed correctly in the mass domain. This correction is not applied in the software of the instrument used. Integrating in the time domain with a constant time interval can be written as the summation in the mass domain.

$$\int I(t)dt = \sum I(m)\Delta t \quad \textbf{(2.9)}$$

After normalization, the *nMMD* follows directly from the summation in the mass domain.

Throughout this thesis, *integration* of a spectrum always refers to the *time* domain and *summation* always refers to the *mass* domain.

For synthetic polymers, it is of utmost importance to obtain a good representation of the MMD obtained by MALDI to compare it with the MMD obtained by the classical polymer characterization methods, such as SEC. Mass discrimination can be prevented if the samples are narrowly distributed in terms of mass. SEC offers an excellent opportunity to split a broad MMD into narrow fractions and, hence, the combination of SEC and MALDI is an attractive approach. The quantitative aspects of mass discrimination, as well the comparison between the MMD from MALDI and from SEC are discussed in Chapter 4.

Reference List

1. Vertes, A.; Irinyi, G.; Gijbels, R. *Anal. Chem.* **1993,** *65*, 2389-2393.
2. Knochenmuss, R.; Lehmann, E.; Zenobi, R. *European Journal of Mass Spectrometry* **1998,** *4*, 421-426.
3. Rashidzadeh, H.; Guo, B. *J. Am. Soc. Mass Spectrom.* **1998,** *9*, 724-730.
4. Goldschmidt, R. J.; Guttman, C. M. *J. Am. Soc. Mass Spectrom.* **2000,** *11* (1095), 1106.
5. Karas, M.; Gluckmann, M.; chaefer, J. *J. Mass Spectrom.* **2000,** *35*, 1-12.
6. Zenobi, R.; Knochenmuss, R. *Mass Spectrom Rev.* **1998,** *17*, 337.
7. Karas, M.; Krüger, R. *Chem. Rev.* **2003,** *103*, 427-439.
8. Siuzdak, G. Mass Spectromerty for Biotechnology, Academic Press, San Diego, **1996**.
9. Watson, J. L. Introduction to Mass spectrometry, Lippencott-Raven, New York, **1997,** *3rd ed.*
10. Juhasz, P.; Vestal, M. L.; Martin, S. A. *J. Am. Soc. Mass Spectrom.* **1997,** *8*, 209-217.
11. Cotter, R. J. Time-of-Flight Mass Spectrometry, American Chemical Society, Washington, D.C., **1997**.
12. Guttman, C. M. MS, John Wiley & Sons, Inc., New York, **2002**.
13. Patterson, S. D.; Katta, V. *Anal. Chem.* **1994,** *66*, 3121-3132.
14. Geno, P. W.; Macfarlane, R. D. *Int. J. Mass Spectrom. Ion Processes* **1989,** *92*, 195-210.
15. Schriemer, D. C.; Li, L. *Anal. Chem.* **1997,** *69*, 4169-4175.
16. Ulmer, L.; Mattay, J.; Torres-Garcia, H. G.; Luftmann, H. *European Journal of Mass Spectrometry* **2000,** *6* (1), 49-52.
17. Nielen, M. W. F. *Mass Spectrom Rev.* **1999,** *18*, 309-344.
18. . *http://polymers.msel.nist.gov/maldirecipes*.
19. Zhu, H. H.; Yalcin, T.; Li, L. *J. Am. Soc. Mass Spectrom.* **1998,** *9*, 275-281.
20. Larsen, B. S.; Simonsick, W. J.; McEwen, C. N. *J. Am. Soc. Mass Spectrom.* **1996,** *7*, 287-292.
21. Lehrle, R. S.; Sarson, D. S. *Rapid commun. Mass Spectrom.* **1995,** *9*, 91-92.
22. Montaudo, G.; Montaudo, M.S.; Puglisi, C.; Samperi, F. *Rapid commun. in Mass Spectrom.* **1995,** *9*, 453-460.
23. Guttman, C. M.; Wetzel, J.W.; Wallace, W.E.; Blair, W.R.; Goldschmidt, R.M.; Vanderhart, D.L.; Fanconi, B.M.; . *Polym. Prepr.* **2000,** *41*, 678-679.

24. Westman, A.; Brinkmalm, G.; Barofsky, D. F. *Int. J. Mass Spectrom. Ion Processes* **1997,** *169/170*, 79-97.

25. McEwen, C. N.; Jackson, C.; Larsen, B. S. *Int. J. Mass Spectrom. Ion Phys* **1997,** *160*, 387-394.

26. Guttman, C. M. *Polym. Prepr.* **1996,** *37*, 837-838.

Chapter 3

Absolute molar-mass distributions

3.1 *Introduction*

The molar mass (M) and the molar-mass distribution (MMD) of polymers are perhaps the most important characteristics for establishing of structure-property relationships for (end product) processing performance. Such relationships are needed not only for the development of new products, but also for quality control and improving existing materials.

Size-exclusion chromatography (SEC), also called gel-permeation chromatography, is the most widely used method to determine the molar mass and the MMD.

During the past several years there have been significant advances in SEC column technology, detection systems, and new applications. Combinations of SEC with molar-mass sensitive detectors are used to determine the *absolute* MMD, while the hyphenation of SEC with other techniques, specifically mass spectrometry, gives rise to accurate and detailed information. The latter hyphenation technique constitutes a two-dimensional separation, which can help us understand complex relationships between, for example, MMD and the chemical composition distribution (CCD).

SEC and MALDI can be used to obtain the MMD. Since SEC is a well-established method for determining the MMD and MALDI is a relative new method, an attempt has been made to compare the MMD obtained by both methods.

In SEC, light-scattering detectors are claimed to measure the absolute MMD, although many parameters need to be calibrated, which may contribute to an erroneous MMD. In this chapter different methods of detection and calibration methods for obtaining the absolute MMD are discussed.

3.2 Size-Exclusion Chromatography (SEC)

SEC belongs to the family of liquid chromatography separation techniques. It separates molecules based on molecular size or, more precisely, based on hydrodynamic volume. In a typical SEC setup a column packed with porous material is flushed with a constant flow of a mobile phase. When a polymer sample is injected into the system and passes through the column, very large molecules will not penetrate into the pores of the packing and will elute first. Smaller molecules, which can penetrate into the pores, will elute at a later time. The sample is separated or fractionated according to molecular size.

The molecules which are too large to penetrate the pores of the column packing elute within the interstitial or exclusion volume V_{ex}, which is the volume of mobile phase between the packing particles. In contrast, molecules smaller than the smallest pore sizes diffuse freely into the pores and have full access to the total permeation volume or total pore volume V_p.

The chromatographic behavior of analytes separated by SEC can be described by the generic SEC equation[1]:

$$V_{ret} = V_{ex} + K_{SEC} \cdot V_p \qquad \textbf{(3.1)}$$

where K_{SEC} is the distribution coefficient, relating the average concentration of the analyte in the pore volume to that in the excluded volume. Two limiting cases can be distinguished: $K_{SEC} = 1$, the molecules can completely enter all the pores and elute at the permeation limit of the column, and $K_{SEC} = 0$, when none of the molecules can enter the pores and they elute at the total exclusion limit. Molecules that can enter parts of the pore volume are in the region where $0 < K_{SEC} < 1$. In this region molecules are separated according to their size. More practically, columns are characterized by the molar-mass range where $0 < K_{SEC} < 1$. Therefore the exclusion limit and the permeation limit are expressed in terms of molar mass (most commonly of polystyrene in tetrahydrofuran (THF)). Calibration standards are normally used to obtain the relationship between molar mass and retention time.

Well-defined standards of known molar masses are used to construct the calibration curve. Note that this calibration is only valid for polymers of the same type and chemical structure. After the calibration curve has been constructed, the molar-mass distribution can be calculated if we assume the detector response to be linearly proportional to the concentration and the separation to be strictly according to molar mass. The relationship between the weight fraction belonging to a specific molar mass between M and $M + dM$ and the normalized detector response w from retention volume v to $v + dv$ is[2]:

$$w(M) = -w(v)\frac{dv}{dM} \quad \text{and} \int_0^\infty w(M)dM = 1 \tag{3.2}$$

In practice the most useful form of the molar-mass distribution is with $\log(M)$ plotted on the abscissa, due to the nearly linear behavior of the logarithm of the molar mass versus the retention volume.

$$w(\log(M)) = w(M)\frac{dM}{d\log(M)} \tag{3.3}$$

Substitution of equation (3.2) in (3.3) gives:

$$w(\log(M)) = w(v)\frac{-dv}{d\log(M)} \tag{3.4}$$

Where $\frac{-dv}{d\log(M)}$ is the inverse of the slope of the calibration curve.

It would be more appropriate to speak of the logarithmic molar-mass distribution, since the molar-mass distribution in SEC is presented with the logarithm of the molar mass on the abscissa and the differential weight fraction $dw(\log(M)/d\log(M)$ on the ordinate. Since the term molar-mass distribution is well established in SEC, the abbreviation MMD (molar-mass distribution) will be used when referring to the logarithmic molar-mass distribution obtained from a SEC experiment. According to the IUPAC nomenclature, *molar mass* is defined as mass divided by amount of substance and is expressed in g/mol.

The quality of the eventual MMD depends greatly on the number of data points used for constructing the calibration curve. However, other parameters should also be taken into consideration. These include the flow rate, type of column packing, number and dimensions of columns, performance of the pump, detector calibration constants, injection volume, detector noise, concentration, etc. In this chapter we focus on the relationship between MMDs obtained by SEC and by MALDI. Therefore, we used the conventional conditions recommended by the suppliers without any optimization of the SEC parameters. The best possible separation by SEC is not the aim of this research.

3.2.1 Experimental

SEC analyses were preformed on a system that consisted of a three-column set (two PLgel Mixed-C 5 μm columns and one PLgel Mixed-D 5 μm column from Polymer Laboratories) with a guard column (PLgel 5 μm, Polymer Laboratories), a gradient pump (Waters Alliance 2695, flow rate 1.0 mL/min isocratic), a photodiode-array detector (Waters 2996) and a differential refractive-index detector (Waters 2414) as concentration detectors, a light-scattering detector (Viscotek), a viscosity detector (Viscotek, dual detector 250). THF (Biosolve, Valkenswaard, the Netherlands) was used as the solvent. THF was filtered twice (0.2 μm filter, Alltech, Breda, the Netherlands) and stabilized with BHT (0.01 v%, Merck, >99% pure). Data acquisition was preformed with the Viscotek TriSec GPC Software (version 3.0 Rev. B.03.04). All detectors were placed in series in the following order: photodiode array (PDA), right-angle light scattering (RALS), viscosity (DP) and differential refractive index (DRI).

3.3 *Calibration methods in SEC*

In SEC two types of standards are used, i.e. narrow standards with a narrow MMD and polymers with a broad molar-mass distribution, but with known characteristic average values of the MMD. Narrow standards were used for the calibration of the column, whereas some broad standards were used to calibrate some instrument factors as discussed later.
The characteristic moments of the MMD are given by[2]:

$$\overline{M}_n = \frac{\int_0^\infty w(M)\cdot d(M)}{\int_0^\infty \frac{w(M)}{M}\cdot d(M)} \quad \overline{M}_w = \frac{\int_0^\infty w(M)\cdot M\cdot d(M)}{\int_0^\infty w(M)\cdot d(M)} \quad \overline{M}_z = \frac{\int_0^\infty w(M)\cdot M^2\cdot d(M)}{\int_0^\infty w(M)\cdot M\cdot d(M)} \qquad \textbf{(3.5)}$$

The polydispersity index (*PDI*) is expressed as:

$$PDI = \frac{\overline{M}_w}{\overline{M}_n} \qquad \textbf{(3.6)}$$

Although some of these values are also reported for a calibration standard, it is the peak molar mass $\left(\overline{M}_p\right)$ which is used for constructing the calibration curve. The peak molar mass is located at the top of the MMD measured by SEC and cannot be calculated from the moments of the MMD (Figure 3-1).

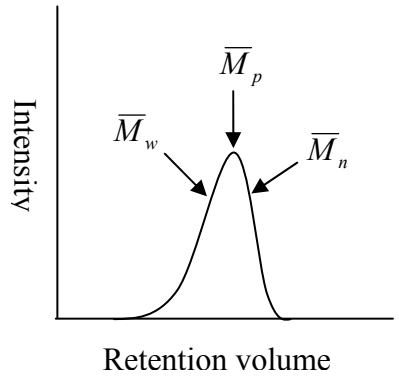

Figure 3-1 The location of the different moments of an MMD and the location of $\overline{M}_p$.

Conventional calibration

By far the most frequently used method for calibration relies on the injection of narrow standards (often polystyrenes). A large range of standards with different molar masses is chosen to cover the entire mass range of the calibration curve. This method is known as conventional calibration. Note that the $\left(\overline{M}_p\right)$ value is not sensitive to band-broadening effects.

The detectors used in this system to measure the concentration (DRI and PDA) do not require any calibration, since relative concentrations suffice.

The quality of the model fitted to the calibration curve obviously influences the accuracy of the MMD. Often a second- or third-order polynomial is used to describe the calibration curve and the correlation coefficient $\left(R^2\right)$ is used as indication of the quality of fit. The value of R^2 is sensitive to the selected order of the polynomial, especially since the number of injected standards is normally rather limited (less then 20). A limited number of data points always provides an improvement of R^2 with increasing order of the polynomial model and over-fitting is a danger. A statistically more-justified parameter is the adjusted correlation coefficient $R_{adj}{}^2$:

$$R_{adj}{}^2 = 1 - \left(1 - R^2\right) \cdot \frac{n-1}{n-p} \qquad \textbf{(3.7)}$$

Where R is the correlation coefficient, n is the number of data points, and p the number of predictors or, in case of a polynomial fit, the order of the polynomial plus one. However, an increase of the polynomial fit will still result in a value more close to unity. An alternative method is suggested with the F-test comparison to test whether an alternative model gives a significant improvement of the fit[3]. The F-test requires the standard deviations of the $\overline{M}_p$ value and the retention time as shown in Appendix 3E.

Universal calibration

As mentioned at the beginning of this chapter, the separation in SEC is based on the hydrodynamic volumes of the molecules. The hydrodynamic volume (V_h) is defined as the product of the molar mass and the intrinsic viscosity $([\eta]\cdot M)$. Plots of $\log([\eta]\cdot M)$ versus retention volume for all polymers of different types, including different conformations (branched, grafted, cyclic, etc), merge into a single plot. This curve, introduced by Benoit et al.[4] is called the universal calibration curve.

Each retention volume of an unknown sample in SEC corresponds to molecules of a given size and thus a corresponding hydrodynamic volume. The unknown molar mass of a sample can be calculated as long as the relation of V_h vs. retention volume is known and the intrinsic viscosity $[\eta](v)$ is measured. Since the relationship between V_h and retention volume can be applied for all polymers (the universal principle), the following relationship is obtained:

$$V_h(v) = [\eta](v)\cdot M_{unknown} \qquad \textbf{(3.8)}$$

Note, again that the quality of the calculated MMD depends on the accuracy of the model describing $\log(V_h(v))$ versus retention volume.

The empirical relation between molar mass and intrinsic viscosity is known as the Mark-Houwink (MH) equation[5]:

$$[\eta] = K\cdot M^{\alpha} \qquad \textbf{(3.9)}$$

Where α and K are constants for a given polymer, solvent and temperature, and M is the molar mass. This relation can be used to express the intrinsic viscosities of Equation (3.8) in terms of molar masses. However, the MH relationship is only valid for molar masses exceeding 20,000 g/mol[6,7].

To measure the intrinsic viscosity Viscotek uses a four-capillary bridge-type cell, analogous to the Wheatstone bridge (see Figure 3-2). The benefit of this instrument is the direct measurement of the specific viscosity (η_{sp}).

$$\eta_{sp} = \frac{4\cdot DP\cdot k_{DP}}{IP\cdot k_{IP} - 2\cdot DP\cdot k_{DP}} \qquad \textbf{(3.10)}$$

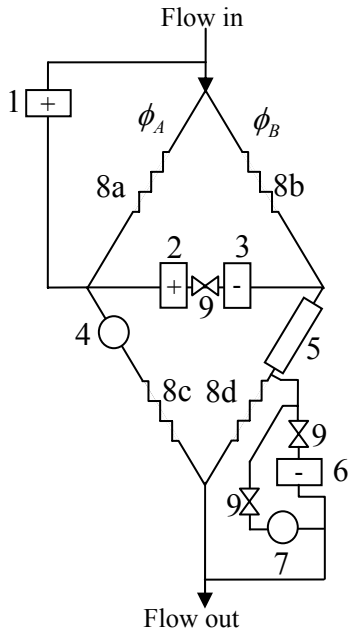

The viscosity bridge has four identical capillary resistors (8). The pressure difference is measured at two locations, across the bridge and inside the bridge. The pressure drop across the bridge is measured by the pressure transducers (1,6) whereas the pressure difference in the bridge is measured by pressure transducers (2,3). These four pressure transducers measure directly the specific viscosity.
The sample cell of a DRI detector is placed inside the bridge (4) and the reference cell of the DRI detector is located at position 7. Under normal working conditions all valves (9) are closed. To purge the pressure transducers and the DRI reference cell, the valves are switched open.
A hold-up reservoir of 19.94 mL is located at number 5.
When the solution with the analyte enters the head of the bridge, the two capillary resistors (8a and 8b) will divide the flow (ϕ_A, ϕ_B).
Half way across the bridge 50% of the eluent will enter the large volume hold-up reservoir and the analyte gets diluted so effectively that the pressure difference between transducers 2 and 3 is totally dominated by the analyte passing capillary 8c.
Note, the DRI detector is referred to as the old DRI detector in this section. It was not used for measuring concentrations. The analyte is diluted by approximately a factor of two due to the hold-up reservoir.

Figure 3-2 Scheme of the Viscotek viscosity detector

Where *IP* is the pressure difference across the bridge and *DP* is the differential pressure within the bridge, k_{DP} and k_{IP} are the calibration factors of the pressure transducers. The setup of the viscosity bridge was modified to put the detectors serial. The large-internal-diameter capillaries used at the end of the bridge were replaced by narrow capillaries and the differential-refractive-index detector was integrated in the bridge. Note, that this DRI detector was not used to determine the concentrations of the polymer in the effluent, due to its low sensitivity. As mentioned in the Experimental section, a Waters DRI detector was placed after the viscosity bridge. Since the old DRI was integrated in the bridge, there was no time difference between the viscosity detector and this detector. In this way the absolute time difference or volume difference could be determined between the Waters DRI detector and the viscosity detector.

The viscosity constant k_{vis} is defined as $\frac{k_{IP}}{k_{DP}}$. Substitution of k_{vis} into formula 3-10 gives:

$$\eta_{sp} = \frac{4 \cdot DP}{IP \cdot k_{vis} - 2 \cdot DP} \qquad \textbf{(3.11)}$$

A viscosity detector yields the intrinsic viscosity ($[\eta]$) from the following equation:

$$[\eta] = \lim_{c \to 0} \left(\frac{\eta_{sp}}{c} \right) \qquad \textbf{(3.12)}$$

$$\eta_{sp} = \frac{\eta - \eta_0}{\eta_0} \quad \textbf{(3.13)}$$

where η_0 is the viscosity of the solvent, η the viscosity of the sample solution, η_{sp} the specific viscosity, c the concentration and η_r the relative viscosity.

Two known methods to extrapolate the concentration to zero are given by Huggins[8] and Kreamer[9]. A practical alternative is the empirical Solomon-Gatesman equation which requires no extrapolation and calculates $[\eta]$ directly[10,11]. This method takes the averages of Huggins and Kraemer equations.

$$[\eta] = \frac{\sqrt{2 \cdot \eta_{sp} - \ln(\eta_{sp} + 1)}}{c} \quad \textbf{(3.14)}$$

Equation (3.11) and (3.14) can be used to determine k_{vis} by measuring standards of known intrinsic viscosities and concentrations.

One of the major drawbacks of capillary viscometers is the presumed exact split of the flow at the entrance of the bridge. When a polymer solution peak passes the cell, the pressure difference within bridge may affect the presumed exact split of the flow. The shift of the peak due to a slight flow-rate imbalance is known as the Lesec effect[12,13]. However, in our setup two DRI signals are obtained, one from the old DRI detector in the bridge and the second one from the DRI detector placed after the viscosity bridge, which is used to monitor the concentration. After the main peak has emerged from the bridge and has been detected by the stand-alone ("new") DRI, it takes some 19.94 mL before a second, shallow and broad peak, which represents the other half of the analyte, can be observed.

Although the second peak was subject to serious band broadening, the areas of both the first and the second chromatogram could still be used to measure the flow split.

The flow-fraction correction factor, ϕ_{fr}, was used to correct the concentrations, since the flow is not exactly equally split at the entrance of the viscosity bridge.

$$\phi_{fr} = \frac{\phi_A}{\phi_A + \phi_B} = \frac{Area_A}{Area_A + Area_B} \quad \textbf{(3.15)}$$

Where ϕ_A and ϕ_B are the flows as shown in Figure 3-2 and $Area_A$ and $Area_B$ are the areas of the main and the second peak, respectively.

At the end of the bridge, pure solvent from the delay column is mixed with the analyte which just passed the right side of the bridge. As a result, the concentration will be a factor two lower than the

concentration in the effluent. Moreover the DRI detector is placed after the viscosity bridge and it is the only detector which measures the two-fold diluted sample. All other detectors experience the "true" concentration. For calculations it is important to have the same concentrations for each detector as explained in section 3.1.5. Note, that placing the DRI detector before the viscosity bridge is not feasible at this moment, since DRI detectors can not withstand high back pressures. No evidence could be found for the Lesec effect (increased flow imbalance with increasing molar mass). With increasing molar mass and decreasing concentration the flow-rate fraction seemed to approach unity and no bridge imbalance could be recorded.

Static light scattering

When the SEC system is equipped with a light scattering detector the absolute molecular-weight distribution of a sample can be obtained. The expressions for $\overline{M}_w$, which can be found in many textbooks are[14]:

$$\frac{K_{LS} \cdot c}{\Delta R(\theta)} = \frac{1}{\overline{M}_w \cdot P(\theta)} + 2A_2 c + 3A_3 c^2 \qquad \textbf{(3.16)}$$

Where, $\Delta R(\theta)$ is the excess Rayleigh ratio (the difference between the Rayleigh ratio of the sample solution and that of the pure solvent, where the Rayleigh ratio is defined as the scattered intensity at the scattering angle θ), c the concentration of the analyte, A_2 and A_3 are the second-, and third-order virial coefficients, $P(\theta)$ is the dissymmetry factor, and K_{LS} a constant defined as:

$$K_{LS} = \frac{4\pi^2 n_0{}^2 (dn/dc)^2}{\lambda_0{}^4 N_A} \qquad \textbf{(3.17)}$$

Where n_0 is the refractive index of the eluent, λ_0 the wavelength in vacuum of the vertically polarized incident light, N_A the Avogadro number and (dn/dc) the specific refractive-index increment, which accounts for the finite change in the eluent refractive index due to the presence of analyte polymer.

In practice $P(\theta)$ is dependent on the angle between the laser and the detector cell and on the squared radius of gyration or indirectly, the molar mass of the scattering molecules. In the setup, the angle between the laser and the detector cell is fixed at 90 degrees. In the present system $P(\theta)$ equals unity for molar masses below 200,000 g/mol. Molar mass exceeding 200,000 g/mol should be interpreted with care. For the calculations of absolute $\overline{M}_w$ values, methods are available to

iteratively calculate the correct $P(\theta)$ for molar masses exceeding 200,000 g/mol, as can be found in literature[15]. Methods to correct $P(\theta)$ will not be discussed since they are beyond the scope of this work.

Equation (3.16) contains the unknown constants K_{LS}, A_2 and A_3. A recent study shows a negligible influence of the third-order virial coefficient, which will therefore not be taken into account[16]. The determination of the second-order virial coefficient requires a multi-angle-light-scattering measurement, which was not preformed. Literature values were taken for the second order virial coefficient ($A_2 = 0.0194 \cdot \overline{M}_w^{-0.286}$). However the concentrations in SEC are usually low and, hence, the term $A_2 c$ (equation 2-13) is usually assumed negligible. The constant K_{LS} requires knowledge of the (dn/dc) values, as discussed in the next section.

Calibration of detector constants

In the previous sections the determination of the calibration constants for the viscosity and light-scattering detectors were already discussed. However, the local concentrations are needed for the calculations of the intrinsic viscosity and the MMD from light scattering.
The concentration detectors, photodiode array (PDA) and differential refractive index (DRI), were used to calculate the actual concentrations. A PDA detector covers a range of wavelengths. The absorbance at each particular wavelength follows the Lambert-Beer law.

$$\text{Absorbance} = \varepsilon \cdot b \cdot c \qquad \textbf{(3.18)}$$

Where ε is the molar absorption coefficient, *b* the path length of the cell, and *c* the analyte concentration.
The following relations were used:

$$c(v,\lambda)_{PDA} = \frac{y(v,\lambda)}{k(\lambda)_{PDA}} \qquad \textbf{(3.19)}$$

$$k(\lambda)_{PDA} = \frac{\int c(v,\lambda)_{PDA}\,dv}{c_{sample} \cdot V_{inj}} = \frac{d\left(\int c(v,\lambda)_{PDA}\,dv\right)}{d\left(c_{sample}\right)} \cdot \frac{1}{V_{inj}} \qquad \textbf{(3.20)}$$

$$c(v)_{DRI} = \frac{y(v) \cdot 2\phi_{fr}}{k_{DRI} \cdot (dn/dc)} \qquad \textbf{(3.21)}$$

$$k_{DRI} = \frac{\int y(v)\,dv \cdot 2\phi_{fr}}{c_{sample} \cdot V_{inj} \cdot (dn/dc)} = \frac{d\left(\int y(v)\,dv\right)}{d\left(c_{sample}\right)} \cdot \left(\frac{2\phi_{fr}}{V_{inj} \cdot (dn/dc)}\right) \qquad \textbf{(3.22)}$$

Where $y(v)$ is the response of the DRI detector at an elution volume v, $y(v,\lambda)$ is the response of the PDA detector at an elution volume v and a given wavelength (λ), c_{sample} the known concentration of a sample, $c(v)_{DRI}$ the local concentration of the sample, (dn/dc) the specific refractive index increment, V_{inj} the injection volume, $\frac{d\left(\int y(v)dv\right)}{d\left(c_{sample}\right)}$ the slope obtained from the area of the raw SEC data chromatograms versus the known injected concentrations, ϕ_{fr} the flow-rate fraction of the viscosity bridge (see paragraph 2.1.3), k_{DRI} the DRI calibration factor, and k_{PDA} the PDA calibration factor.

To correct for the sample dilution after the viscosity bridge, ϕ_{fr} has to be multiplied by a factor of two.

The value of k_{DRI} is still dependent on the value of (dn/dc), whereas k_{PDA} is dependent on the value of ε. Unfortunately, both the values of (dn/dc) and of ε are dependent of the molar mass and/or the end groups. The (dn/dc) of polystyrene in THF becomes constant when the molar mass exceeds 10,000 g/mol[17]. The empirical relationship between molar mass and (dn/dc) can be written as:

$$(dn/dc) = a + \frac{b}{M} \qquad \textbf{(3.23)}$$

Where *a* and *b* are constants and *M* is the molar mass. The (dn/dc) value is mainly affected for molar masses under 1000 g/mol.

The last system-dependent correction is the inter-detector-delay volume. The consequence of connecting detectors in series is a time lag between the detectors. Moreover, the calculation of the intrinsic viscosity requires knowledge of the concentration and the specific viscosity of the same sample volume, which is detected at different times. The determination of the time lag between the viscosity and DRI detectors was already discussed in section 2.1.3. The time lag between a UV detector and a DRI detector can be simply determined by the volume difference, the so-called the inter-detector-delay volume, between the corresponding observed maxima in the detector responses. However, the inter-detector-delay of the light-scattering-detector and the DRI detector cannot be determined by the observed maxima in the detector responses. The light-scatting-detector response is proportional to the product of the concentration *and* the molar mass (formula 2-13), whereas the response of the DRI detector is only proportional to the concentration. No attempt was made to

correct for the difference in responses. Instead of using a narrowly distributed standard, a broad standard with known molar-mass averages was used to determine the inter-detector-delay volume. Note, that the other constants of the light-scattering detector can be determined independently of the inter-detector-delay volume, since they only require the total peak areas.

3.4 *Band broadening in SEC*

A known phenomenon in SEC is band broadening, which obviously affects the experimentally determined MMD. In this work all band-broadening effects are merged into one parameter (σ). Different types of band broadening are extensively discussed elsewhere[18].

A concentration profile of a sample in a column is subjected to band broadening when it passes through a column. The relation between the MMD and the Gaussian band broadening is given by Tung's[19] equation:

$$y(v) = \int w(v^1) \cdot G(v - v^1)\, dv^1 \qquad \textbf{(3.24)}$$

Where $w(v^1)$ is the unbiased true MMD, $y(v)$ the experimental SEC chromatogram, v and v^1 are the respective retention volumes, and $G(v)$ is the Gaussian band-broadening function. The MMD can be corrected directly, so that equation (3.24) can be written in a more useful form[20]:

$$w(\log M') = \int_0^\infty \frac{1}{\sigma \cdot \left(\frac{d\log(M)}{-dv}\right) \cdot \sqrt{2 \cdot \pi}} \exp\left(- \frac{(\log M' - \log M)^2}{\left(\frac{d\log(M)}{-dv}\right)^2 \cdot 2\sigma^2} \right) \cdot w(\log M) \cdot d\log M \qquad \textbf{(3.25)}$$

where σ is the dispersion constant, $\left(\frac{d\log(M)}{-dv}\right)$ the slope of the calibration curve, $w(\log M')$ the apparent MMD and $w(\log M)$ the "true" MMD . Many researchers[19,21-25] put a lot of effort in solving Equation (3.25) for $w(\log M)$. Strictly speaking, the exact solution of Equation (3.25) requires the "true" MMD to be known and is therefore very hard to obtain.

An alternative method to estimate the effect of band broadening in SEC involves using a longer column. That would allow an assessment of the effect of the importance of band broadening in the SEC in comparison with MALDI. In order to be able to compare the experimentally determined MMDs from SEC and from MALDI, the latter was subjected to an artificial band-broadening effect. The details of this procedure will be discussed in Chapter 4.

3.5 *Results*

Some calibration curves require the calibration constants to be known. Therefore the calibration constants will be discussed first.

The calibration constants are either system dependent or eluent dependent. Note that none of the calibration parameters in Table 1 are affected by the column performance.

Table 1 Calibration parameters for the calculation of the molar-mass distribution (MMD).

System-dependent parameters	Eluent-dependent parameters
$k_{vis} = 1.065 \pm 0.04$	$(dn/dc) = 0.185 \pm 0.002$ mg/g
$IDD_{DRI-LS} = 0.530 \pm 0.010$ mL	$K_{LS} = 1.18 \cdot 10^{-5} \pm 0.02 \cdot 10^{-5}$
$IDD_{DRI-DP} = 0.422 \pm 0.010$ mL	$k_{DRI} = 11699 \pm 46$ mV
$IDD_{DRI-UV} = 0.660 \pm 0.004$ mL	$k_{PDA} = 8602 \pm 37$ mV
$\phi_{fr} = 0.988 \pm 0.012$	

The pressure difference measured by the pressure transducers is recorded in Volts. The value of k_{vis} close to unity implies that the conversion from Volts to Pascals is nearly the same for both transducers.

The inter-detector-delays (IDDs) were calculated from the time difference between the $\bar{M}_p$ values for all standards. An average value was calculated (see appendix 3A). The correct IDD_{DRI-LS} could not be obtained from the $\bar{M}_p$ values as explained in section 3.1.5. Broad standards of known average molar-masses were used to fit the IDD_{DRI-LS}. Since only a limited number of broad standards were measured, the standard deviation of the IDD_{DRI-LS} was computed from the $\bar{M}_p$ values.

The calculated ϕ_{fr} is close to unity, which implies that the splitting performs very well. A value lower than one means that slightly less than half of the solution takes the short path through the viscosity bridge and that the concentration measured by the DRI represents slightly less than half of the total analyte.

The (dn/dc) value and its standard deviation were taken from literature[14].

No significant influence was observed of the second virial coefficient in determining K_{LS}, due to the low (enough) concentrations. The standards with molar masses exceeding 200,000 g/mol were neglected due to the angle dependence (section 0). The k_{DRI} and k_{PDA} values were calculated as described in section 0.

The calculation of MMDs from SEC data was described briefly for three different methods, conventional calibration, universal calibration, and light scattering.

For the conventional and universal calibration twelve narrow polystyrene standards were injected twice. The calibration curves are shown in Figure 3-3 and Figure 3-4.

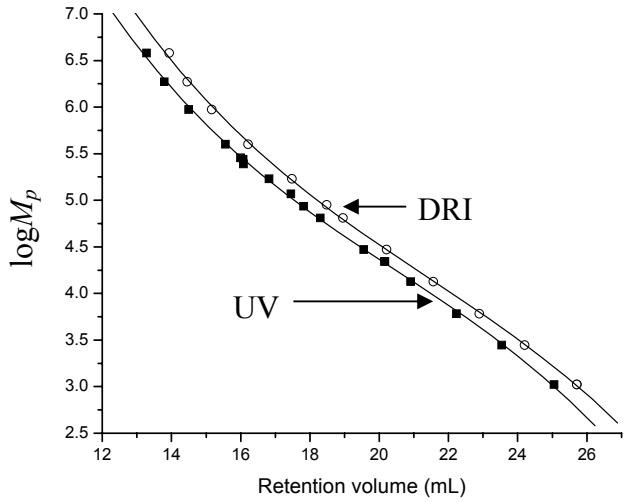

Figure 3-3 The calibration curves of polystyrene standards for UV and DRI.

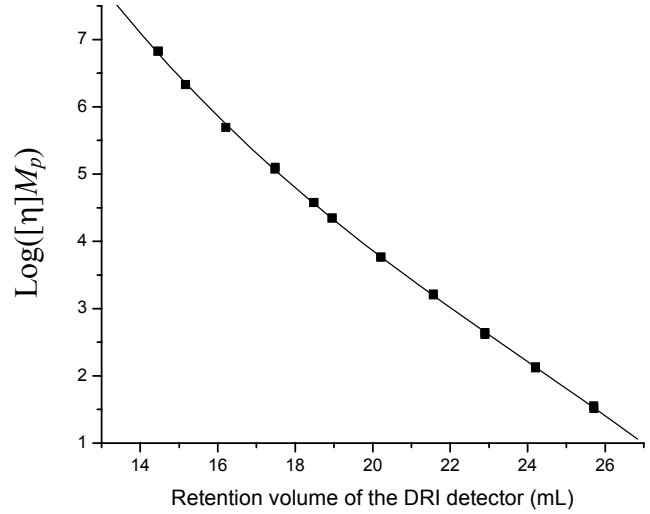

Figure 3-4 Universal calibration curve obtained using polystyrene standards.

In order to decide which type of calibration is needed (classical or inverse) the error in both the molar mass and retention volume, for each data point, was determined (see appendix 3E). The relative error in the retention time is nearly 10 times smaller than the error in the molar mass, hence, classical calibration will be used taking only the error in the molar mass is taken into account.

The most appropriate order of the polynomial fit could not be determined from the values of $R_{adj}{}^2$ as shown in Figure 3-5. The $\log\left(1-R_{adj}{}^2\right)$ seems to reach a constant value while increasing the polynomial fit, however the "correct"order of the polynomial fit cannot be seen from this plot.

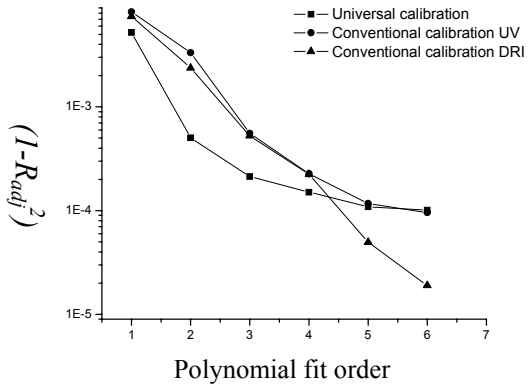

Figure 3-5 $\log\left(1-R_{adj}{}^2\right)$ versus the order of the polynomial equation used to fit the calibration curves of Figure 3-3 and Figure 3-4.

To perform a F-test the standard deviation of the molar mass need to be known. The molar mass values provided by MALDI and SEC were used to calculate the molar mass error of each data point. The F-test comparison method was used to validate whether an increase of the polynomial order is significant as described elsewhere[3]. For all calibration curves a fifth- or sixth-order polynomial was used (see appendix 3F).

For the sake of completeness the Mark-Houwink (MH) constants were determined.
A plot of the logarithm of the intrinsic viscosity versus the logarithm of the molar mass can be used to obtain the MH constants, as shown in Figure 3-6. A clear deviation from the linear MH relationship was observed for molar masses below 20,000 g/mol. A third-order polynomial was used to cover the entire mass range (1050– 3.8 10^6 g/mol). If the principle of universal calibration can be applied and the molar masses are below 20,000 g/mol, then the third-order polynomial is recommended.

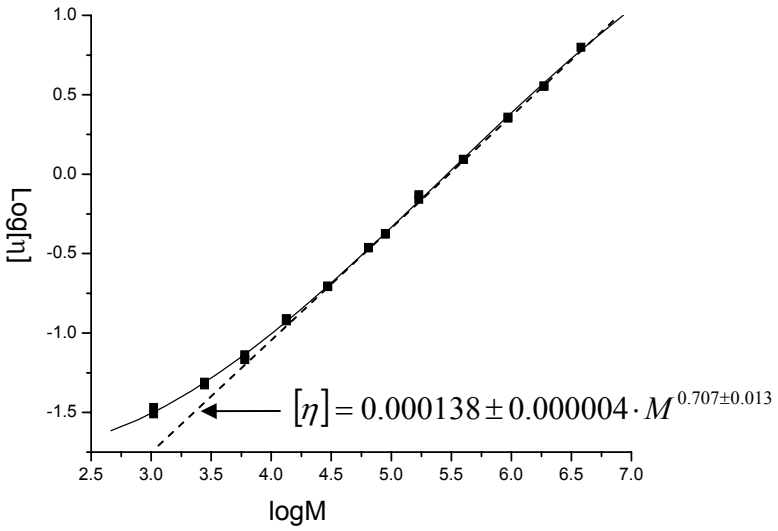

Figure 3-6 Relationship between intrinsic viscosity and molar mass. All polystyrene standards were injected twice. The dashed line represents the linear MH equation. The solid line represents a third-order polynomial.

After all calibration parameters were determined, four broad standards were measured. The fourth standard is a blend of narrow polystyrene standards as will be discussed in Chapter 4. Some of the characteristic values from literature are given in Table 2.

All calculated characteristic values of the four standards are given in Appendix 3A with the calibration-parameter values listed in Table 1.

An alternative method to calculate $\overline{M}_n$, the Goldwasser[26] method, is extremely sensitive for baseline settings and is, unfortunately, of no practical use. No attempts were made to optimize the $\overline{M}_n$ values obtained by the Goldwasser method, since the necessary slight changes in baseline settings had no significant effect on the characteristic values as obtained from the other methods.

Table 2 The characteristic values of broad standards of polystyrene as listed in literature.

	$\overline{M}_n$ g/mol	$\overline{M}_w$ g/mol	$[\eta]$ dl/g [e]
Dow 1683[a]	100,000	250,000	0.843
Dow 1683[b]	95,930	242,900	-
PS 280 [c]	-	274,126	0.891
SRM 706 [d]	-	285,000 +/- 2000	-

a) American Polymer Standards Corporation, b) International GPC symposium 1996, J.Lesec and M.Millequant, pg. 87, c) Viscotek Cooperation, d) National Institute of Standards and Technology (NIST) .

e) Eluent THF at 30 °C

Table 3 shows the obtained moments for two different parameter settings. It is at least remarkable, that the values of the PS280 ($\overline{M}_w, [\eta]$) seem to agree very well with the values given in Table 2 whereas the other values of the broad standards deviate from the corresponding literature values. The $\overline{M}_w$ of Dow 1683 and the SRM 706 are both too far off (see Table 3, method 1).

Table 3 Deviations of the broad standards for both parameters settings using light scattering as calibration method.

	Method 1[†]		Method 2[*]	
	$\overline{M}_n$ g/mol	$\overline{M}_w$ g/mol	$\overline{M}_n$ g/mol	$\overline{M}_w$ g/mol
Dow 1683	97,550	266,600	101,400	255,400
PS 280	123,400	276,650	125,550	265,100
SRM 706	123,900	296,400	126,750	284,500
Deviation Dow 1683 (%)	-0.4	8.2	0.4	3.0
Deviation PS 280 (%)	-	0.9	-	-4.2
Deviation SRM 706 (%)	-	4.0	-	-1.3

[†] The parameter settings for each method are listed in Appendix 3A-3B.

A much better agreement between the standards of Dow 1683 and SRM 706 (see Table 3, method 2) is found in appendix 3B, where only a few calibration parameters were adjusted.
For further calculations the second calibration-parameter settings were chosen. A very thorough study has recently been published on obtaining the accurate $\overline{M}_w$ of the SRM 706[16].

Error analysis

Erroneous MMDs are the result of propagating errors of calibration methods, calibration constants, variation in system performance and erroneous reference data.

Reference materials

The $\overline{M}_p$ values of standards materials are given by the supplier, but rarely the standard deviation is reported. Since there is no absolute method to directly measure the $\overline{M}_p$ value of a narrow standard, one should rely on the $\overline{M}_n$ and $\overline{M}_w$ determined by classical methods or by mass spectrometry i.e. MALDI.
The $\overline{M}_p$ values obtained by MALDI were found to be in excellent agreement with the $\overline{M}_p$ values given by the supplier (appendix 3E). The transformation of the MALDI distribution to a *w*(logM) distribution, as in SEC, is described in more detail in Chapter 4. However, the transformation hardly affects the value of $\overline{M}_p$ (except for molar masses below 2,000 amu). In order to obtain the $\overline{M}_p$ value from a MALDI spectrum, the entire distribution is converted to a w(logM) distribution. The conversion is discussed in detail in Chapter 4.
Moreover, the universal calibration curve requires, besides the same $\overline{M}_p$ values, the known intrinsic viscosities of the polymer standards, making this calibration method more error-sensitive than conventional calibration.

Calibration method

Different methods for calibration have been tested to obtain the MMD. Instead of looking at the entire MMD, the average molar masses ($\overline{M}_n$, $\overline{M}_w$ and $\overline{M}_z$) are compared for each calibration method. Unfortunately the unbiased absolute moments for the broad distributions are unknown as references. It is assumed that light scattering provides the most reliable moments and, therefore, all moments are compared to the average molar masses obtained by light scattering. The values are shown in Table 4.

Table 4 The relative deviation obtained for conventional calibration (CC) and universal calibration (UC). All calibration methods are compared to the moments obtained by light scattering of the standard SRM 706.

moments	CC-LS deviation (%)	UC-LS deviation (%)
$\overline{M}_n$ g/mol	0.8	-3.8
$\overline{M}_w$ g/mol	-0.8	-1.7
$\overline{M}_z$ g/mol	-5.7	-6.1

Calibration-parameter uncertainties affecting the moments calculated by light scattering

To investigate the effect of all calibration-parameter uncertainties, again the average molar masses are computed and their deviation reported. The values of the root-mean-squares (RMS) are listed in Table 5 expressed in g/mol for the broad standard PS280. The relative contributions of the uncertainties of all calibration parameters can be found in appendix 3C. The values for $\overline{M}_w$, $\overline{M}_z$ were strongly affected by the uncertainty of the K_{LS} . The value of $\overline{M}_n$ was strongly affected by the uncertainty of IDD_{DRI-LS} .

Table 5 The errors in the calculated characteristic values of the polystyrene PS280 broad standard.

	Target value	RSM (g/mol)	Std. dev. %
$\overline{M}_n$ g/mol	123,100	4,788	4.1
$\overline{M}_w$ g/mol	276,500	5,244	2.2
$\overline{M}_z$ g/mol	423,300	5,993	1.8

System performance

Since there are always small variations in the SEC performance the maximum error among all reinjected broad standards is reported in Table 6.

Table 6 The maximum relative error among all reinjected broad standards.

	Max. error %
$\overline{M}_n$ g/mol	2.7
$\overline{M}_w$ g/mol	2.0
$\overline{M}_z$ g/mol	4.2

An overview of the various sources of error is given in table 7.

Table 7 Overview of the maximum error in the molar-mass moments.

	Calibration curve	Light scattering	Repeatability	
	Max. error %	Std. dev. %	Max. error %	Tot. Max error. %
$\overline{M}_n$ g/mol	3.8	4.1	2.7	<5%
$\overline{M}_w$ g/mol	1.7	2.2	2.0	<2.5 %
$\overline{M}_z$ g/mol	6.1	1.8	4.2	<7.5%

The presented errors do not represent an in-depth thorough study or a full error analysis and should be interpreted with some care. In this example, the average molar masses of the MMD were used to indicate the quality of the calibration parameters. However, the best calibration for light scattering and viscosity measurements requires a complete analysis of a sample including, the molar mass, the intrinsic viscosity, the radius of gyration, the hydrodynamic radius, all moments of these molar-mass distribution, and the MH constants. Each calibration parameter affects at least one of these values in different ways. If each calibration parameter responds in different ways, then errors may cancel or amplify each other. Such a thorough error analysis is beyond the scope of this thesis.

Axial dispersion corrections

Practical experience shows that axial-dispersion corrections have a limited effect on the computed average molar-masses of the MMD, but strongly affect e.g. the values of the MH constants. Due to their limited effect on the MMD no further attempts were made to optimize the axial-dispersion correction parameters.

3.6 *Conclusions*

Calibration methods were compared for one purpose only, i.e. to obtain the most accurate MMD. Besides conventional calibration, there are many parameters that affect the outcome of the MMD in more-advanced calibration methods, such as universal calibration and triple detection (no need for a calibration curve). A pragmatic approach to determine each parameter carefully (and independently) did not yield the best results. The calibration parameters, such as light-scattering constant K_{LS} and IDD_{DRI-LS} required adjustment to obtain significantly better results. These two parameters turned out to be the most critical parameters in the determination of the MMD moments. Throughout all the measurements, conventional calibration and light-scattering detection seemed to correspond rather well, whereas somewhat larger differences were found for universal calibration. In the end, if the molar masses are not too high (<500,000 g/mol) and the absolute MMD is required within less than one percent error, fractionation of the sample and MS analysis seems to be a (very)

attractive alternative, at least within the limits of applicability of MALDI-TOF-MS.

Reference List

1. Mori, S.; Barth, H. G. Size Exclusion Chromatography, Springer-Verlag, Berlin Heidelberg New York, **1999**.

2. Shortt, D. W. *Journal of Liquid Chromatography* **1993,** *16* (16), 3371-3391.

3. van Herk, A. M. *Journal of Chemical Education* **1995,** *72*, 138-140.

4. Grubisic, Z.; Rempp, P.; Benoit, H. *J Polym Sci Polym Lett Ed* **1967,** *5*, 753.

5. Sakurada, I. *Kolloid Z.* **1938,** *82*, 345.

6. Fox, T. G.; Kinsinger, J. B.; Mason, H. F.; Schuele, E. M. *Polymer* **1962,** *3*, 71.

7. Altares, T.; Wyman, D. P.; Allen, V. R. *J Polym Sci Polym Lett Ed* **1964,** *A2*, 4533.

8. Huggins, M. L. *J. Am. Chem. Soc.* **1942,** *64*, 2716.

9. Kraemer, E. O. *Ind. Eng. Chem.* **1938,** *30*, 1200.

10. Solomon, O. F.; Gotesman, B. S. *Makromol. Chem.* **1967,** *104*, 177.

11. Solomon, O. F.; Ciuta, I. Z. *J. Appl. Polym. Sci.* **1962,** *6*, 683.

12. . *Abstr. Pap. Am. Chem. Soc.* **1993,** *206* (130-PMSE).

13. Lesec, J.; Millequant, M.; Havard, T. *ACS Symp. Ser.* **1993,** ***521***, 220-230.

14. Mori, S.; Barth, H. G. Size Exclusion Chromatography, Springer-Verlag, Berlin Heidelberg New York, **1999**.

15. Mori, S.; Barth, H. G. *Size Exclusion Chromatography, Springer Verlag Berlin Heidelberg New York,* **1999**.

16. Guttman, C. M.; Blair, W. R.; Fanconi, B. M.; Goldschmidt, R. J.; Wallace, W. E.; Wetzel, S. J.; VanderHart, D. L. *NIST Special Publication* **2003,** 260-152.

17. Bahr, U.; Deppe, A.; Karas, M.; Hillenkamp, F.; *Anal. Chem.* **1992,** *64*, 2866-2869.

18. Popovici, S. *Towards Smal and Fast Size-Exclusion Chromatography, PhD Thesis, University of Amsterdam* **2004**.

19. Tung, L. H. *J. Appl. Polym. Sci.* **1966,** *10*, 375.

20. Tung, L. H.; Runyon, J. R. *J. Appl. Polym. Sci.* **1969,** *13*, 2397-2409.

21. Meira, G. R. *"Data reduction in size exclusion chromatography" in Modern Methods of Polymer Characterization, H. G. Barth, J. W. Mays, eds (Wiley, New York)* **1991**.

22. Styring, M. G.; Hamielec, A. E. *"Determination of Molecular Weight Distribution by Gel Permeation Chromatography", Determination of Molecular Weight, A. R. Cooper, ed., Wiley, New York* **1989**.

23. Hamielec, A. E. *"Correction for Axial Dispersion", Steric Exclusion in Liquid Chromatography of Polymers, J. Janka, ed., Dekker, New York* **1984**.

24. Yau, W. W.; Kirkland, J. J.; Bly, D. D. *Modern Size-Exclusion Liquid Chromatography, Wiley, New York* **1979**.

25. Yau, W. W.; Stoklosa, H. J.; Bly, D. D. *J. Appl. Polym. Sci.* **1977,** *21* (1911).

26. Goldwasser, J. M. *International GPC Symposium, Newton, MA, October* **1989**.

Appendix 3A

The calculated characteristic values for the four broad standards. The instrumental settings used are listed at the top of the table based on the average values of the Viscotek Cooperation standards. All standards were injected twice.

Method 1

$k_{vis} = 1.064 \pm 0.04$				$(dn/dc) = 0.185 \pm 0.002$ g/mL				$\phi_{fr} = 0.988 \pm 0.012$	
$IDD_{DRI-LS} = 0.530 \pm 0.010$ mL				$K_{LS} = 1.18 \cdot 10^{-5} \pm 0.02 \cdot 10^{-5}$ V					
$IDD_{DRI-DP} = 0.422 \pm 0.010$ mL				$k_{DRI} = 11699 \pm 46$ V					
$IDD_{DRI-UV} = 0.660 \pm 0.004$ mL				$k_{PDA} = 8602 \pm 37$ V					
File Name		psmix2-1	psmix2-2	STB_41-1	STB_41-2	STB47-1	STB47-2	STB50-1	STB50-2
Description		-	-	Dow1683	Dow1683	Viscotek PS280	Viscotek PS280	SRM 706	SRM 706
Conventional	$\overline{M}_n$	5090	5050	103200	103000	123700	123800	124800	126800
Universal	$\overline{M}_n$	4670	4930	89300	85000	101700	104700	101400	102100
	$\overline{M}_{n_gold}$ [3]	4690	5220	89100	93400	98800	103400	101100	103000
Light scatering	$\overline{M}_n$	6390	6140	97500	97600	123200	123600	122300	125500
Conventional	$\overline{M}_w$	13100	13100	266700	266000	266800	267000	282900	282900
Universal	$\overline{M}_w$	12400	12500	264400	263900	260900	261000	268500	268100
Light scatering	$\overline{M}_w$	13800	13800	266600	266000	276200	277100	296400	296400
Conventional	$\overline{M}_z$	23400	23600	488900	487300	428400	429100	449500	447900
Universal	$\overline{M}_z$	22700	22600	463000	461800	419300	416300	419300	419600
Light scatering	$\overline{M}_z$	22900	23600	452900	451100	422800	424400	449800	448000
Conventional	$\overline{M}_p$	20500	20700	266100	275900	266100	275900	296900	296900
Universal	$\overline{M}_p$	19300	19700	274300	284300	266100	276000	289100	288200
Light scatering	$\overline{M}_p$	21300	21700	279500	289400	285900	296700	321700	321700
Universal	α	0.559	0.601	0.667	0.668	0.629	0.641	0.666	0.654
Light scatering	α	0.666	0.693	0.715	0.72	0.705	0.71	0.722	0.719
Universal	-logK	-3.177	-3.367	-3.648	-3.654	-3.424	-3.487	-3.603	-3.535
Light scatering	-logK	-3.659	-3.79	-3.916	-3.944	-3.865	-3.887	-3.95	3.929
Universal	$[\eta]$ dl/g	0.116	0.113	0.858	0.856	0.897	0.899	0.963	0.967
Light scatering	$[\eta]$ dl/g	0.116	0.111	0.853	0.852	0.89	0.893	0.954	0.958

[3] The method to calculate $\overline{M}_n$ without the use of a DRI detector is known as the Goldwasser method.

Appendix 3B

The calculated characteristic values for the four broad standards. The instrumental settings used are listed at the top of the table and based on the average values of the DOW 1683 and the SRM 706. All standards were injected twice.

Method 2

$k_{vis} = 1.050 \pm 0.04$				$(dn/dc) = 0.185 \pm 0.002$ mL/g				$\phi_{fr} = 0.988 \pm 0.012$	
$IDD_{DRI-LS} = 0.510 \pm 0.010$ mL				$K_{LS} = 1.12 \cdot 10^{-5} \pm 0.02 \cdot 10^{-5}$ V					
$IDD_{DRI-DP} = 0.410 \pm 0.010$ mL				$k_{DRI} = 11699 \pm 46$ V					
$IDD_{DRI-UV} = 0.660 \pm 0.004$ mL				$k_{PDA} = 8602 \pm 37$ V					
File Name		psmix2-1	psmix2-2	STB_41-1	STB_41-2	STB47-1	STB47-2	STB50-1	STB50-2
Description		-	-	Dow1683	Dow1683	Viscotek PS280	Viscotek PS280	SRM 706	SRM 706
Conventional	$\overline{M}_n$	5090	5060	103300	103200	124000	124000	125000	126600
Universal	$\overline{M}_n$	4920	5200	107400	104500	115100	118300	120600	117800
	$\overline{M}_{n_gold}$ [4]	5900	5500	83200	95400	100600	105100	103000	103200
Light scatering	$\overline{M}_n$	5440	4890	101400	101400	124600	126500	125600	127900
Conventional	$\overline{M}_w$	13200	13100	266100	265500	266200	266400	282300	282200
Universal	$\overline{M}_w$	12800	12900	278400	276400	271300	271400	280200	279000
Light scatering	$\overline{M}_w$	13400	13600	255600	255200	264300	265900	284600	284400
Conventional	$\overline{M}_z$	23600	23400	485100	483700	425300	425300	446200	444600
Universal	$\overline{M}_z$	23200	22900	516300	506200	446400	443000	448900	445500
Light scatering	$\overline{M}_z$	24000	25500	420300	419400	394900	397000	422200	420400
Conventional	$\overline{M}_p$	20500	20700	266100	275900	266100	275900	296900	296900
Universal	$\overline{M}_p$	20000	20400	276600	288000	270600	280800	294600	294200
Light scatering	$\overline{M}_p$	20800	21500	270800	280000	276400	286700	310700	310500
Universal	α	0.565	0.608	0.671	0.672	0.632	0.644	0.666	0.654
Light scatering	α	0.608	0.636	0.728	0.734	0.707	0.717	0.725	0.721
Universal	-logK	-3.216	-3.409	-3.685	-3.689	-3.455	-3.519	-3.622	-3.553
Light scatering	-logK	-3.408	-3.534	-3.984	-4.014	-3.867	-3.918	-3.956	-3.936
Universal	$[\eta]$ dl/g	0.114	0.112	0.844	0.843	0.882	0.884	0.945	0.948
Light scatering	$[\eta]$ dl/g	0.114	0.112	0.844	0.843	0.882	0.885	0.945	0.948

[4] The method to calculate $\overline{M}_n$ without the use of a DRI detector is known as the Goldwasser method.

Appendix 3C

All Standards of Viscotek Corporation used to obtain for the calibration curves.

				Retention volumes (mL)				Inter-detector delay (mL)				
Name		$\overline{M}_p$	Conc. mg/mL	UV	LS	DP	DRI	IDD_{DRI-UV} [5]	IDD_{DRI-DP} [6]	IDD_{DRI-LS} [6]	k_{vis}	K_{LS} [6]
STB	53	1050	2.067	25.054	24.989	25.274	25.713	0.657	0.439	0.724	1.148	1.26E-05
STB	53	1050	2.067		25.174	25.270	25.709	-	0.439	0.535	1.041	1.12E-05
STB	54	2790	1.570	23.538	23.638	23.763	24.201	0.663	0.438	0.563	1.095	1.12E-05
STB	54	2790	1.570		23.572	23.766	24.201	-	0.435	0.629	1.048	1.08E-05
STB	55	6040	1.264	22.234	22.340	22.463	22.895	0.662	0.432	0.555	1.091	1.16E-05
STB	55	6040	1.264		22.329	22.462	22.896	-	0.434	0.567	1.012	1.15E-05
STB	56	13400	1.032	20.907	21.009	21.140	21.563	0.658	0.423	0.554	1.036	1.16E-05
STB	56	13400	1.032		21.015	21.143	21.567	-	0.424	0.552	0.991	1.15E-05
STB	57	29600	0.744	19.554	19.663	19.790	20.212	0.658	0.422	0.549	1.038	1.18E-05
STB	57	29600	0.744		19.667	19.790	20.211	-	0.421	0.544	1.049	1.17E-05
STB	58	64500	0.689	18.302	18.413	18.542	18.956	0.653	0.414	0.543	1.049	1.19E-05
STB	58	64500	0.689		18.412	18.540	18.954	-	0.414	0.542	1.059	1.19E-05
STB	59	89300	0.510	17.819	17.940	18.069	18.480	0.662	0.411	0.540	1.106	1.19E-05
STB	59	89300	0.510		17.940	18.070	18.481	-	0.411	0.541	1.120	1.19E-05
STB	60	170000	0.489	16.816	16.943	17.072	17.479	0.664	0.407	0.536	0.980	1.19E-05
STB	60	170000	0.489		16.944	17.073	17.482	-	0.409	0.538	1.082	1.18E-05
STB	61	400000	0.405	15.556	15.674	15.797	16.209	0.653	0.412	0.535	1.085	1.18E-05
STB	61	400000	0.405		15.674	15.797	16.209	-	0.412	0.535	1.085	1.18E-05
STB	62	940000	0.349	14.499	14.628	14.745	15.164	0.664	0.419	0.536	1.089	1.23E-05
STB	62	940000	0.349		14.626	14.744	15.163	-	0.419	0.537	1.074	1.24E-05
STB	63	1870000	0.268	13.793	13.917	14.038	14.458	0.667	0.420	0.541	1.123	1.29E-05
STB	63	1870000	0.268		13.921	14.042	14.462	-	0.420	0.541	1.120	1.30E-05
STB	64	3800000	0.185	13.277	13.354	13.490	13.886	0.611	0.396	0.532	1.052	1.19E-05
STB	64	3800000	0.185		13.360	13.495	13.891	-	0.396	0.531	1.052	1.21E-05
Average								0.660	0.422	0.543	1.065	1.18E-05
Std. dev.								0.004	0.010	0.010	0.040	2E-07

[5] The UV signal was only recorded once of the injected standards.

[6] All gray marked values were excluded from the calculation of the average values and their standard deviation.

Appendix 3D

The influence of the calibration-constant errors on the characteristic values of the MMD. All values are expressed in percentages.

	IDD_{DRI-DP}	IDD_{DRI-LS}	k_{vis}	K_{LS}	k_{DRI}	dn/dc	Tot. deviation (%)
$\overline{M}_n$	0.12	3.49	0.04	1.71	0.38	1.09	4.1
$\overline{M}_w$	0.02	0.47	0.20	1.83	0.42	1.09	2.2
$\overline{M}_z$	0.07	0.71	0.27	1.19	0.43	1.09	1.8
α	2.46	1.83	0.21	0.07	0.00	0.00	3.1
-logK	2.52	1.90	0.55	0.08	0.04	0.21	3.2
$[\eta]$ dl/g	0.39	0.00	3.76	0.00	0.40	1.08	1.2

Appendix 3E

The most probable $\overline{M}_p$ values determined by MALDI and by the supplier.

Sample	$\overline{M}_p$ MALDI	$\overline{M}_p$ SEC	$\log\left(\overline{M}_{p(MALDI)}\right) - \log\left(\overline{M}_{p(SEC)}\right)$	Retention time (min)	Retention time difference[a] (min)
STB53	1257	1050	0.078[7]	25.711	-0.004
STB54	2766	2790	-0.004	24.201	0.003
STB55	5994	6040	-0.003	22.896	0.001
STB56	13491	13400	0.003	21.565	0.004
STB57	29639	29600	0.001	20.212	-0.001
STB58	63996	64500	-0.003	18.955	-0.002
STB59	86621	89300	-0.013	18.481	0.001
STB60	167592	170000	-0.006	17.481	0.003
STB61	395832	400000	-0.005	16.209	-0.002
STB62	932875	940000	-0.003	15.164	-0.001
STB63	-	1870000	-	14.460	0.004
STB64	-	3800000	-	13.889	0.005
Average			± 0.004 (0.13%)[b]		± 0.003 (0.03%)[b]

a) The difference in retention time was obtained after measuring each narrow standard twice.
b) The percentage is expressed as the average value difference of the maximum and minimum values

[7] Relatively large difference between $\overline{M}_p$ values of low molar mass standards ($\overline{M}_p$ < 2,000 g/mol) is always observed and not included for the calculation of the average.

Appendix 3F

To check whether an alternative model B gives a significant improvement of the fit over model A, the following statistical test was made:

$$\frac{ss_B\left(\widehat{\Theta}\right)-\frac{ss_A\left(\widehat{\Theta}\right)}{p_A-p_B}}{\frac{ss_A\left(\widehat{\Theta}\right)}{i-p_A}} \geq F_z\left(p_A-p_B, i-p_A\right) \qquad \textbf{(A3-1)}$$

Where $F_z\left(p_A-p_B, i-p_A\right)$ represents a value from the F-distribution at level z and at p_A, p_B and $i-p_A$ degrees of freedom and $ss_A\left(\widehat{\Theta}\right), ss_B\left(\widehat{\Theta}\right)$ the estimated sum of squares. The model B represents a higher polynomial fit order then model A.

Polynomial order	$\frac{ss_B\left(\widehat{\Theta}\right)-\frac{ss_A\left(\widehat{\Theta}\right)}{p_A-p_B}}{\frac{ss_A\left(\widehat{\Theta}\right)}{i-p_A}}$			$F_z\left(p_A-p_B, i-p_A\right)$		
	DRI	UV	Universal	DRI	UV	Universal
2	20.4	45.3	188.8	4.5	4.3	4.4
3	52.4	70.1	26.9	4.6	4.4	4.4
4	16.1	25.6	8.5	4.7	4.4	4.5
5	5.9	63.1	7.6	4.7	4.4	4.5
6	0.2	27.6	2.2	4.8	4.5	4.5
7	0.2	3.7	0.4	5.0	4.5	4.6
Appropriate polynomial order	5	6	5			

The appropriate polynomial order is based on the criterion given by equation **A3-1**.

Chapter 4

The relationship between the MMD from MALDI and from SEC

4.1 *Introduction*

In case of a homopolymer, the main limiting factor that stands between MALDI and the MMD is formed by ionization-efficiency differences within samples that are heterogeneous in terms of size, mass or chain length. This phenomenon, which is generally denoted as mass discrimination makes the determination of molar-mass distributions (MMD) by MALDI an ongoing challenge. Various publications[1-8] have shown that accurate MMDs can be obtained for polymers with a narrow MMD or low polydispersity index (PDI<1.2). However, for samples with a high polydispersity, both underestimation and overestimation of the high-mass fractions have been reported[9,10]. In the literature many factors have been reported to contribute to mass discrimination. These include sample preparation, desorption/ionization mechanisms, ion focusing/transmission, mass-dependent detection and detector saturation. All these factors contribute to an erroneous MMD.

Concerning mass discrimination, it is our experience that the recently reported matrix, trans-2-[3-(4-tert-butylphenyl)-2-methyl-2-propenylidene]malononitrile (DCTB)[11], exhibits significantly less mass than other commonly used matrices. Mass discrimination can be investigated by the comparison of molar-mass distributions obtained by methods without mass discrimination such as SEC. Besides the fact that SEC is a relative method, SEC and MALDI-TOF-MS data are presented in a different way, as logarithmic molar-mass distributions and number distributions, respectively. In order to compare the two distributions, the conversion of MALDI-TOF-MS spectra to a logarithmic molar-mass distribution requires careful attention. Numerous authors compare average

values of the MMD (number molar-mass and weight-average molar mass), whereas only very few authors[12,13] compare the total MMD. Moreover, the suggested methods for comparing these distributions are not always consistent.
In this chapter mass discrimination will be quantitatively investigated by comparing MMDs obtained by different methods of calibration in Size-Exclusion Chromatography (SEC) and MALDI-TOF-MS for a broad mixture of polystyrenes (PDI>1.2).

4.2 *Experimental*

In order to create a well-defined broad polystyrene standard, six narrow standards were mixed.These were PS1 1950 g/mol of Polymer Laboratories, PS2 3770 g/mol of Polymer Standards Service, PS3 7000 g/mol of Polymer Laboratories, PS4 10000 g/mol of Pressure Chemicals, PS5 22000 g/mol of Polymer Laboratories and PS6 37000 g/mol of Pressure Chemicals, respectively. All standards were dissolved in air-stabilized tetrahydrofuran (THF, Biosolve, Valkenswaard, the Nederlands) and mixed in equal weights. The standards were used for calibration of SEC using the given $\overline{M}_p$, the most probable peak molar mass values from the supplier (see section 3.3).

MALDI-TOF-MS analysis was carried out on a Voyager DE-STR from Applied Biosystems (laser frequency 20 Hz, 337nm and a voltage of 25kV). The matrices used were trans-2-[3-(4-tert-butylphenyl)-2-methyl-2-propenylidene]malononitrile (DCTB), which was synthesized according to reference[11], dithranol (Aldrich, 99% pure), 2,5-dihydroxybenzoic acid (DHB, Aldrich 99% pure) and (4-(Hydroxybenzylidene)-malononitrile (DCTB-OH, Sigma, purity value not available). Silver trifluoracetate (Aldrich, 98%) was added as cationic ionization agent. The matrix was dissolved in THF at a concentration of 40 mg/mL. Silver trifluoracetate was dissolved in THF at a concentration of 1 mg/mL. Polymer was dissolved in THF at approximately 1 mg/mL.
All the spectra were acquired on the Voyager DE-STR in the linear mode. For each spectrum 1000 laser shots were accumulated. In a typical MALDI experiment, the matrix, salt and polymer solution were premixed in the ratio 5 μL sample: 5 μL matrix: 0.5 μL salt. Approximately 0.5 μL of the obtained mixture was hand spotted on the target plate. More detailed information about the instrumental settings can be found in section 2.2.

SEC analyses were performed on a system, which consisted of a two-column set (PLgel Mixed-D 5μm Polymer Laboratories) with a guard column (PLgel 5μm Polymer Laboratories), an isocratic pump (Gyncotek P580, Separations, flow rate of 1.0 mL/min), a UV detector (Spectra Physics Linear^{TM} UV-VIS 200, 254 nm) as concentration detector and THF as the solvent.

A fraction collector (Millipore) was used to collect 60 fractions of 9 droplets each. The mixture of the polystyrene standards was injected 20 times and the corresponding fractions were collected. All 60 fractions were re-injected in the SEC system.
This SEC setup was used exclusively for the fractionation and the re-injections. The MMDs were determined with the SEC setup described in Chapter 3.

4.3 *Results and discussion*

The broad polystyrene standard mix of six narrow standards was analyzed with SEC as described in Chapter 3 to obtain the MMD. The calibration parameters obtained by the broad standards (Chapter 3, method 2 appendix A2) were used to compute the MMD moments.

Table 8 The MMDs obtained of a mixture of six narrow standards by different methods.

	Conv. Calibration	Univ. Calibration	Lightscattering detection	Maximum deviation
$\overline{M}_n$	5075	5060	5165	<5%
$\overline{M}_w$	13150	12850	13500	<2.5%
$\overline{M}_z$	23500	23050	24750	<7.5%

The overlay of the total MMD can be found in appendix A1. To compare the MMD obtained by MALDI with SEC, the MMD obtained by lightscattering will be used.

4.3.1 The relationship between the MMD from MALDI and from SEC

In a MALDI-TOF-MS spectrum the signal is proportional to the number of ions of a certain mass. As long as all ions are singly charged, the intensity in MALDI hereafter baseline subtraction (see section 2.3), normalizing the spectrum and summation of each peak in the mass domain, represents the number mass distribution *nMMD* (more details about how to interpret spectra will be discussed in Chapter 5 and 6). The jth number fraction $n_j(M_j)$ of the *nMMD* is related to the jth mass fraction $w_j(M_j)$ of the MMD by:

$$w_j(M_j) = n_j(M_j)M_j \qquad \textbf{(4-1)}$$

The logarithmic mass distribution as function of the number distribution is given after substitution of equations 3.3 and 4.1:[13-15]

$$w(\log(M)) = n(M)M\frac{dM}{d\log(M)} \quad \textbf{(4-2)}$$

Which can be simplified further to:

$$w(\log(M)) = n(M)M^2\ln(10) \quad \textbf{(4-3)}$$

4.4 *SEC and MALDI-TOF-MS*

In order to record MALDI-TOF-MS spectra without mass discrimination, the polydispersity of the analyzed sample has to be low (PDI < 1.2)[16-18]. SEC was used to fractionate the high-polydispersity sample into fractions that fulfill this low-polydispersity requirement.

The fractions were re-injected into SEC and the concentration was recorded as function of the elution volume. After baseline subtraction and integration of the peak of interest, the peak area of the chromatogram was calculated to determine the mass of the injected polymer fraction. Figure 4-1 indicates the concentrations of the collected fractions as a function of the fraction number.

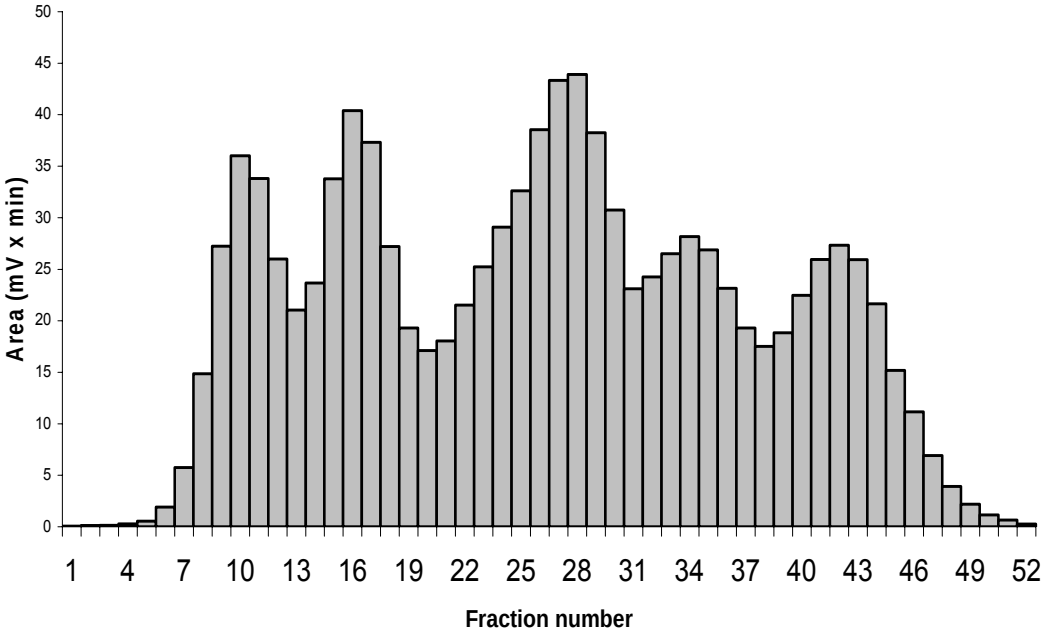

Figure 4-1 Area of re-injected collected fractions from the SEC chromatogram as function of fraction number.

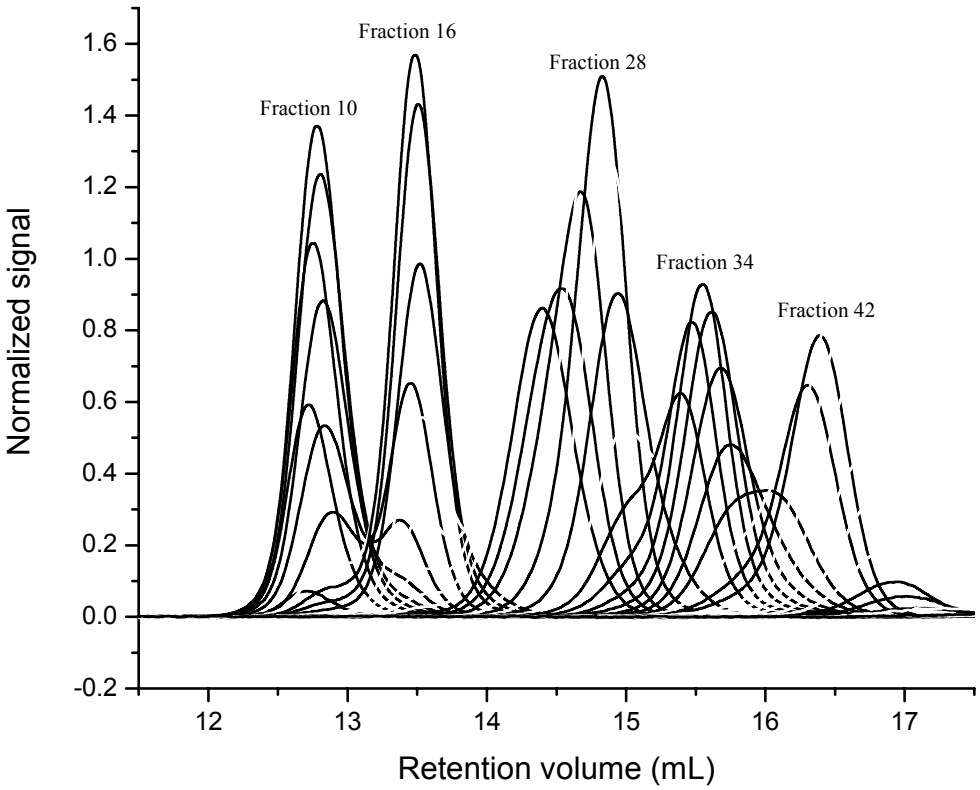

Figure 4-2 Re-injected chromatograms of all 60 collected fractions of a mixture of six narrowly distributed polystyrene standards.

MALDI-TOF-MS spectra were acquired from all polymer fractions collected from the SEC fractionation. The spectra where normalized by area, which resulted in a normalized number distribution *nMMD* for each fraction.

The SEC chromatograms of the mixture of narrow polystyrene standards are shown in Figure 4-2.

Since the injected mass of each fraction is known (Figure 4-1), the chromatogram of the entire sample can be reconstructed. The summation of all these relative chromatograms corrected for their weight should yield the original chromatogram:

$$R(v) = \sum_{i=1}^{i=60} R_i(v) \cdot weight_i \qquad \textbf{(4-4)}$$

Where R_i is the normalized (by area) SEC chromatogram, *i* the corresponding fraction number, $weight_i$ the weight of fraction *i* and $R(v)$ the chromatogram of the entire sample.

Figure 4-3 shows the match between the original chromatogram and the constructed chromatogram. This result implies that the complete MMD can be constructed from the MMDs of the individual fractions obtained from either SEC or MALDI. However MALDI measures a number distribution, which leads to the following description.

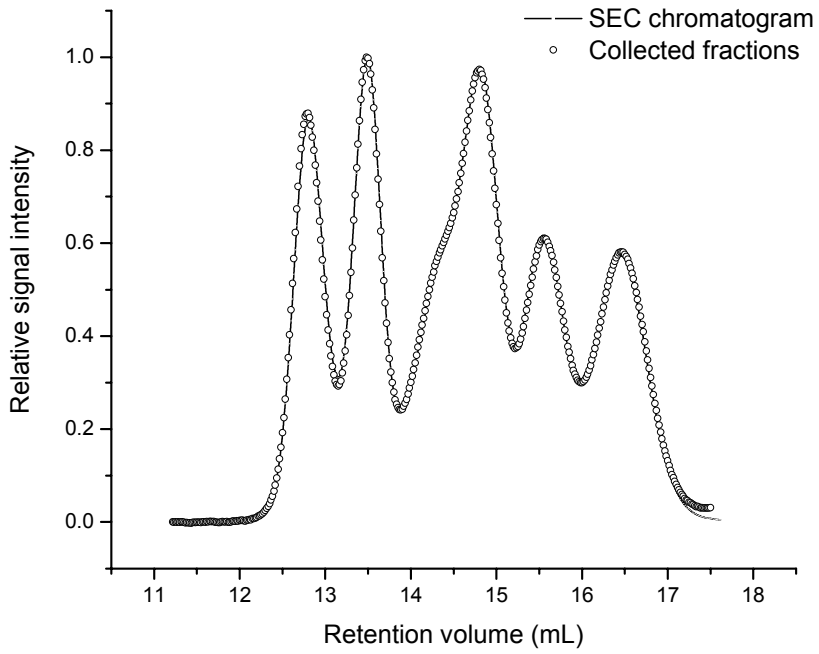

Figure 4-3 Reconstructed chromatogram of all collected fractions. The solid line represents the original chromatogram, the open circles represents the reconstructed chromatogram.

The total number of ions detected by MALDI from polymer chains having a length *j* is obtained after integration of the MALDI spectra within a certain mass window. The width of this mass window equals the mass of one repeat unit. The area represents the total number of polymer chains of a given length. Depending on the end groups, repeat unit mass and the salt used (section 5.1.1), the integration limits can be calculated and the spectrum can be processed to yield the number distribution.

The total number distribution $n_t(M)$ can be obtained by summation of the number distributions of all fractions. However each polymer fraction requires a scaling factor since fractions were collected by weight instead of by number. For each fraction the following equation can be applied:

$$\left(n(M)\right)_i \cdot f_i = n_i(M) \qquad \textbf{(4-5)}$$

Where *i* is the fraction number, $n(M)$ the normalized number distribution ($\sum n(M) = 1$) obtained from the MALDI measurement, f the correction factor for proper scaling and $n_i(M)$ the scaled number distribution of fraction *i*.

The following equation was obtained for the MMD as described in appendix 4A:

$$w\log(M) = \sum_{i=1}^{60}\left(\left(n(M)M^2\right)\cdot\frac{w}{\left(\overline{M}_n\right)}\right)_i \cdot \ln(10) \qquad \textbf{(4-6)}$$

Where *w* is the weight of a fraction, $\overline{M}_n$ the number-average molar mass, *i* the fraction number and *M* the molar mass. The result of computing all fractions into one MMD distribution is shown in Figure 4-4.

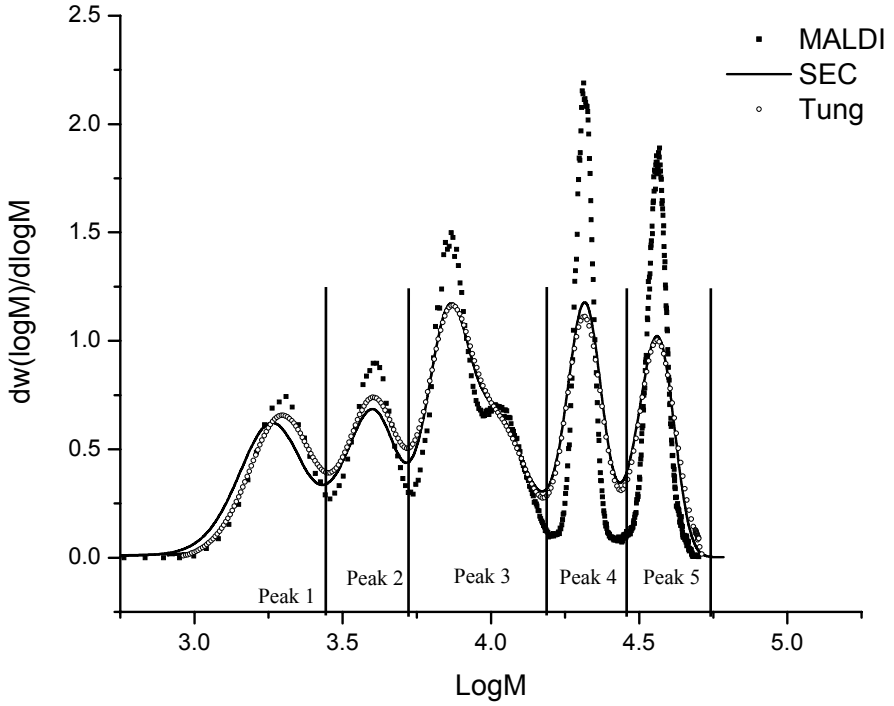

Figure 4-4 A comparison of the MMD obtained by MALDI and SEC. The MALDI signal was subjected to broadening by Tung's equation so that the two MMDs could be compared.

Table 9 MMD moments obtained by MALDI and by other methods.

	MALDI	Conv. Calibration	Univ. Calibration	Triple detection	Error relative# to MALDI (%)
$\overline{M}_n$	5271	5075	5060	5165	3.2
$\overline{M}_w$	13111	13150	12850	13500	0.4
$\overline{M}_z$	23822	23500	23050	24750	0.2

The average moment of the three calibration methods was taken to compare with MALDI.

The MMDs obtained by MALDI-TOF-MS and by SEC are plotted in Figure 4-4. The slightly shift in the lower mass region (peak1) results in a relatively large error in the value of $\overline{M}_n$ as seen in Table 9. The values obtained by conventional calibration are closest to those obtained by MALDI. In theory, if SEC would not suffer from column broadening, these numbers should be identical. Since broadening mainly affects the resolution of the peaks, the area under each peak should be the same for both distributions. A comparison of peak areas can be found in Table 10.

Table 10 The areas of the peaks indicated in Figure 4-4.

	Area MALDI	Area SEC
Peak1	0.180	0.181
Peak2	0.162	0.159
Peak3	0.336	0.332
Peak4	0.170	0.171
Peak5	0.152	0.157
Total area	1.000	1.00

Table 10, confirms that a complete MMD without mass discrimination can be constructed from MALDI-TOF-MS data of fractions obtained from SEC.

To visualize the effect of column broadening in SEC, the MMD reconstructed from the MALDI-TOF-MS data of the fractionated sample was subjected to axial dispersion by Tung's equation as described in section 3.4.

$$w(\log M') = \int_0^{\infty} \frac{1}{\sigma \cdot \left(\frac{d\log(M)}{-dv}\right) \cdot \sqrt{2 \cdot \pi}} \exp\left(-\frac{(\log M' - \log M)^2}{\left(\frac{d\log(M)}{-dv}\right)^2 \cdot 2\sigma^2} \right) \cdot w(\log M) \cdot d\log M \qquad \textbf{(4-7)}$$

Where σ is the dispersion constant, $\frac{d\log(M)}{-dv}$ the slope of the calibration curve, $w(\log M')$ the apparent MMD, and $w(\log M)$ the "true" MMD. In contrast to all methods describing the chromatographic band broadening, the "true" MMD is not known, since it is the desired outcome of the selected method. In this case Tung's equation is used in the opposite way, since mass discrimination was reduced to a minimum and the "true" MMD obtained by MALDI was used to compute the apparent MMD.

A good fit was obtained with a constant Gaussian broadening of $\sigma \cdot \frac{d\log(M)}{-dv} = 0.052$. Figure 4-4 clearly shows the broadening of SEC at higher masses. The apparent MMD (Tung) is clearly broadened too much at the lower mass tail of the lowest molar mass distribution (the lowest molar mass standard). The observed band broadening can only be visualized if the polydispersity of the sample is less than the observed band broadening. Especially towards the lower mass range of this particular set of columns, the contribution of the polymer polydispersity starts to overshadow the observed band broadening. If the polymer polydispersity dominates the observed band broadening, than it also represents the true (continuous) molar-mass distribution. The column performance in terms of band broadening is extensively discussed elsewhere[19].

Taking into account the calculated areas (Table 10) as well the MMDs, (Figure 4-4) a very close approximation of the true MMD is achieved. This so-called true MMD is needed to compare the MMD obtained with MALDI for the total sample (without fractionation and with a high polydispersity).

Figure 4-5 shows the MMD obtained from one single measurement of the total sample versus the MMD obtained from the fractionated sample. It shows that mass discrimination increases with increasing mass. Both MMDs are normalized.

To calculate the mass discrimination, the area of the first or the second peak (Figure 4-5) is used to rescale the MMD obtained for the non-fractionated sample. The discrimination factor is expressed as the ratio of peak areas of both samples ("true"peak area over discriminated peak area).

As can be seen in Table 11 the highest molar mass, peak 5 (37000 g/mol), is suppressed by a factor 14.5 for this polystyrene sample with a polydispersity of 2.5. Surprisingly also the first peak is suppressed by a factor of 1.8.

As mentioned in section 2.3 the different types of matrices can perform very differently for the same sample. The effect of different types of matrices on the MMD is shown in Figure 4-6. The mass discrimination factors are listed in Table 11. Besides DCTB, no other matrix could visualize the two highest molar mass standards clearly.

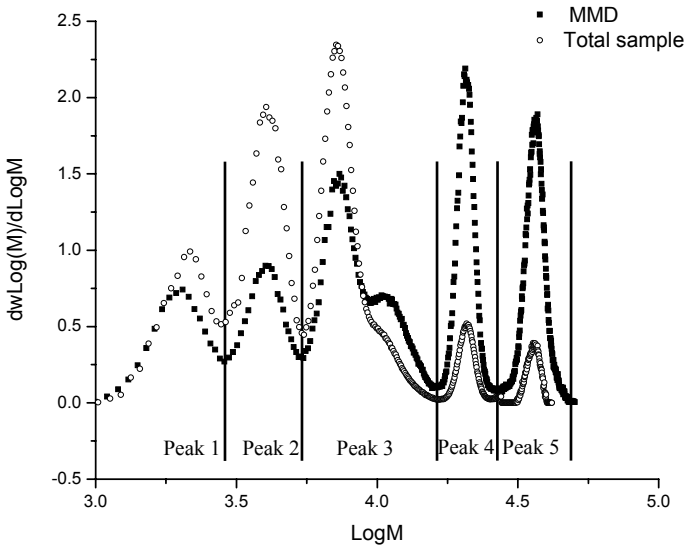

Figure 4-5 MMD obtained after fractionation is indicated by the solid black squares. The MMD obtained from one MALDI experiment is indicated by open circles.

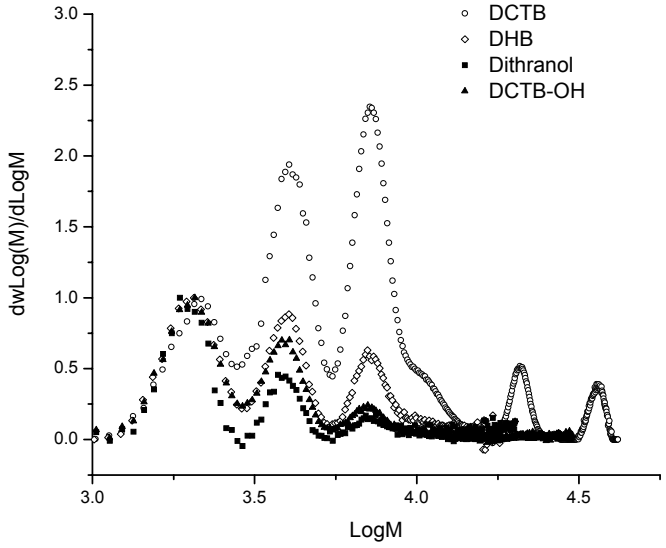

Figure 4-6 The MMD of the same sample measured with different matrices. DCTB clearly shows the least mass discrimination.

Table 11 Discrimination factors calculated from the peak areas of Figure 4-6. for different types of matrices.

	MMD area of:		Mass discrimination factor			
	fractionated sample	non-fractionated sample	DCTB	DHB	Dithranol	DCTB-OH
Peak1	0.180	0.102	1.8	1.0	1.0	1.0
Peak2	0.162	0.159	1.0	2.7	1.5	1.7
Peak3	0.336	0.181	1.8	10.4	4.7	10.5
Peak4	0.170	0.018	9.5	∞	∞	∞
Peak5	0.152	0.010	14.5	∞	∞	∞
Total area	1.000	0.471				

4.5 *Conclusions*

By creating a well known, synthetic reference sample, we have been able to quantitatively access the mass discrimination occurring in MALDI-TOF-MS analysis of polystyrene.
When MALDI-TOF-MS spectra are acquired of broad polystyrenes (PDI > 1.2) mass discrimination does occur. The "true" MMD, without mass discrimination, could be constructed from MALDI-TOF-MS data of fractions obtained from SEC. For polystyrene the matrix trans-2-[3-(4-tert-Butylphenyl)-2-methyl-2-propenylidene]malononitrile reduces the mass discrimination to less then a factor 14.5 over a broad mass range (1000 - 37000 g/mol) compared to the "true" MMD. This makes this matrix superior to other tested matrices in terms of mass discrimination.
Mass discrimination on both the low and the high molar mass tail was observed for the broad polystyrene standard. A possible reason for the mass discrimination on the low molar mass tail could be detector saturation effects. A relatively high laser intensity was needed to obtain reasonable intensities for the highest molar masses. These high laser intensities could lead to saturation effects of the detector due to an increase of low-molar-mass species.
Polystyrene polymers larger than 10,000 g/mol can lead to agglomerates as shown in appendix 4E. During the laser ablation, high-molar-mass species are not completely "disentangled" in the gas phase. In general, this phenomenon alters the MMD of broad distributions and it is hard to prevent (although dilution of the sample may help). However, this error can be safely neglected compared to the observed mass discrimination.

SEC

Column band-broadening effects could be described very well by axial dispersion. Moreover, within a molar mass range of 1000 - 37000 g/mol, the increase of the band broadening with increasing molar mass could be described by a dispersion constant independent of molar mass.
The computed $\overline{M}_w$ and $\overline{M}_z$ of MALDI and SEC were found to be in excellent agreement. The small deformation of the lower mass region (peak1) results in a relatively high error in the value of

$\overline{M}_n$ as seen in Table 9. Moreover, this effect has also already been observed in appendix 3E for the lowest-molar-mass standard. In general, polystyrene standards of molar masses lower than 2500 g/mol show a small discrepancy between $\overline{M}_p$ values given by their suppliers and observed with MALDI.

The theoretical conversion of MALDI spectra to SEC chromatograms was confirmed by the experiments. Note that proper baseline corrections are crucial to obtain reliable MMDs.

Reference List

1. Tang, X.; Dreifuss, P. A.; Vertes, A. *Rapid commun. Mass Spectrom.* **1995,** *9*, 1141-1147.
2. Shimada, K.; Lusenkova, M. A.; Sato, K.; Saito, T.; Matsuyama, S.; Nakahara, H.; Kinugasa, S. *Rapid commun. Mass Spectrom.* **2001,** *15*, 277-282.
3. Schriemer, D. C.; Li, L. *Anal. Chem.* **1997,** *69*, 4169-4175.
4. Rashidzadeh, H.; Guo, B. *Anal. Chem.* **1998,** *70*, 131-135.
5. Karas, M.; Hillenkamp, F. *Anal. Chem.* **1988,** *60* (20), 2299-2301.
6. Hanton, S. D. *Chem. Rev.* **2001,** *101*, 527-569.
7. Belu, A. M.; DeSimone, J. M.; Linton, R. W.; Lange, G. W.; Friedman, R. M. *J. Am. Soc. Mass Spectrom.* **1996,** *7*, 11-24.
8. Axelsson, J.; Scrivener, E.; Haddleton, D. M.; Derrick, P. J. *Macromolecules* **1996,** *29*, 8857-8882.
9. Hanton, S. D.; Clark, P. A.; Owens, K. G. *J. Am. Soc. Mass Spectrom.* **1999,** *10*, 104-111.
10. McEwen, C. N.; Jackson, C.; Larsen, B. S. *Int. J. Mass Spectrom. Ion Phys* **1997,** *160*, 387-394.
11. Ulmer, L.; Mattay, J.; Torres-Garcia, H. G.; Luftmann, H. *European Journal of Mass Spectrometry* **2000,** *6* (1), 49-52.
12. Wallace, W. E.; Guttman, C. M. *J. Natl. Inst. Stand. Technology* **2002,** *107*, 1-17.
13. Guttman, C. M.; Blair, W. R.; Danis, P. O. *Journal of Polymer Science PartB: Polymer Physics* **1997,** *35*, 2409-2419.
14. Byrd, M. H. C.; McEwen, C. N. *Anal. Chem.* **2000,** *72*, 4568-4576.
15. Shortt, D. W. *Journal of Liquid Chromatography* **1993,** *16* (16), 3371-3391.
16. Spickermann, J.; Martin, K.; Räder, H. J.; Müllen, K.; Schlaad, H.; Müller, A. H. E.; Krüger, R.-P. *European Journal of Mass Spectrometry* **1996,** *2*, 161-165.
17. Montaudo, G.; Montaudo, M.S.; Puglisi, C.; Samperi, F; *Macromolecules* **1995,** *28*, 7983-7989.
18. Montaudo, G.; Montaudo, M.S.; Puglisi, C.; Samperi, F.; *Rapid commun. Mass Spectrom.* **1995,** *9*, 453-460.
19. Popovici, S. *Towards Smal and Fast Size-Exclusion Chromatography, PhD Thesis, University of Amsterdam* **2004**.

Appendix 4A

The total number distribution $n_t(M)$ can be obtained by summation of the number distributions of all fractions after scaling the fractions relative to their weight. For each fraction the following formula can be applied:

$$\left(n(M)\right)_i \cdot f_i = n_i(M) \qquad \textbf{(A4-8)}$$

Where *i* is the fraction number, $n(M)$ the normalized number distribution ($\sum n(M) = 1$) obtained from the MALDI measurement, f the correction factor for proper scaling and $n_i(M)$ the scaled number distribution of fraction *i*.
The following formula was obtained for the total number distribution:

$$\sum_{i=1}^{60} n_i(M) = n_t(M) \qquad \textbf{(A4-9)}$$

The total weight of each fraction *i* (w_i) can be calculated by:

$$\left(\sum M \cdot n(M)\right)_i = w_i \qquad \textbf{(A4-10)}$$

Note w_i represents the total weight of a fraction whereas the $w(M)$ represents the molar weight *fraction* of a molar mass distribution.
Substitution of equation A4.1 into A4-3 gives:

$$\left(\sum M_i \cdot \left(n(M)\right)_i \cdot f_i\right) = w_i \qquad \textbf{(A4-11)}$$

Since the scaling factor is a constant within each fraction it can be put outside the summation en written explicit:

$$f_i = \frac{w_i}{\sum M_i \cdot \left(n(M)\right)_i} \text{ or } \qquad f_i = \frac{w_i}{\left(\sum M \cdot n(M)\right)_i} \qquad \textbf{(A4-12)}$$

Since the *n(M)* distribution is normalized by number ($\sum n(M) = 1$) the number average molar mass can be simplified to:

$$\overline{M}_n = \sum \left(n(M) \cdot M\right) \qquad \textbf{(A4-13)}$$

In general, equation A4-5 becomes for every fraction:

$$f_i = \frac{w_i}{\left(\overline{M}_n\right)_i} \qquad \textbf{(A4-14)}$$

The total number distribution can be written as the summation of the number distribution for all fractions by substitution of equation A4-7, A4-1 into A4-2:

$$n_t(M) = \sum_{i=1}^{60} \left(\left(n(M)\right)_i \cdot \frac{w_i}{\left(\overline{M}_n\right)_i} \right) = \sum_{i=1}^{60} \left(n(M) \cdot \frac{w}{\left(\overline{M}_n\right)} \right)_i \qquad \textbf{(A4-15)}$$

The logarithmic molar mass distribution can be obtained after substitution of equation A4-8 into equation 4.3 (see section 4.2.1):

$$w\log(M) = \sum_{i=1}^{60}\left(\left(n(M)M^2\right)\cdot\frac{w}{\left(\overline{M}_n\right)}\right)_i \cdot \ln(10) \qquad \textbf{(A4-16)}$$

This equation can also be written in terms of molar weight fractions:

$$w\log(M) = \sum_{i=1}^{60}\left(w(M)\cdot w\right)_i \cdot \ln(10) \qquad \textbf{(A4-17)}$$

The advantage of equation A4-9 is that all terms are still expressed as number distributions as measured directly by the MALDI.

Appendix 4B

The MALDI-TOF-MS raw data spectra of a mix of six narrow polystyrene standards measured with different matrixes.

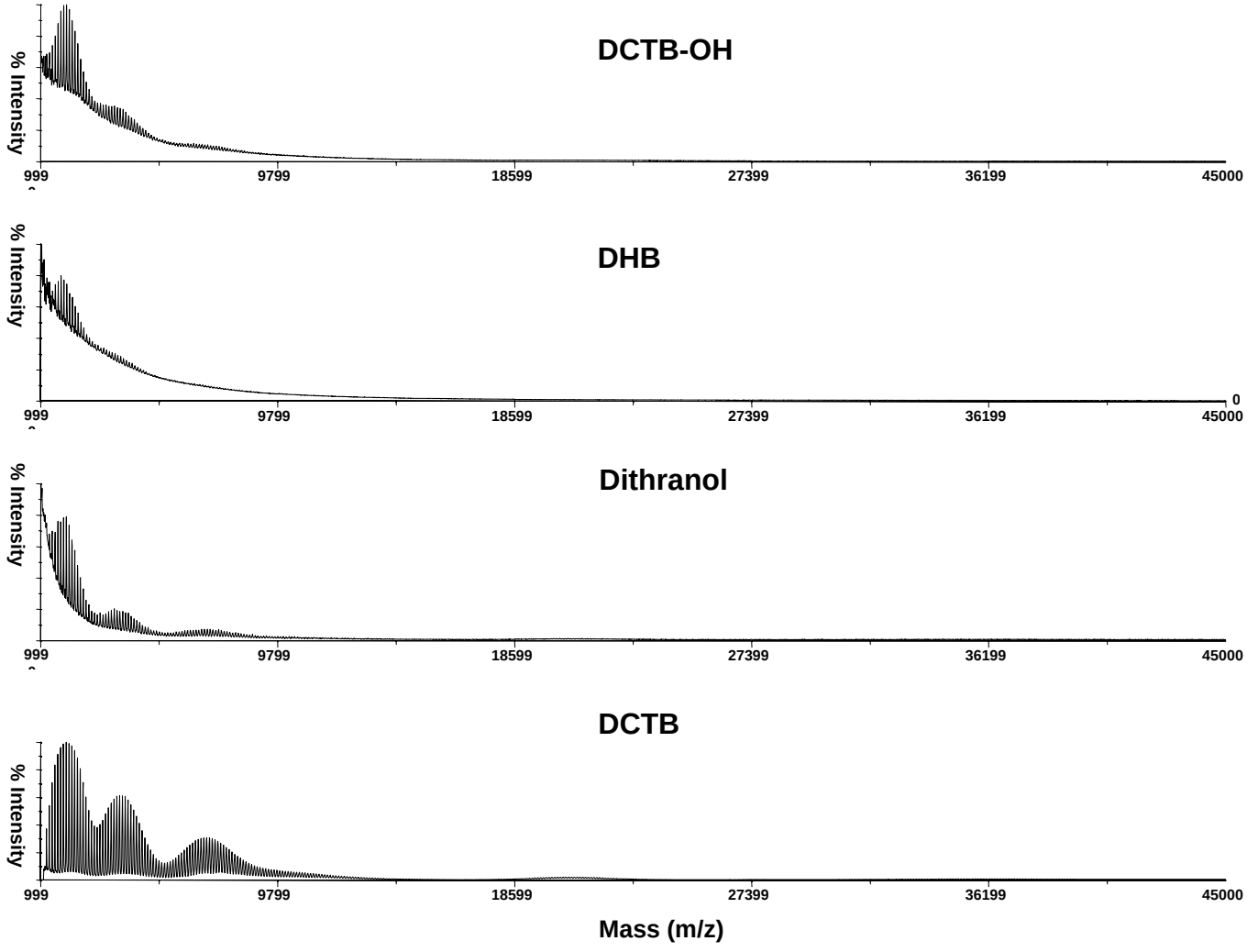

Appendix 4C

The polydispersity of each fractionated polymer sample of a mixture of six narrow polystyrene standards.

Fraction nr.	D (Mw/Mn)	File name	D (Mw/Mn)	Fraction nr.	D (Mw/Mn)
PS2_01	1.02	PS2_21	1.06	PS2_41	1.04
PS2_02	1.02	PS2_22	1.05	PS2_42	1.04
PS2_03	1.01	PS2_23	1.04	PS2_43	1.04
PS2_04	1.09	PS2_24	1.04	PS2_44	1.04
PS2_05	1.04	PS2_25	1.04	PS2_45	1.04
PS2_06	1.03	PS2_26	1.03	PS2_46	1.04
PS2_07	1.03	PS2_27	1.03	PS2_47	1.04
PS2_08	1.02	PS2_28	1.03	PS2_48	1.04
PS2_09	1.03	PS2_29	1.03	PS2_49	1.05
PS2_10	1.02	PS2_30	1.04	PS2_50	1.05
PS2_11	1.03	PS2_31	1.06	PS2_51	1.05
PS2_12	1.04	PS2_32	1.05	PS2_52	1.03
PS2_13	1.06	PS2_33	1.05	PS2_53	-[#]
PS2_14	1.07	PS2_34	1.04	PS2_54	-[#]
PS2_15	1.04	PS2_35	1.04	PS2_55	-[#]
PS2_16	1.03	PS2_36	1.04	PS2_56	-[#]
PS2_17	1.03	PS2_37	1.05	PS2_57	-[#]
PS2_18	1.03	PS2_38	1.06	PS2_58	-[#]
PS2_19	1.05	PS2_39	1.06	PS2_59	-[#]
PS2_20	1.08	PS2_40	1.05	PS2_60	-[#]

[#] Fractions 53 through 60 did not yield a significant response due to the low amount of material present.

Appendix 4D

The MMD obtained by conventional calibration, universal calibration and light scattering.

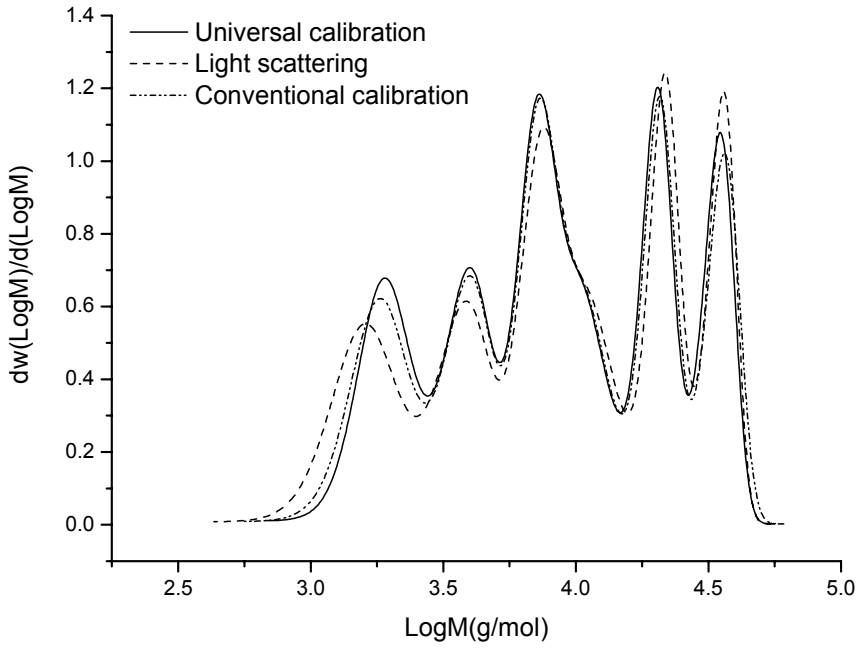

Appendix 4E

The MALDI spectrum of the well defined broad polystyrene standard consisting of six narrow standards.

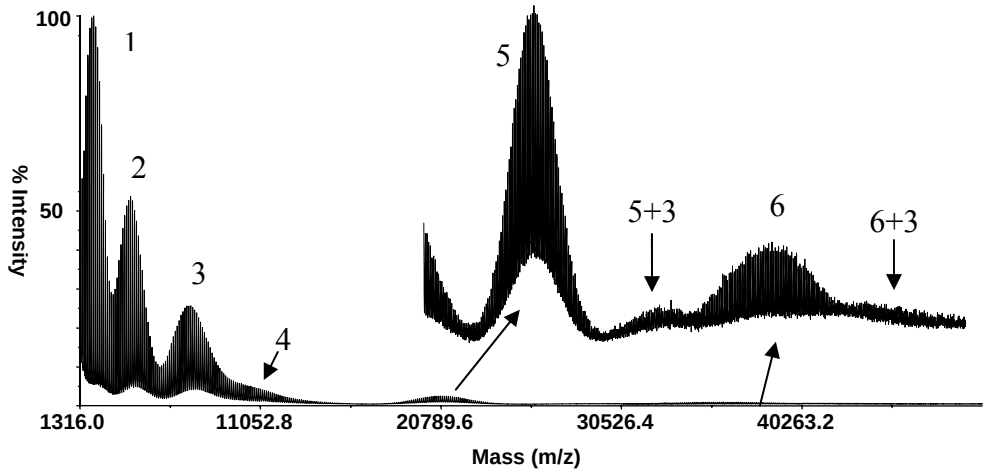

All six peaks of the individual standards are marked. Note that peak four merged together with peak three and is much broader in terms of chain numbers resulting in a broader peak, where the individual peak maximum of the fourth standard is no longer observed. The formation of agglomerates is also observed i.e. peak three and peak five (5+3). Even the combination of peak five and peak six was observed (not shown). Although multiple peak formation leads to biased molar mass distribution, the effects are rather weak in terms of intensity.

Chapter 5

MALDI of homopolymers

5.1 *Introduction*

MALDI-TOF-MS spectra of homopolymers contain information on end groups and molar-mass distributions. Unfortunately this information is not the direct outcome of the analysis and, hence, mathematical operations are needed. We developed software based on the definitions described in the next paragraph to extract information from spectra. Since this chapter only deals with homopolymers we will add some definitions for copolymers in chapter 6.

5.2 *Definitions*

5.2.1 Determination of numbers of repeat units and end-group masses

The observed mass of a singly charged copolymer chain in MALDI-TOF-MS is described by the following equation:

$$m_{obs} = m_A \cdot nr_A + m_{ion} + m_{end1} + m_{end2} \qquad \textbf{(5.1)}$$

where m_{obs} is the observed mass of a peak in the MALDI-TOF-MS spectrum, m_A is the mass of the repeat unit, nr_A is the number of repeat units, m_{ion} the mass of the adduct ion and m_{end1}, m_{end2} are the masses of the end groups. The total end-group mass $(m_{end1} + m_{end2})$ can be calculated from the above equation as long as the number of repeat units and the adduct mass are known (normally the adduct-ion mass is known, since salt is added for the analysis). However, for a given peak mass we do not know how many repeat units are present.

Let there be two polymers, one with two identical end groups, the mass of which equals 2/3 of the mass of a repeat unit, and the second polymer has one end group with a mass equal to 2/3 of the mass of a repeat unit, whereas the mass of the other end group equals 5/3 of the mass of a repeat unit (see Figure 5-1).

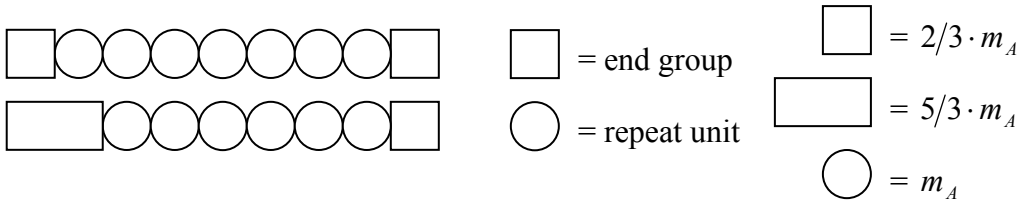

Figure 5-1 Schematic polymer chains having different end-group masses and different numbers of repeat units, but the same overall molar mass.

The total masses of both schematic polymer chains are identical;
$(2 \cdot (2/3) + 7)m_A = (5/3 + 2/3 + 6)m_A$, although the end-group mass and the number of repeat units for both polymer chains are different. As a consequence, the solutions for the end group mass become a function of the number of repeat units. Therefore we define the residual mass (m_{res}) as being the minimum total end-group mass, and the corresponding maximum number of repeat units (nr_{A_Max}):

$$m_{res} = m_{obs} - m_A \cdot nr_{A_Max} - m_{ion} \quad \textbf{(5.2)}$$

$$nr_{A_Max} = INT\left(\frac{m_{obs} - m_{ion}}{m_A}\right) \quad \textbf{(5.3)}$$

Note that the m_{res} of both chains in Figure 5-1 would be $1/3 \cdot m_A$ and the maximum number of repeat units 8.
The solutions for the total end-group masses for a singly charged peak in a MALDI-TOF-MS spectrum can now be written in a more general form:

$$(m_{end})_n = m_{res} + m_A \cdot n \quad \textbf{(5.4)}$$

Where $(m_{end})_n$ represents all the solutions for the total end-group masses for a given residual mass, *n* equals the maximum number of times one repeat unit mass would "fit" within the total end groups (e.g. an end-group mass of 154 amu can be considered as one repeat unit of styrene (104 amu) and an m_{res} of 50), or in other words where *n* is the smallest integer part of the ratio m_{end}/m_A.

5.2.2 End-group Correlation Function (ECF)

We just defined a method to calculate for each peak all possible total end group masses. However, since most polymers only have few different end groups, only one peak of each series should be sufficient to determine the end-group masses. Figure 5-2 shows a typical MALDI-TOF-MS spectrum of a homopolymer of styrene with two series of peaks having different total end-group masses.

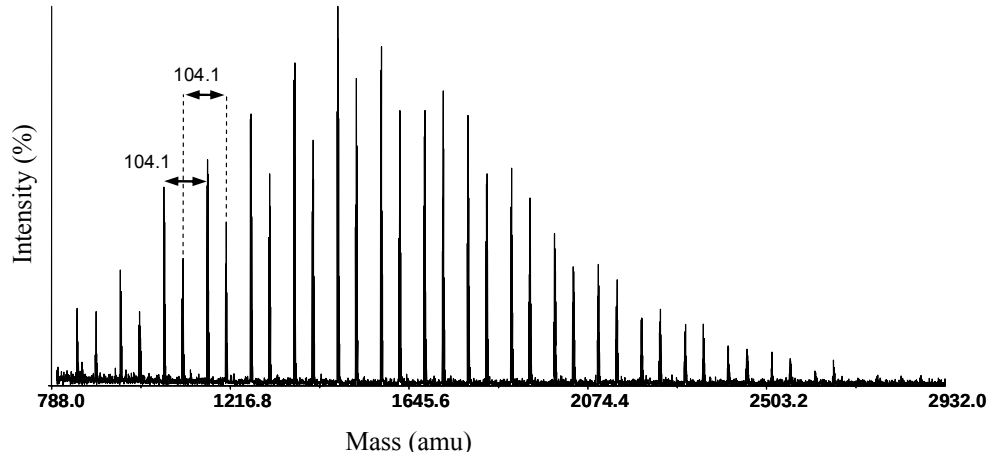

Figure 5-2 A MALDI-TOF-MS spectrum of polystyrene, reflective positive-ion mode, DCTB as matrix and Ag^+ as a cationization agent. The two different series of peaks differ by 104.1 amu, the mass of one repeat unit of styrene.

To obtain the highest possible precision for end-group analysis with MALDI-TOF-MS, we introduce the End-group Correlation Function (ECF). This function finds the maximum correlation of a given end-group mass along the entire spectrum.

$$ECF(m_{end}) = \sum I\left(m_A \cdot nr_A + m_{ion} + m_{end}\right) \tag{5.5}$$

Where I is the corresponding intensity of the spectrum at a given mass, and $ECF(m_{end})$ the end-group correlation at any given end-group mass.

Note that while calculating the ECF as a function of the end-group mass, the upper value of m_{end} must be selected at least equal to the mass of a repeat unit in order to find all end-group masses. The mass step-size of m_{end} is set the same as the maximum mass difference between two consecutive data points (normally at the end of the spectrum since the data is acquired in the time domain). The result of a calculated ECF is shown in Figure 5-3.

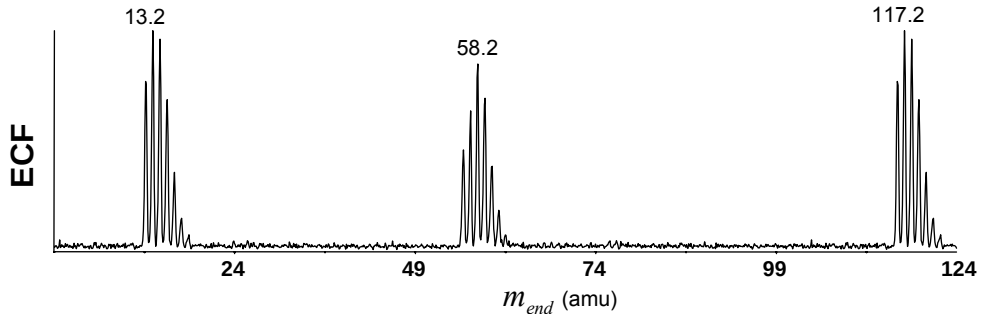

Figure 5-3 The result of the calculation of the end-group correlation function (arbitrary units) of a polystyrene sample (Figure 5-2).

The repeat unit mass of polystyrene equals 104.1 amu therefore all peaks below 104.1 amu must be different end groups. Figure 5-3 shows the existence of two well resolved peak clusters at 13.2, 58.2 amu respectively. The clusters present the "average-isotopic" distributions, since the shape of the isotopic distributions slightly changes along the molar-mass scale, which affects the accuracy of the end group mass. Figure 5-4 shows a change in peak-maximum-average repeat mass of less then 0.1 amu. The peak maximum is defined as the corresponding mass of the most abundant peak within the isotope cluster of a given number of repeat units. The average mass of a repeat unit is calculated by the corresponding mass of the peak maximum divided by the number of repeat units resulting in the peak-maximum-average repeat mass.

According to equation **(5.2)** the accuracy of m_{res} depends on the product of $m_A \cdot nr_{A_Max}$. The deviation between the value of the peak-maximum-average repeat mass and the average mass of the monomer decreases with an increase of the number of repeat units resulting in saw-toothed function of $m_A \cdot nr_{A_Max}$ (the absolute error of m_{res}) versus number of repeat units (see Figure 5-4). The end-group calculation must be applied to the entire mass range to obtain accurate end-group masses. As long as a mass range of at least 11 repeat units are used to compute the end-group masses, the obtained deviation is between -0.6 amu and -0.4 amu for polystyrene. It is more convenient to shift the end-group masses by 0.5 amu resulting in a deviation of ±0.1 amu. The ECF functions shown is this thesis are already corrected for the deviation depending on the mass range and the type of polymer. Besides such a correction, the spectrum typically deviates by 0.5 amu using the instrument default calibration.

The two peaks at 13.2 and 58.2 amu (Figure 5-3) are the residual masses for the end groups of the spectrum in Figure 5-2. The general solutions for the end groups become:

$$\left(m_{end}\right)_1 = 13.2 + m_A \cdot n \text{ and } \left(m_{end}\right)_2 = 58.2 + m_A \cdot n \qquad \textbf{(5.6)}$$

An experienced user of the MALDI would have noticed immediately the difference in the isotopic patterns of Figure 5-2 (not visible). This is also noticed in Figure 5-3. Before starting to assign the other end group, it is wise to check whether all species are charged with the same cation. Preparing the sample with a different salt should yield all species shifted in the same manner. The expert user would recognize a mass difference close to 44 as the difference between Ag and Cu. A small trace of a copper salt turned out to be the cause of the "second end group" in the present case. This example underlines the need to verify whether all species are ionized by the same cation.
In some cases a higher accuracy is needed and equation **(5.5)** needs to be modified and needs as input the repeat mass and an approximation of the end-group mass. The repeat mass can be obtained by the Auto Correlation Function (ACF) discussed in the next section, whereas the approximated end-group mass is obtained by equation **(5.5)**.

$$ECF_{HR}(m_{end}) = \sum\left(\sum_{IMax(nr_A)}^{IMax(nr_A)+m_A} I\left(m\left(IMax\right)+m_{end}\right)\right) \tag{5.7}$$

Where ECF_{HR} is the high resolution end group determination, $m(IMax)$ the corresponding mass of the maximum intensity within the isotopic cluster at a given number of repeat units. Note that the m_{end} must be lower then the mass of a repeat unit in contrast to equation **(5.5)**.

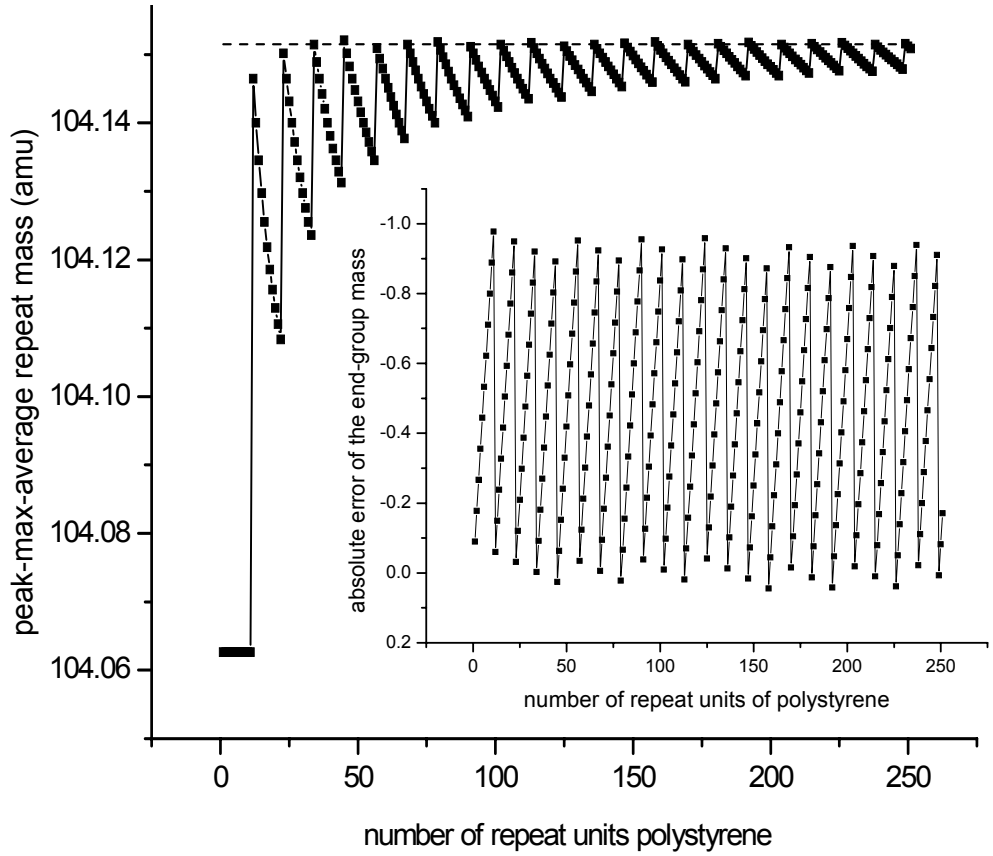

Figure 5-4 The peak-maximum-average repeat mass is the most abundant peak in an isotopic cluster divided by the number of repeat units. The dashed line is the average molar mass of the repeat units. The graph demonstrates the mass shift of repeat unit mass if only the most abundant peak of an isotopic distribution is taken into account.
The insert shows the saw-toothed function of the absolute error of the end-group mass versus the number of repeat units.

5.2.3 Auto-Correlation Function (ACF)

The last part of this section deals with the determination of the repeat-unit mass (m_A) or the identification of the monomer used in the polymerization. Figure 5-5 shows a spectrum of a polymer with four different end groups. Although the repeat mass is the same as in Figure 5-2 this is not immediately clear from the spectrum.

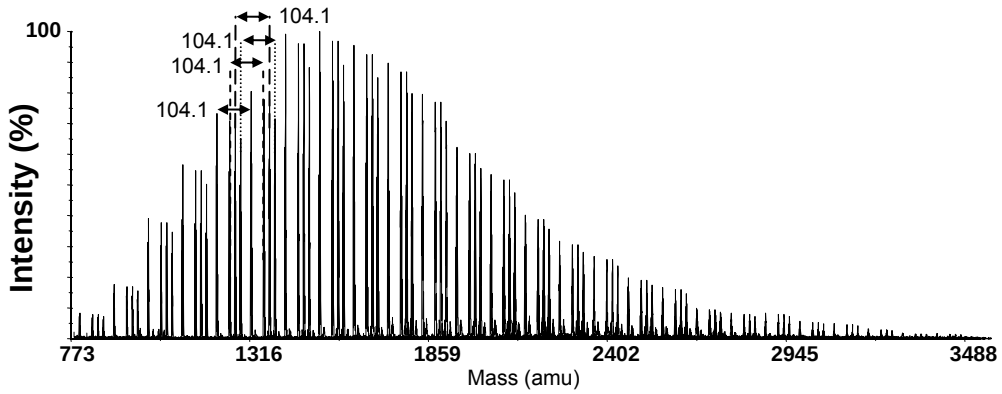

Figure 5-5 A MALDI-TOF-MS spectrum of polystyrene with four distinct series of peaks with a mass increment of 104.1 amu, the mass of one repeat unit styrene.

The auto-correlation function[2] (ACF) returns the maximum correlation for any chosen repeat unit mass, in this case the maximum correlation is found at a mass difference of 104.1, 208.2, 312.3… etc. (see Figure 5-6).

$$ACF(m_{rep}) = \frac{\sum I(m) \cdot \sum I(m + m_{rep})}{\left(\sum I(m)\right)^2} \tag{5.8}$$

Where m_{rep}, the mass step-size, is set equal to the maximum mass difference between two consecutive data points. The observed mass difference of 104.1 amu corresponds to the mass of a styrene repeat unit.

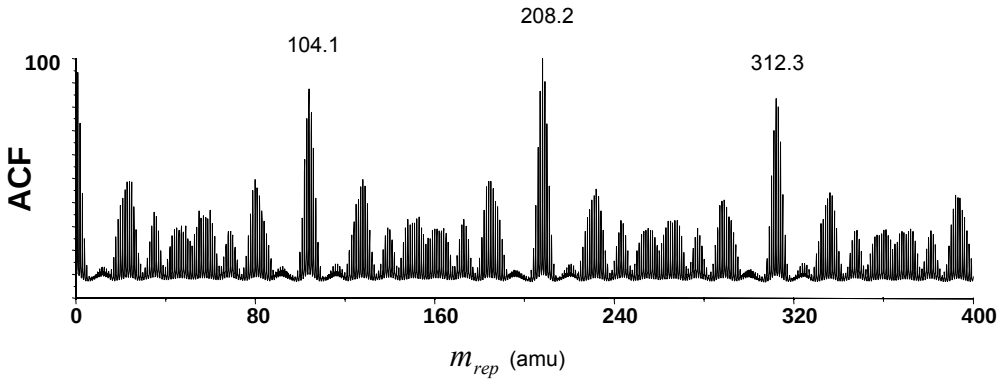

Figure 5-6 The result of the auto-correlation function for a polymer with a repeat unit mass of 104.1 amu which corresponds with the mass of a styrene repeat unit.

The ACF does not return the exact average mass of a repeat unit but the "local" average repeat mass in the mass range of interest. The problem is similar to the peak-maximum-average-repeat mass (see Figure 5-4). As a consequence, the ACF will always return a slightly lower repeat-unit mass compared to the exact average repeat-unit mass. All deviations are typically below 0.1 amu and decrease with increasing mass. Note that these minor deviations do not hamper the identification of the monomer used in the polymerization.

5.2.4 Conclusion

The aim of the concepts described above is to obtain a user-independent method for the interpretation of MALDI-TOF-MS spectra. In summary:

- ACF reveals the repeat mass (m_A), which suggests the polymer identity. Isomers cannot be distinguished based on mass.
- ECF reveals the number of different end-group combinations and the corresponding residual masses (m_{res}) .

The generic solution, equation **(5.4)**, is obtained for each total end-group mass from one MALDI-TOF-MS spectrum. However, for each polymeric series only one of these values for the total end-group mass is correct. At this point chemistry and mathematics must come together. Chemical information is needed to reduce the number of possible solutions for the end-group masses. The next section will demonstrate the need for both mathematics and chemistry. In order to demonstrate the use of the previously derived equations, the data will be analyzed first in the conventional way (only taking a limited region of the entire spectrum and trying to explain every peak).

5.3 *End-group analysis with MALDI-TOF-MS to reveal the initiator functionality*

5.3.1 Introduction

Control Radical Polymerization (CRP) enables synthesis of complex architectures (gradient, block, graft, ect.). The three most effective methods of CPR include Nitroxide Mediated Polymerization (NMP), atom-transfer radical polymerization (ATRP) and Reversible Atom Fragmentation Transfer (RAFT) polymerization[3,4]. Restricting our discussion to the ATRP of methyl methacrylate (MMA), it has been observed that multifunctional halides, such as trichloroalkanes, successfully initiate the polymerization of MMA via ATRP[5]. However, there is no direct measurement for the initiator functionality (mono-, di-, or trifunctional in the case of trichloroalkanes). It is well known that the initiation of the ATRP process largely determines the overall control achieved during the polymerization.

Polymer-end-group analysis is an effective way to establish the initiation mechanism of functional halide initiators. In recent years, MALDI-TOF-MS has been employed as an effective tool from characterization of polymers, obtained via controlled radical polymerization, clearly giving insight into comonomer incorporation, end-group assignment etc. Recently published article gives an excellent review of the use of soft-ionization techniques such as ESI and MALD-TOF-MS for the analysis of polymers. MALDI-TOF-MS is an effective technique for end-group analysis. However, in MALDI the presence of weak carbon-halogen bonds leads to fragmentation despite the soft nature of MALDI. This results in poorly resolved spectra[6,7] and affects the accuracy of the end-group analysis,.

In this study, polymer samples were thermally treated prior to MALDI-TOF-MS analysis to obtain high-resolution spectra. This allows the determination of the true initiator functionality of 2,2,2-trichloroethanol (TCE).

Experimental

A typical polymerization was carried out in a 50-mL three-neck round-bottom flask. *p*-Xylene (11.05 g, 0.10 mol), MMA (2.42 g, 0.02 mol), CuCl (0.037 g, 0.4 mmol), and $CuCl_2$ (0.003 g, 0.02

mmol) were accurately weighed and transferred to the flask. The ligand, *N,N,N′,N″,N″*-pentamethyldiethylenetriamine (PMDETA) (0.07 g, 0.4 mmol) was then added. After the reaction mixture was purged with argon for 30 min, the flask was immersed in a thermostated oil bath, maintained at 90 ºC, and stirred for 10 min. A light green, slightly heterogeneous reaction mixture was obtained. The initiator, TCE (0.15 g, 0.10 mL, 1.00 mmol) was added slowly using a degassed syringe. The reactions were carried out under an argon atmosphere. Samples were withdrawn at suitable time periods throughout the polymerization. Pre-determined amounts of the sample were transferred immediately after withdrawal into GC vials and diluted with 1,4-dioxane, to subsequently determine the monomer conversion using GC. The remaining sample was diluted with THF and passed through a column packed with aluminum oxide prior to SEC and MALDI-TOF-MS measurements.

Materials

Methyl methacrylate (MMA, 99+%) was distilled and stored over molecular sieves at -15°C. *p*-Xylene (99+% HPLC grade Aldrich, Zwijndrecht the netherlands) was stored over molecular sieves and used without futher purification. *N,N,N′,N″,N″*-pentamethyldiethylenetriamine (PMDETA, Aldrich 99%), 2,2,2-trichloroethanol (TCE, Aldrich, 99%), *p*-toluenesulphonyl chloride (pTsCl, Aldrich, 99%), copper (I) bromide (CuBr, Aldrich, 98%), copper (II) bromide ($CuBr_2$, Aldrich, 99%), copper (I) chloride (CuCl, Aldrich, 98%), copper (II) chloride ($CuCl_2$, Aldrich, 98%), aluminum oxide (activated, basic, for column chromatography, 50-200 μm), tetrahydrofuran (THF, Biosolve, Valkenswaard, the Nederlands), ethyl 2-bromoisobutyrate initiator (EBriB, Aldrich, 99%), and 1,4-dioxane (Aldrich, AR-grade) were used as supplied. The ligand *N*-*n*pentyl-2-pyridylmethanimine (PPI) was synthesized as described by Haddleton *et al*[8]. and distilled prior to use.

MALDI-TOF-MS instrument

MALDI-TOF-MS measurements were performed on a Voyager-DE-STR (Applied Biosystems, Framingham, MA, USA) instrument equipped with a 337nm nitrogen laser. All spectra were acquired in the positive-ion reflectron mode. Trans-2-[3-(4-tert-butylphenyl)-2-methyl-2-propenylidene]malononitrile (DCTB) was used as matrix. Sodium trifluoracetate (Aldrich, 98%) was added as the cationic ionization agent (approximately 1 mg/mL dissolved in THF). The matrix was dissolved in THF at a concentration of 40 mg/mL. The dissolved-polymer concentration was approximately 1 mg/mL. In a typical MALDI experiment, the matrix, salt and polymer solutions were premixed in the ratio: 5 μL sample: 5 μL matrix: 0.5 μL salt. Approximately 0.5 μL of the obtained mixture were hand spotted on the target plate. For each spectrum 1000 laser shots were accumulated.

Fourier-Transform Infrared Spectroscopy (FTIR)

The FTIR spectra were recorded with a BioRad Excalibur 3000 series spectrometer. One hundred scans at a resolution of 4 cm^{-1} were signal-averaged, and the BioRad Merlin software was used to analyze the spectra. Samples were prepared by casting films from a dilute polymer solution on KBr discs for FTIR measurements. These films were thin enough to be within the range where the Lambert-Beer law could be applied.

Results and discussion

MMA was polymerized by ATRP using EBriB, p-TsCl, or TCE as initiator. The characteristics of the experiments are summarized in Table 12.

Table 12 Homopolymerization of MMA (ATRP)

Entry	Initiator	Reaction time (min)	Conversion (%)	Molar mass (g/mol)	PDI
1	pTsCl[a,b]	230	74.0	7.1×10^3	1.08
2	TCE[a,b]	180	45.0	2.8×10^3	1.25
3	EBriB[c,b]	240	85.0	5.1×10^3	1.22

a) Target $\overline{M}_n$ =5000 g/mol; [Initiator]:[CuCl]:[PMDETA] = 1:0.5:0.5, reaction temperature = 90°C.

b) Volume (*p*-xylene)/(monomer) = 1/0.5

c) Target $\overline{M}_n$ =6000 g/mol; [Initiator]:[CuBr]:[PPI] = 1:1:2, reaction temperature = 90°C.

In Figure 5-7, the FTIR spectrum of PMMA with bromine end groups is shown after heating overnight at different temperatures. The carbonyl band is clearly visible at 1730 cm^{-1} regardless of the temperature at which the sample was treated. Upon increasing the temperature to 140 – 160 ºC a slight shoulder is developing at 1782 cm^{-1}. This shoulder is tentatively assigned to the formation of a lactone at the chain end. It was particularly significant at temperatures in the range of 140 – 160ºC.

MALDI-TOF-MS is known as a soft ionization technique. However, it has been reported that polymers with halogen end groups can fragment during the measurements[7,9], due to the weakness of the carbon-halogen bond. One of the possible side reactions in the specific case of PMMA is the formation of lactones. This lactone formation during the measurements lowers the resolution, and complicates the interpretation of the MALDI-TOF-MS spectra. The reduction in resolution is the result of fragmentation during the laser ablation and/or during the time of flight. Molecules that fragment in the flight tube will have the proper kinetic energy and arrive at the correct time in the linear mode. In the reflector mode, these ions are reaccelerated with the mass of the charged fragment and arrive at the wrong time, leading to spectral differences between the linear and the reflector modes.

In the present study the problem of reduced resolution in MALDI-TOF-MS was solved by heating samples overnight at 150ºC, resulting in quantitative formation of the chain-end lactones. FTIR spectroscopy was used to monitor the formation of lactones as a function of temperature.

p-toluene sulphonyl chloride (p-TsCl)

The use of p-TsCl as intiator leads to chlorine-end-functionalized PMMA (PMMA-p-TsCl). Figure 5-9a and Figure 5-9b show the MALDI-TOF-MS spectra of the PMMA-pTsCl before and after heating, respectively. Figure 5-9c shows the theoretical spectra of the proposed structures A, B and C (Figure 5-8).

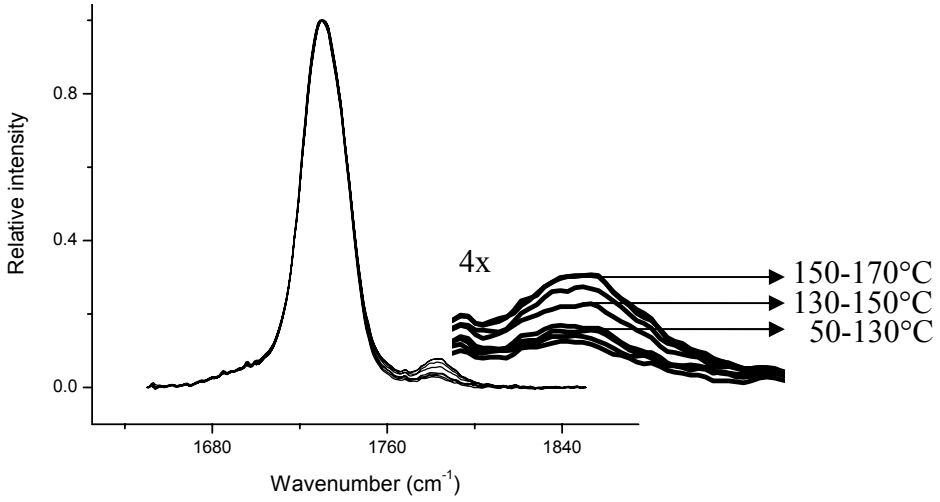

Figure 5-7 The FTIR spectra of bromine-end-functional PMMA (initiated with EBriB) as a function of temperature. The shoulder at 1782 cm^{-1} is enlarged to show the increase with temperature.

The presence of three peaks (denoted A, B and C) indicates the existence of polymer chains with three different end groups. The peaks at lower mass carry the same respective end groups, but contain a smaller number of MMA repeat units. Compared to untreated PMMA, the heat-treated PMMA shows an increased resolution within peaks B and C, whereas the resolution within peak A remains the same. No conclusion can be drawn from the relative changes in intensities of peaks A and C before and after heating, since MALDI-TOF-MS is not a quantitative technique.

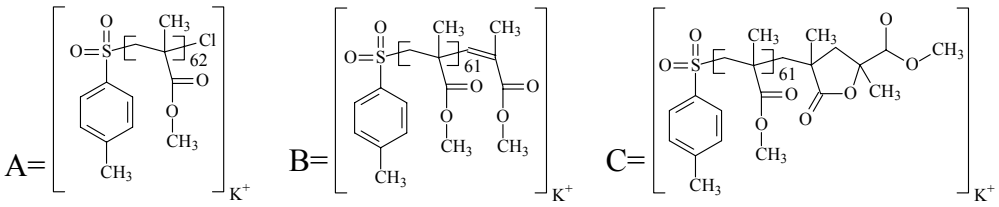

Figure 5-8 Different proposed structures for the observed peaks of PMMA-pTsCl. The theoretical isotope patterns are depicted in Figure 5-9c.

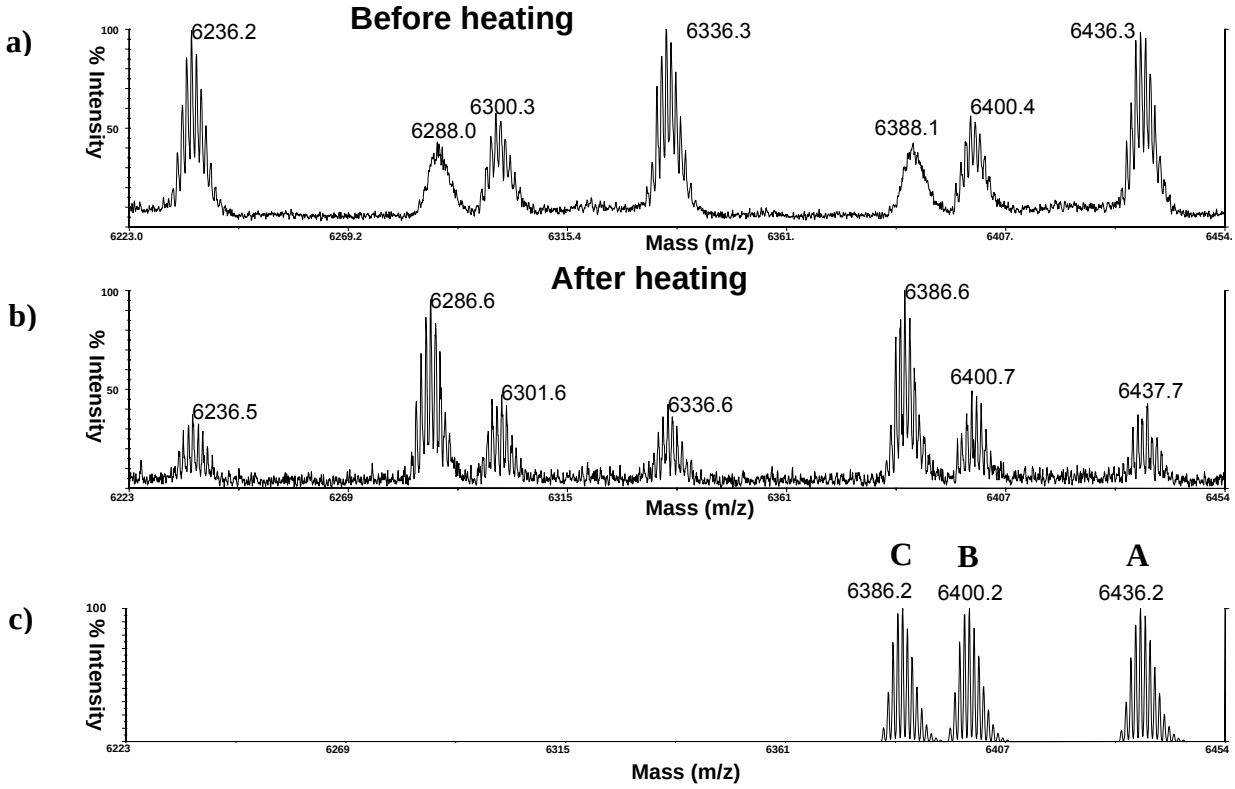

Figure 5-9 Figures (a) and (b) show the MALDI-TOF-MS spectra of the PMMA-pTsCl before and after heating, respectively. Figure (c) shows the theoretical spectra of the proposed structures A,B and C (Figure 5-8).

The peaks assigned to structure **A** corresponds to a PMMA chains with a chlorine end group. The peak assigned to structure **B** corresponds to a polymer chain that has lost HCl. The peak assigned to structure **C** corresponds to a polymer chain with a lactone end group, formed upon the loss of CH_3Cl. All peaks show excellent agreement between the observed and theoretical masses.

From the above spectra it is evident that thermal treatment increases the resolution. The more-accurate masses and isotope patterns simplify the interpretation of MALDI-TOF-MS spectra of fragmenting polymers, since the shape of the isotopic pattern is related to the number of chlorine atoms present. The masses of polymer fragments are slightly biased towards higher masses, due to fragmentation as discussed in section 2.1.3 and at the beginning of this section.

Despite the observed fragmentation, the spectra obtained for PMMA-pTsCl polymers are relatively simple. Polymers with more than one chlorine atom are more challenging.

2,2,2-Trichloroethanol (TCE)

The use of 2,2,2-trichloroethanol (TCE) as initiator in an ATRP reaction also leads to chlorine end-functionalized PMMA (PMMA-TCE). In contrast to PMMA-pTsCl, all three chlorine atoms from the initiator can theoretically initiate the polymerization. This may even lead to three arm star or branched architectures beside the linear chains. As far as we know, there is no unambiguous evidence for the mono-functional initiation of TCE. In comparison with on the MALDI-TOF-MS analysis of PMMA-pTsCl, more-complicated spectra were expected for PMMA-TCE, due to the presence of three chlorine atoms. If all three chlorines initiate the reaction, then a maximum of three lactone groups can be formed. Similarly, a bi-functional initiation may lead to two lactone groups. In summary, a maximum of ten different end groups may be expected in the MALDI-TOF-MS spectra of PMMA-TCE. Table 13 summarizes all possible peaks, the corresponding mass losses, and the number of chlorine atoms.

Each peak (A through J) represents a different combination of end groups. Note that the mass difference between peak F (formed via the loss of two CH_3Cl molecules) and peak A, of 101 amu, is almost the same as the mass of a repeat unit of MMA (100.1 amu). However, the numbers, of Cl atoms for peaks A and F are different. The same situation holds for peaks B and I, and C and J, where the mass difference of the corresponding end groups is also nearly identical to the mass of a repeat unit.

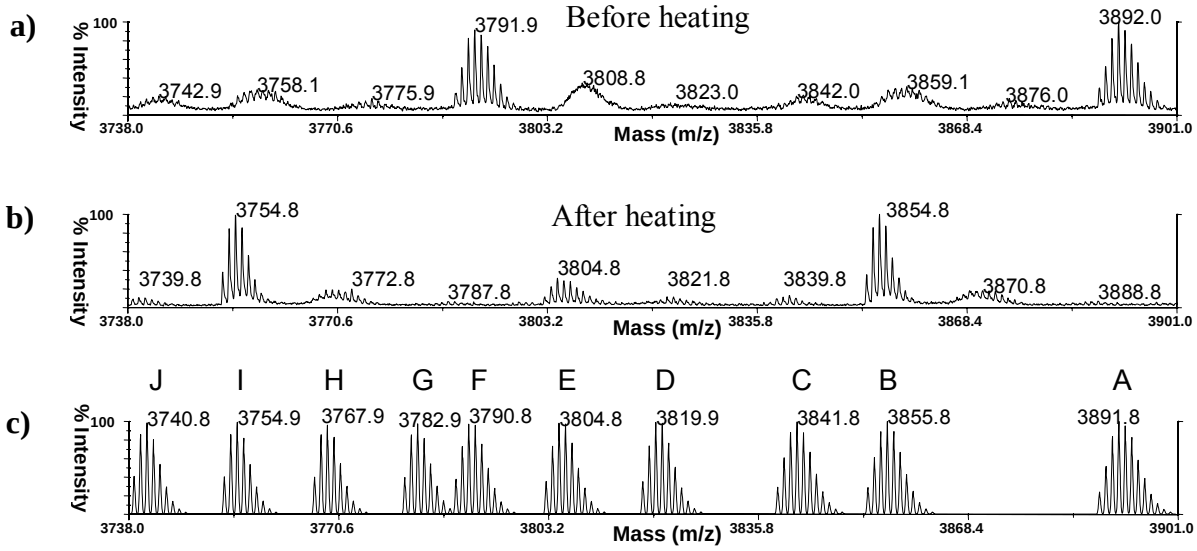

Figure 5-10 MALDI-TOF-MS analysis of PMMA-TCE. Spectrum (a) shows the untreated sample and spectrum (b) shows the effect of heating the sample at 150ºC overnight. Spectrum (c) shows the theoretical isotope distributions of 37 repeat units of PMMA with different end groups (Table 2, peaks A through J). The displayed mass corresponds to the most abundant isotope.

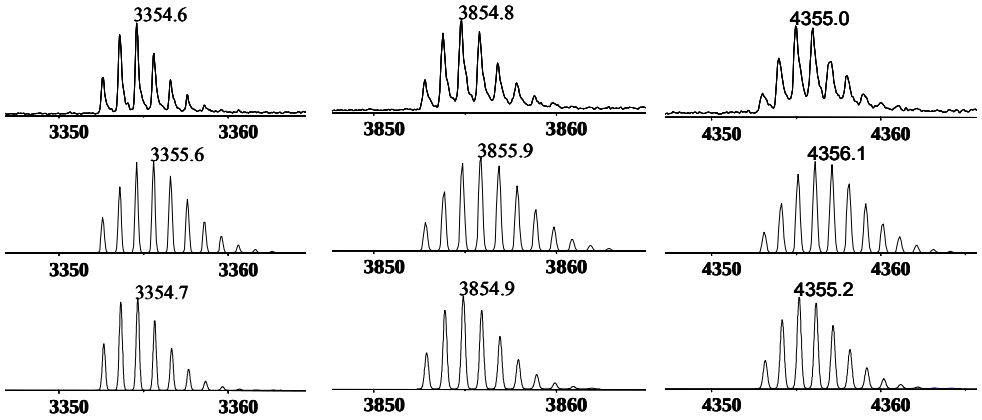

The spectra of PMMA-TCE.

The theoretical spectra of structure B.

The theoretical spectra of structure I.

Figure 5-11 The upper trace shows enlarged parts of the spectrum at different mass intervals. The middle and lower trace show the corresponding theoretical isotope patterns of structures B and I, respectively.

Figure 5-10a and Figure 5-10b show the spectra of PMMA-TCE before and after heating. The most-relevant proposed structures can be found in appendix 5A. For each peak (A through J) the theoretical isotope pattern is shown in Figure 5-11c.

In the spectrum of the sample before heat treatment (Figure 5-10a), only one peak shows sufficient resolution to allow unambiguous assignment. The observed isotope pattern of the peak at 3892.0 amu (Figure 5-10a) is compared with the theoretical isotope patterns of peaks A and F (Figure 5-10c). Based on the width of the isotope pattern it is concluded that the peak at 3892.0 amu should be assigned to structure A (appendix 5A). A general observation is that the width of the isotope pattern increases with the number of chlorine atoms due to the chorine isotopes (Cl_{35} and Cl_{37} with corresponding intensity 1:0.32). The peak at 3791.9 amu (Figure 5-10a) is assigned to a chain with identical end groups as that at 3892.0 amu, but with one MMA repeat unit less incorporated. No further attempts were made to identify the remaining peaks due to a lack of resolution.

Table 13 All possible structures sorted by increasing mass loss relative to peak A. The fourth column refers to the number of Cl atoms present in the polymer.

Peak	Fragment[#]	mass loss (amu)	Description	Cl atoms present	End group mass (amu)
A	-	0.0	-	3	149.40
B	-(HCl)	36.5	HCl	2	112.94
C	-(CH_3Cl)	50.5	1 Lactone	2	98.90
D	-2(HCl)	72.9	2HCl	1	76.48
E	-(CH_3Cl)(HCl)	86.9	1 Lactone+HCl	1	62.46
F	-2(CH_3Cl)	101.0	2 Lactones	1	48.43
G	-3(HCl)	109.4	3HCl	0	40.02
H	-2(CH_3Cl)	123.4	1 Lactones+2HCl	0	25.99
I	-2(CH_3Cl)HCl	137.4	2 Lactones+HCl	0	11.97
J	-3(CH_3Cl)	151.5	3 Lactones	0	98.06

[#] The loss of a CH_3Cl group corresponds with a formation of a lactone.

At this point it is not possible to deduce the initiator functionality from the MALDI-TOF-MS analysis (Figure 5-10a), since isomeric structures may result from initiation by TCE as shown in Figure 5-13. For obvious reasons, these structures can not be distinguished by mass spectrometry.The spectrum of the heat-treated sample (Figure 5-13b) shows the most abundant peaks at 3754.8, 3854.8 etc., which can be assigned to either peak B or peak I. The lack of a broad isotope pattern indicates the absence of chlorine atoms. Therefore, structure I was assigned to masses 3854.8 and 3754.8. Probably the most convincing evidence for this assignment is shown in Figure 5-11. Three expansions of the mass spectrum are shown that are related to identical end groups at different chain length. The experimental spectrum consistently shows the third isotopic peak as the most abundant one. This feature is recognized in structure I whereas structure B shows the fourth peak to be the most abundant.

The last situation in which an observed mass can be assigned to two different end groups, which differ by nearly the mass of a repeat unit concerns peaks C and J.

The low intensity of the observed peaks 3739.5, 3839.8 etc. (Figure 5-10b) does not allow us to judge which isotope pattern (C or J) should be assigned to these peaks. However, we know that upon thermal treatment the vast majority of (chain end) chlorine atoms are converted to lactones, which leads to a significant increase in the intensity of the peaks, as seen in the heat-treated PMMA-pTsCl. Since peak I, which corresponds to the formation of two lactones, is the most abundant peak after heat treatment, we can rule out the existence of structure J. Structure J represents trifunctional initiation, which would result in three Cl end groups, and, therefore, in three lactones as the dominant peak after heat treatment.

In case of the presence of a small amount of trifunctional initiator, the peak assignment of the structures C and J cannot be made based on mass. However, the relative end-group intensities of structure J (the formation of three lactones) should show a different relationship across the molar mass range (a higher functionality leads in this case to a higher molar mass) compared to the other functional initiators, since structure J is the only structure that can be obtained upon heat treatment after trifunctional initiation. Figure 5-12 shows an overlay of the relative intensities of all relevant structures versus the molar mass. The similar behavior of all peaks indicates the presence of one type of initiator functionality. Note that small amounts of trifunctional initiators do not lead to a significant increase in the polydispersity measured by SEC.

The peaks at 3739.8, 3839.8 etc. are assigned to structure C. At this point all the peaks with two possible structures are assigned (C and J, A and F, and B and I). Peak A (3892.0) completely disappears during heat treatment, indicating lactone formation.

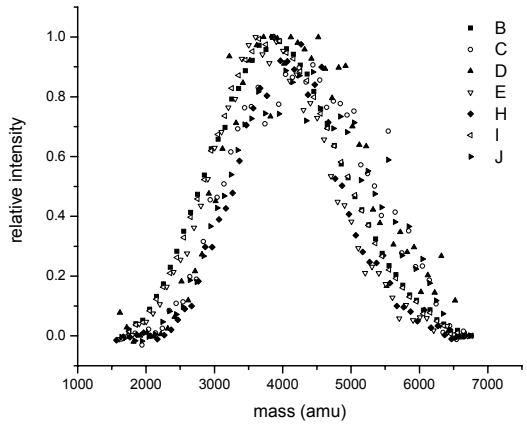

Figure 5-12 The relative abundance of the observed end groups corresponding to the structures B, C, D, E, H, I and J (see Table 2). No significantly different relative intensities for the end-groups were observed across the molar mass distribution.

The peaks at 3772.8, 3804.8, and 3821.8 are very weak and are assigned to structures H, E, and D, respectively (Figure 5-10b). Structure G is not observed in Figure 5-10b.

In summary, structures I, E, and H are the relevant ones in the heat-treated sample. Moreover, peak I, corresponding to the formation of two lactone groups, is dominant. Note that a maximum of two lactones are formed after heat treatment.

Initiator functionality

In this section an attempt is made to reveal the functionality of the TCE initiator based on the results of MALDI-TOF-MS analysis of samples before and after heat treatment. Figure 5-13 shows the possible polymer structures formed via mono-, di- and tri-functional initiation. All have exactly the same mass. Note that all these structures lead to different numbers of lactones after heat treatment.

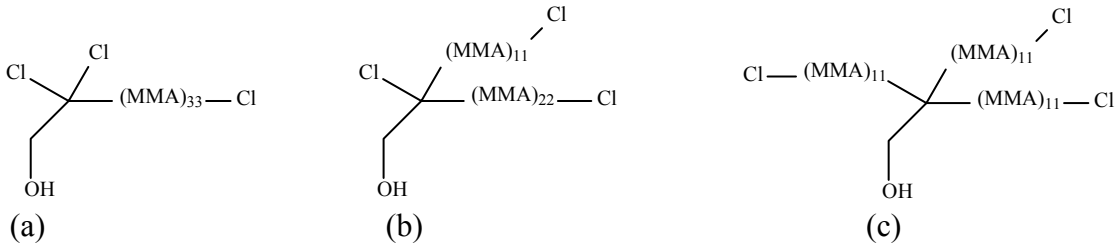

Figure 5-13 The different topologies that result from mono-, di- and tri-functional initiation. All structures have identical masses.

When considering the mechanism of lactone formation upon heat treatment, mono-functional initiation of TCE (Figure 5-13 structure (a)) leads to the formation of two lactones[7], one lactone is formed by an end-functional Cl atom (Figure 5-14(a)). We postulate a second possibility for the

lactone formation by one Cl atom of the initiator (Figure 5-14(b)), which is basically the same reaction as the former lactone formation, *i.e.* reaction of the ε-OCH_3 with the terminal Cl atom.

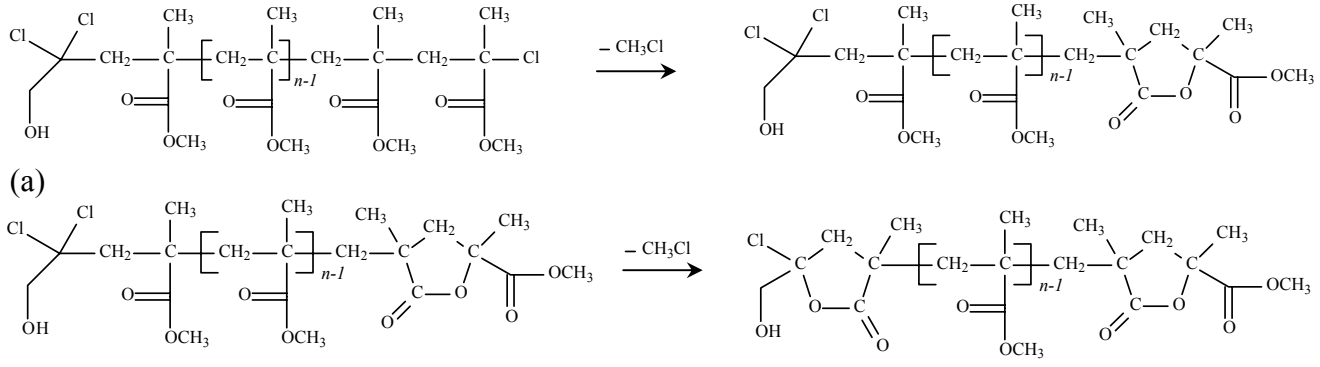

Figure 5-14 (a) Schematic illustration of the reaction by which an end-functional chlorine atom leads to lactone formation. (b) Schematic illustration of the reaction by which a chlorine atom at the initiator leads to lactone formation.

Table 14 Maximum number of lactones formed in relation to the initiator functionality.

Functionality of initiator	Max. nr. of lactones formed	Nr. of lactones observed
mono-functional	2	2
di-functional	3	2
tri-functional	3	2

Such dual lactone formation is not possible for initiators with one chlorine atom, such as pTsCl. Similarly, structures (b) and (c) in Figure 5-13 would show a maximum of three lactones after heat treatment. In case of a di-functional initiator (Figure 5-13) one of the Cl atoms in Figure 5-14b is replaced by a bulky polymer chain and the lactone formation needs to take place in the middle of the polymer chain. However in the "conventional" lactone formation (Figure 5-14b) the two groups next to the Cl atom (methylester and methyl group) do not hinder the lactone formation, since the second methylester in the backbone forms the lactone. Although the kinetics of the second postulated lactone formation will be different, the steric hindrance of the bulky polymer chain is unlikely to prevent the lactone formation.

The numbers of lactones observed (Table 14) provide strong evidence for a mono-functional initiation of TCE in ATRP.

Conclusion

MALDI-TOF-MS is demonstrated to be a very powerful technique for end-group analysis to study initiator functionalities, as long as well-resolved spectra can be obtained.

The MALDI-TOF-MS analysis of PMMA-pTsCl confirms the formation of lactones upon thermal treatment. Furthermore, the heat treatment increases the resolution of MALDI-TOF-MS spectra and

simplifies the end-group characterization of polymer systems with weak carbon-halogen bonds. The results of the MALDI-TOF-MS analysis of PMMA-TCE samples before and after thermal treatment, in combination with the maximum number of lactones formed, prove the mono-functional initiation of TCE.

5.3.2 The use of the ECF function

The crucial part in the work described above is the correct interpretation of spectra obtained by MALDI. In this section the strength of the ECF function is shown.
The ECF of the earlier discussed spectra (Figure 5-10) is shown in Figure 5-15.

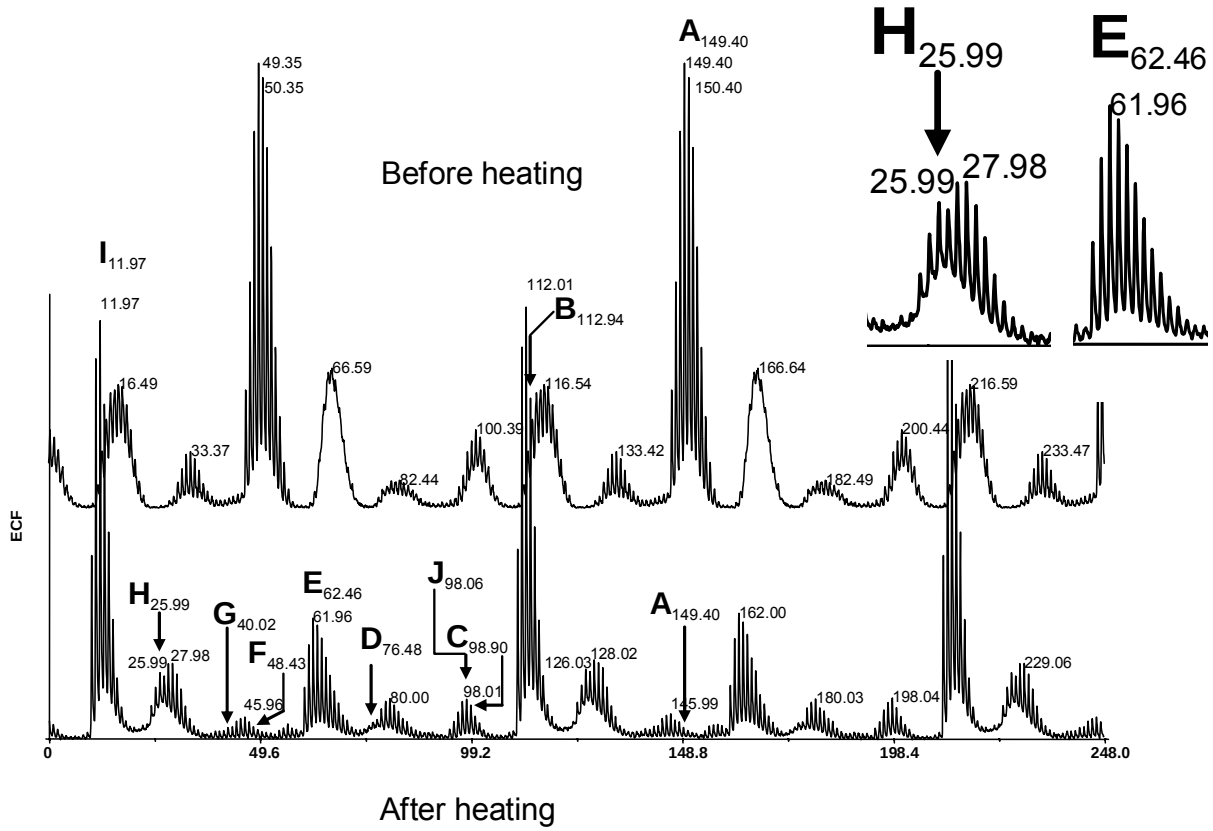

Figure 5-15 End-group correlation function (ECF) of spectra shown in Figure 5-10. The labels A through J correspond to the structures in Table 2. The label subscript refers to the most-abundant theoretical-isotope end-group mass of the corresponding structure.

The ECF function not only calculates the masses of all end groups present in the spectrum, but also improves the resolution of the computed end groups. The improved resolution helps to assign and to exclude possible structures. The labels A through J corresponds to the structures in Table 13. The subscript of each label refers to the most abundant theoretical-isotope end-group mass of the corresponding structure and, if present, should be found at the "top" of an isotope pattern (as long as no isotope overlap takes place). Structure B has an end-group mass of 112.94 amu and is clearly not on the "top" of the isotope pattern compared to structure I. To exclude peak overlap, the isotope pattern should be considered as discussed in the previous section. Since their most abundant isotope

is not located on the "top" of an isotope pattern, peaks A, D, G and F are either absent, or show isotope overlap. The latter suggests the amount of these structures to be negligible. Structures C and J may show isotope overlap, whereas the remaining structures E and H can be easily assigned. However, the ECF function reveals some new insights in the two structures H and E and this will be discussed in more detail.

The ECF "isotope distribution" represents an average isotope distribution of the peaks within a chosen mass range and it does not correspond to the isotope distribution of the end-group structures. The structures H and E are obviously too broad to contain zero or one Cl atom, respectively (see Table 13). The insert of Figure 5-15 reveals that structure H seems to be "bimodal" and structure E could be the result of two overlapping distributions, both with a mass difference of only two amu. The PMMA-pTsCl system indicated the loss of a Cl atom by, besides lactone formation, a cleavage of an HCl group (formation of a double bond, see Figure 5-9). No evidence was found for other end groups such as a saturated bond[9](the exchange of a Cl atom for a H atom).
For PMMA-TCE, structure H will be observed after one lactone formation and twice the loss of the (remaining) Cl atoms. In case of Figure 5-13b, each Cl atom has at least one H atom available for HCl cleavage resulting in double bonds. However, the loss of two HCl groups and the formation of a lactone in case of Figure 5-13a or Figure 5-14a is impossible, due to the formation of <u>two</u> double bonds on one and the same carbon atom. The only way to split off two HCl groups is via hydrogen abstraction of other species, resulting in one double bond (see Figure 5-16) or via the loss of Cl_2 and the rearrangement of one hydrogen atom.

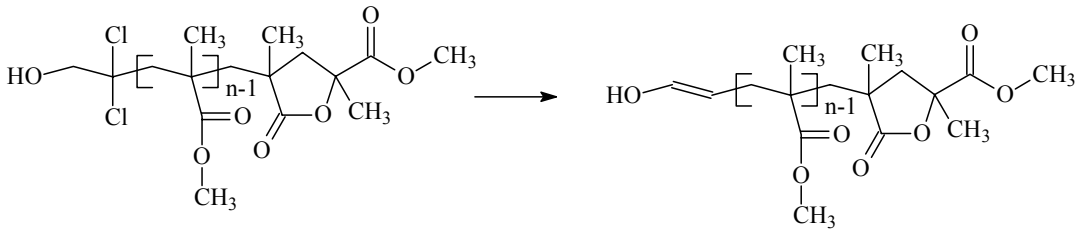

Figure 5-16 The loss of two Cl atoms after lactone formation cannot lead to more than one double bond, as long as the lactone is located at the end of the chain.

The suggested structure has an end-group mass that is of two amu higher than structure H. But, if the lactone formation takes place at the initiator side (Figure 5-14b) than the remaining two Cl atoms at the initiator and the "active" side can easily undergo HCl cleavage which corresponds with the structure H. The broad isotope distribution of structure E may be the result of two overlapping isotope distributions, also with a mass difference of two amu.
The structure of Figure 5-13b (bi-functional initiation) cannot lead to structures as shown in Figure 5-16 due to the fact that there are always hydrogen atoms present for the HCl cleavage and no

evidence was found for the exchange of a Cl atom for a H atom (which could theoretically lead to the same structure as shown in Figure 5-16) in the case of PMMA-pTsCl.
In the case where TCE is mono-functionally initiating and the lactone formation occurs at the "active" end of the chain, the loss of two Cl atoms must lead to structures with two amu difference compared to the loss of the HCl molecules. The absence of these structures in PMMA-pTsCl systems excludes the di-functional or tri-functional initiation of TCE since a structure with two amu difference, compared to structure H, cannot be formed. In addition to the previous conclusion, the number of lactones formed and the use of the ECF function both support the mono-functional initiation of TCE.

In summary, the ECF improves the resolution of a spectrum since it takes the entire mass range into account. The improved resolution lead to a more-accurate interpretation of spectra and, it can reveal small changes in isotope patterns, which are hard to observe from an enlarged part of a spectrum. One may call the ECF the "end-group fingerprint", since it includes all the end-group information present in the spectrum for homopolymers. The end group analysis for copolymers will be discussed in the next chapter.
In some cases the ECF function is not accurate enough to distinguish between end-group masses. An accurate end-group-resolution function may help, as shown in the next sections.

5.4 *Copolymerization of polyketones*

Over the last decades numerous new well-defined transition-metal-based polymerization catalysts have been reported. The so-called "single-site" catalysts may not always behave as such, since polydispersities in excess of two have been observed. Polymers which are formed via "single-site" catalysts are supposed to yield a Flory-Schulz molar-mass distribution with a polydispersity of two. The Flory-Schulz distribution is based on the assumption that polyaddition of monomers at equilibrium conditions is independent of the size of the molecule. The high polydispersities found in practice have been attributed to the occurrence of "multiple-site" catalyst during the polymerization.
The copolymerization of ethylene and carbon monoxide is known to lead to perfectly alternating polyketone. The proposed mechanism of the copolymerization is described elsewhere[1].
In this study the end groups of the perfectly alternating copolymerization were studied by MALDI-TOF-MS. The MMDs obtained with MALDI and SEC was compared to the theoretical Flory-Schulz distribution.

Materials

Phosphorus trichloride (PCl_3,Aldrich, 99.999%), diethylamine ($(Et_2)_2NH$,Aldrich, 99.5%), diethyl ether ($(Et_2)_2O$ were distilled before use. *N,N,N′,N′*- tetramethylethylenediamine (TMEDA, Aldrich 99%) was refluxed over CaH_2 and distilled before use. Acrylonitrile (Aldrich, 99%) was degassed before use. Reacting gases, carbon monoxide (CO) and ethylene were supplied by Hoek Loos (CO: 99.97% pure, ethylene: 99.95% pure). Pd(acetylacetonate)$_2$ (i.e. Pd(acac)$_2$ was supplied by Degussa. hydrochloric acid diethyl ether solution (HCl/Et_2O, Aldrich, 2M), Aldrich, 98.0%), butyllithium solution, 2.5 M in hexane(n-BuLi), lithium aluminum hydride ($LiAlH_4$, Aldrich, reagent grade 95%), potassium hydroxide, (KOH, VWR) and 1,1,1,3,3,3-Hexafluoro-2-propanol (HFIP, Biosolve, Valkenswaard, the Nederlands), di- *p*-Tolylether (Aldrich, 99%) and Trifluoromethanesulfonic acid (CF_3SO_3H, Aldrich, 99%) were used as supplied.

Synthesis of the palladium(II) complex

Starting from di-*p*-tolylether, the synthesis of the diphosphine ligand has been accomplished according to the scheme shown below, following a procedure similar to the one reported in literature.[10]

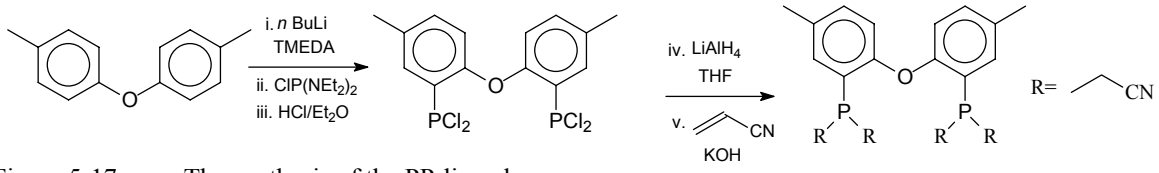

Figure 5-17 The synthesis of the PP-ligand.

The palladium complex suitable for the catalysis was prepared stepwise starting from Pd(acac)$_2$ (see scheme below) following the literature procedure.[11]

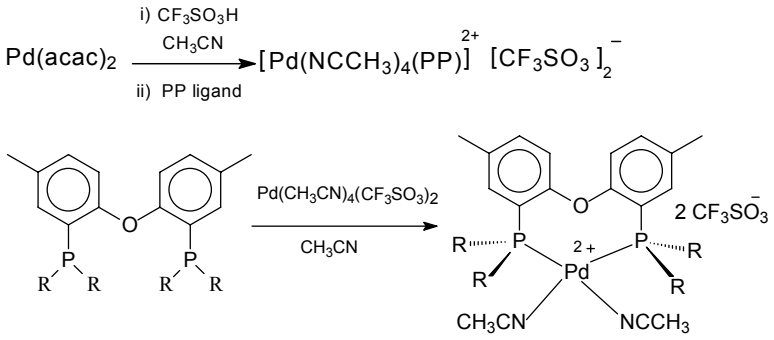

Figure 5-18 The synthesis of the palladium(II) complex.

Experimental

In a typical experiment of copolymerization of ethylene and carbon monoxide, a solution of the desired palladium complex (0.02 mmol) in 10 ml of anhydrous MeOH was injected, under argon atmosphere, into a 75 mL stainless-steel autoclave, previously evacuated by a vacuum pump. The

autoclave was flushed three times with 3 bar of ethylene, then pressurized with ethylene at 25 bar and carbon monoxide at 25 bar at room temperature and then heated to 60ºC. Stirring (1000 rpm) was applied during the reaction. After 2 hours, the reaction was stopped by cooling the autoclave using an ice bath. After the unreacted gases were released, the reaction mixture was filtered. The white solid was washed with methanol and dried under reduced pressure. MALDI was performed on the solid fraction.

Size-Exclusion Chromatography (SEC)

SEC analyses were performed on a system, which consisted of a two-column set (PSS PFG columns linear XL, Polymer Standards Service), an isocratic pump (Gyncotek P580, Separations, flow rate of 0.4 mL/min), an ultraviolet (UV) detector (Waters 486, 230nm) and a differential refractive-index (DRI) detector (Waters 410) as concentration detectors, and HFIP as eluent.

MALDI-TOF-MS instrument

The instrument conditions, matrix and salt concentration used are the same as described in section 5.3.1. The sample was dissolved in HFIP. The best spectra were obtained after first depositing the sample on the target (0.2μL) and subsequently adding the mixture of the matrix and salt solution.

5.4.1 Results and discussion

A typical spectrum of the ethylene-carbon-monoxide copolymer is shown in Figure 5-19. It is the perfect alternating behavior of the copolymer which makes the spectrum look like that of an ordinary homopolymer with a "total" repeat mass of a CO unit and an ethylene unit[11,12]. The insert (upper right corner of Figure 5-19) suggests the presence of at least two different end groups. However, the mass difference between the peaks at 1583.736 amu and 1611.732 amu corresponds to either the mass of a CO unit (28.0104 amu) or an ethylene unit (28.0432 amu). With the use of the mathematical tools described in section 5.2 we tackle the first question: What are the exact end-group masses?

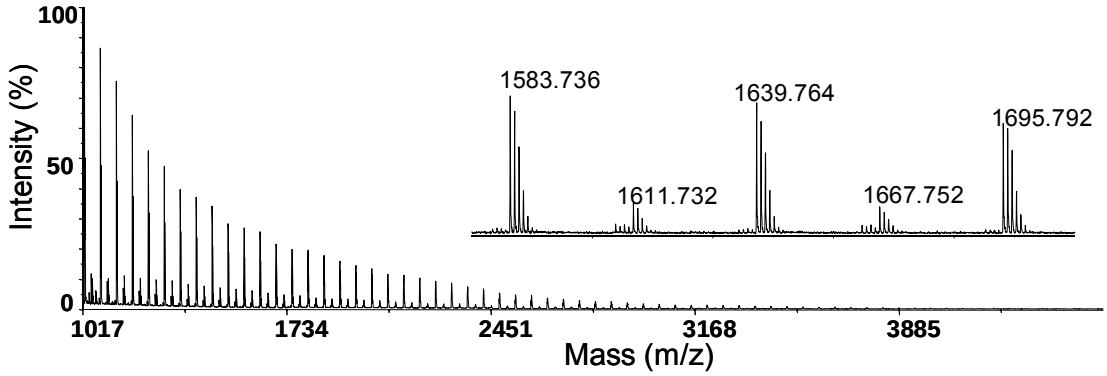

Figure 5-19 A spectrum of an ethylene-carbon-monoxide copolymer. The perfectly alternating copolymer makes the spectrum look like a homopolymer. All species are charged with potassium. The insert suggest the presence of at least two different end groups.

For completeness, the autocorrelation function (ACF) returns the combined mass of the repeat units of CO and ethylene, 56.048 amu. The outcome of the ACF always returns a slightly lower value than the theoretical mass of a CO-Ethylene unit (56.064 amu), as explained in section 5.2.3.

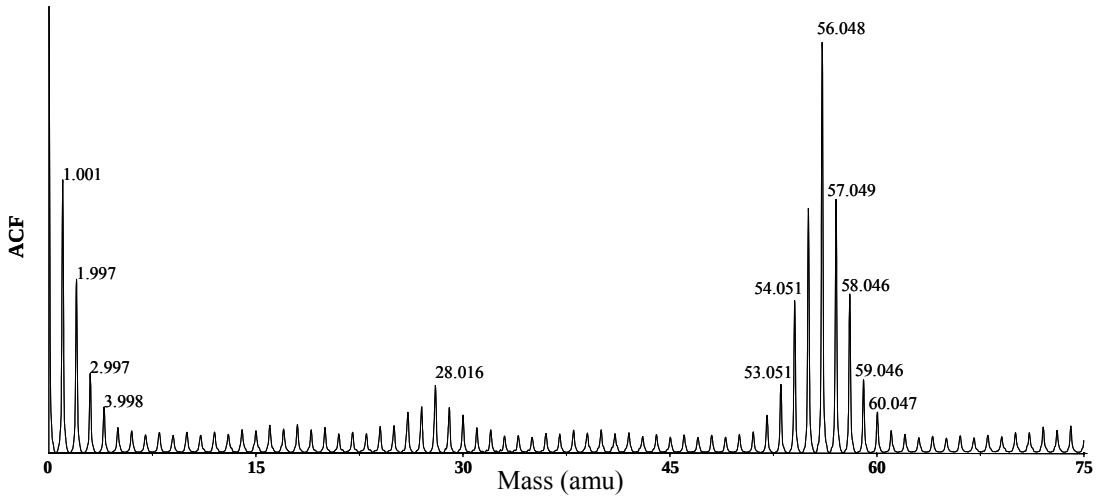

Figure 5-20 The autocorrelation function of the spectrum shown in Figure 5-19**.**

Figure 5-21 shows the end-group-correlation function of the copolymer. The two dominant peaks in the spectrum suggest end-groups masses of 31.999 amu and 3.934 amu. Note that all end-group masses higher by the repeat mass unit (56) are part of the general solution given by equation **(5.4)**. It is surprising that the mass difference of the two end-group masses coincides with the mass of exactly one repeat unit of either a CO or an ethylene unit. A more-plausible explanation would be termination of the growing polymer after only one CO or ethylene has been incorporated instead of a CO-ethylene unit. Also relatively small defects in the copolymerization (and not being perfectly alternating) lead to a different end group. In literature the mechanism of CO/Ethylene copolymerization has been proposed by Drent and coworkers[1]. It is shown in Figure 5-22.

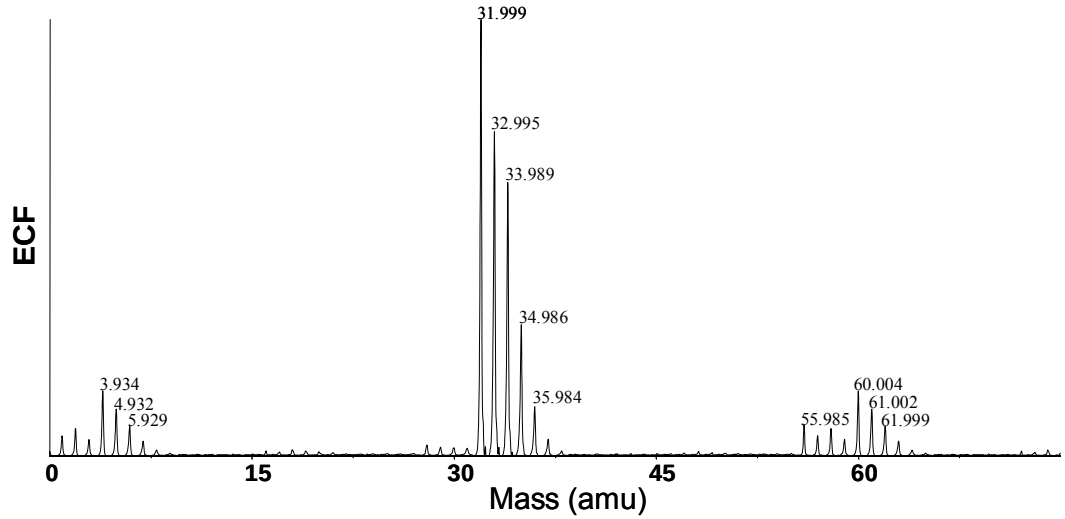

Figure 5-21 The end-group-correlation function of the spectrum shown in Figure 5-19.

The following structures were suggested to arise from after termination by protonolysis or methanolysis: di-ketones, keto-esters and di-esters. At low temperatures (< 85°C), the majority of the products are keto-esters and keto-ethers, with only a small quantity of di-esters and diketones. At higher temperatures the ratio di-ketones/keto-esters/di-esters gets close to 1:2:1[1]. Since the experiments were performed at low temperatures, the majority of the expected products are keto-esters.

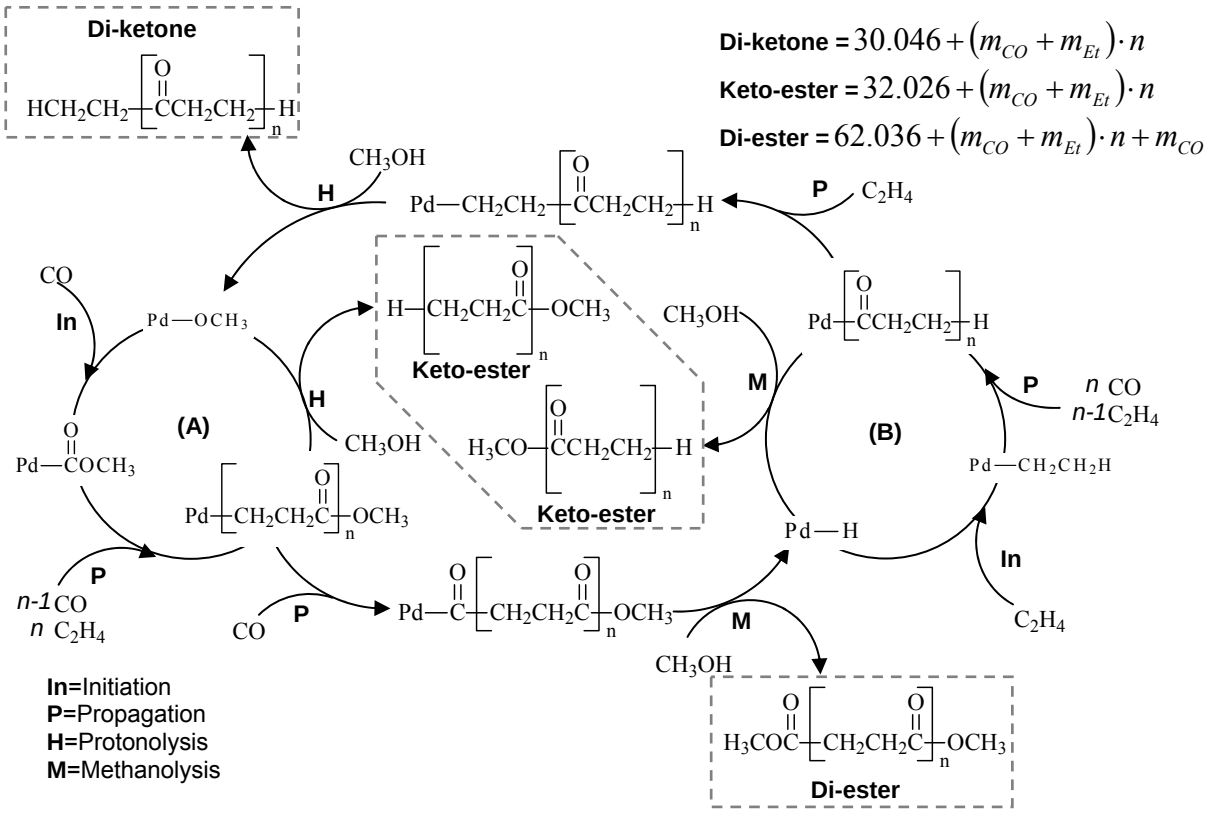

Figure 5-22 Proposed mechanism of carbon monoxide and ethylene copolymerization[1].

The general forms of the end-group masses are listed on the top right of Figure 5-22.

The calculated end-group-mass of 31.999 amu corresponds with the suggested structure of the keto-ester. However the other end-group-mass, 3.934 amu, cannot be explained by one of the suggested structures above. The mass difference of the end groups (28.065 amu) +0.05/-0.95 amu (see section 5.2.2) is either a CO unit or an ethylene unit (the error is too large to assign the mass difference to either). The mechanism in Figure 5-22 suggests in each initiation-propagation-termination cycle (A and B) always a prefectly alternating structure. A double ethylene insertion is known to be possible, whereas a double CO insertion does not occur for thermodynamic reasons[13,14].

With the ECF_{HR} (see section 5.2.2) the mass difference of the end groups could be assigned to the mass of a CO unit.

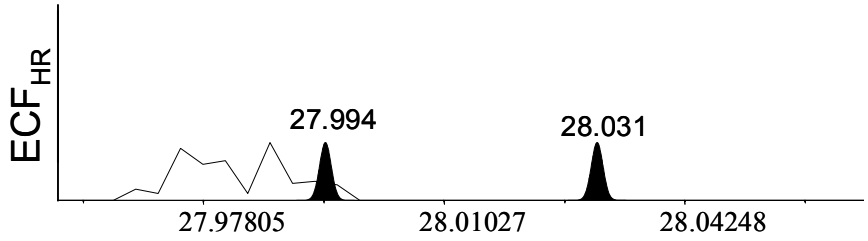

Figure 5-23 The solid Gaussian peak at 27.994 corresponds to the mass of CO whereas 28.031 corresponds to the mass of ethylene. The experimental values with an average of 27.978 ±0.02 amu indicate the CO mass difference of the end groups.

There are only two possibilities to add a CO unit to the keto-ester. The first possibility is straightforward. Add either a CO unit or subtract one ethylene unit (minus one ethylene unit plus the mass of the repeat unit, or the addition of a CO unit results in the same mass). The end group becomes an aldehyde. The second possibility is subtracting an ethylene unit. Here, we assume that at least once the double-ethylene insertion took place. Two methods were employed to find defects in the alternating system. The first test simply calculates the mass difference as a function of the number of repeat units. In case a defect (one double-ethylene insertion) is present, the mass difference will be 0.037 amu higher.

Figure 5-24 shows the persistent mass difference of consecutive repeat units as function of the number of repeat units. Due to a loss of resolution with increasing number of repeat units, the mass difference starts to scatter. The linear fit indicates an average constant mass difference and, therefore, no evidence of one (or more) double ethylene insertions was found. The second method implies the use of an internal calibration standard. An internal calibration standard eliminates the error of spot-to-spot variation, which is at least 0.02 amu and thus not acceptable in the present case. In this procedure a polymer with known end groups was added to the sample and spotted on the target. The error in the internal calibration standard was found to be less than 0.003, amu which was sufficient. An enlarged part of the spectrum can be seen in Figure 5-25. The excellent match between the perfectly alternating keto-ester structures again proves the error-free alternating system.

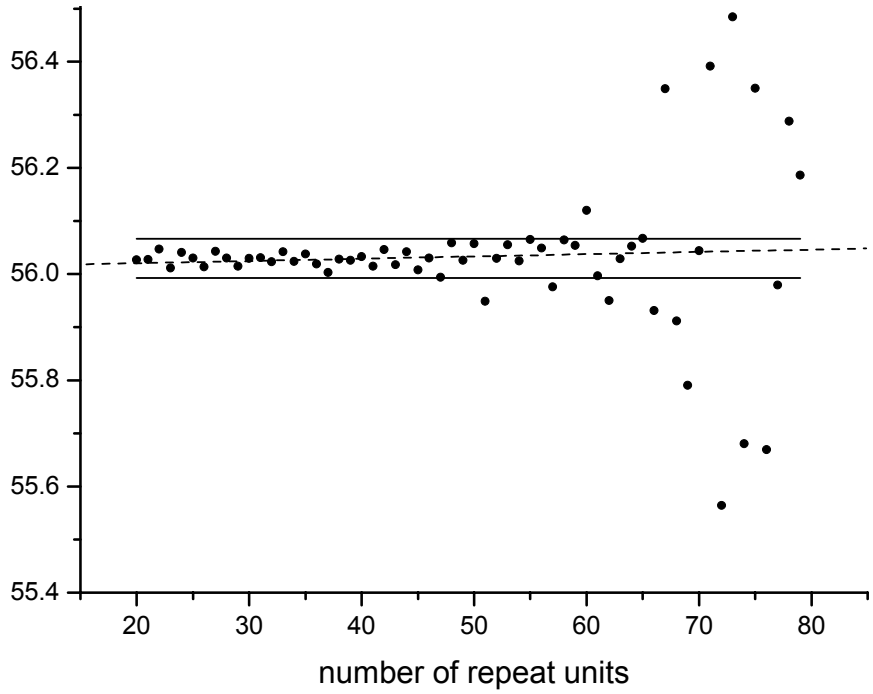

Figure 5-24 Mass difference of consecutive repeat units as a function of the number of repeat units. The upper solid line indicates the expected mass deviation (0.037 amu) if double-ethylene insertion would take place once. The bottom solid line indicates the opposite mass deviation (-0.037 amu). The dashed line presents the linear fit.

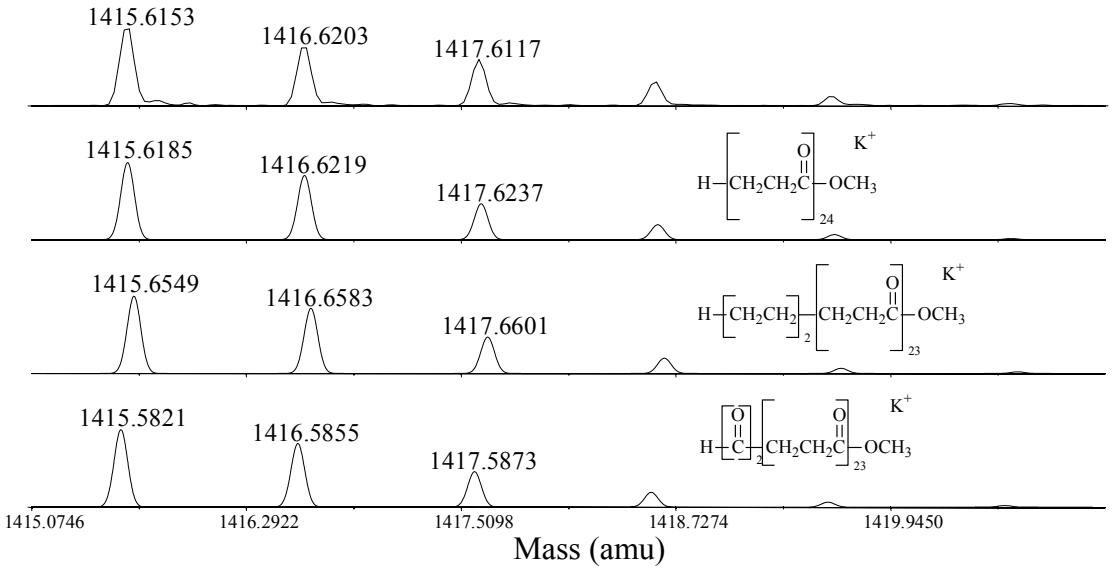

Figure 5-25 The upper trace is the measured sample after internal calibration was applied. The lower traces are the simulated spectra of the given structures on the right side of the picture. Although the bottom-trace structure is not thought to occur, it is depicted here for completeness.

The perfectly alternating copolymerization leads to the conclusion that the mystery peak can only be explained by an aldehyde end group. No further attempts were made to assign the remaining end groups due to the weak intensity as shown in Figure 5-19.

The molar mass distribution (MMD)

In order to compare the molar-mass distribution to the theoretical Flory-Schulz distribution, some modifications need to be made. The equation describing a Flory-Schulz distribution is given below.

$$w_i = i(1-p)^2\, p^{i-1} \qquad \textbf{(5.9)}$$

Where w_i is the weight fraction, i the chain length, and p the degree of polymerization. For a copolymer, the chain length is not exactly proportional to the molar mass, since monomers can have different masses. However, in this case the mass difference of the monomers can be safely neglected with respect to the resolution of SEC.

As described in section 4.3.1 equation 4-3, the number distribution is proportional to the logarithmic MMD by M^2. Since $w_i = n_i M$, the weight distribution is thus proportional to the MMD by M. The chain length can be related to the molar mass, resulting in the modified Flory-Schulz distribution.

$$w(\log M) = \left(\frac{M}{m_A + m_B} (1-p)^2\, p^{\frac{M}{m_A+m_B}-1} \right) M \ln(10) \qquad \textbf{(5.10)}$$

Where m_A and m_B are the masses of the monomers ($m_A \approx m_B$). Note that the entire MMD is described by only one parameter, p.

Figure 5-26 shows the MMD obtained by SEC and by MALDI. The MMD is somewhat narrower than the theoretical Flory-Schulz distribution. No explanation could be given for the shape of the obtained MMD. Due to the low UV absorption of polyketones at 230 nm, no useful UV signal was obtained. Despite the shape of the MMD, the polydispersity did not exceed the value of two. The synthesized palladium(II) complex (see Figure 5-18) acts like a single-site catalyst.

5.5 *Conclusions*

The most abundant end groups in the MALDI-TOF-MS spectrum were assigned to a keto-ester and to an aldehyde. No other structures, such as, di-keto-ester or di-ketone were observed. The copolymerization of CO and ethylene results in a perfectly alternating copolymer. No evidence of double ethylene insertion was observed. The MMD obtained by SEC and MALDI was found to be in good agreement with, but somewhat narrower than the Flory-Schulz distribution. No explanation could yet be given for the obtained shape of the MMD.

In summary, the end-group correlation function (can be used to determine end-group-masses within 0.02 amu. A typical example is the difference between a CH_4 group and a O atom. In contrast to the ECF function, some brute processing power is needed to obtain an with a resolution of 0.001 amu, which makes this function less attractive for daily-routine data-analysis.
The ECFfunction can also be used to study the presence of small defects in the polymer sequence of monomers of nearly the same mass.

However, the majority of the copolymer systems contain monomers of different masses and different topologies, i.e. random, gradient, etc. The data analysis of such complex copolymers is discussed in the next chapter.

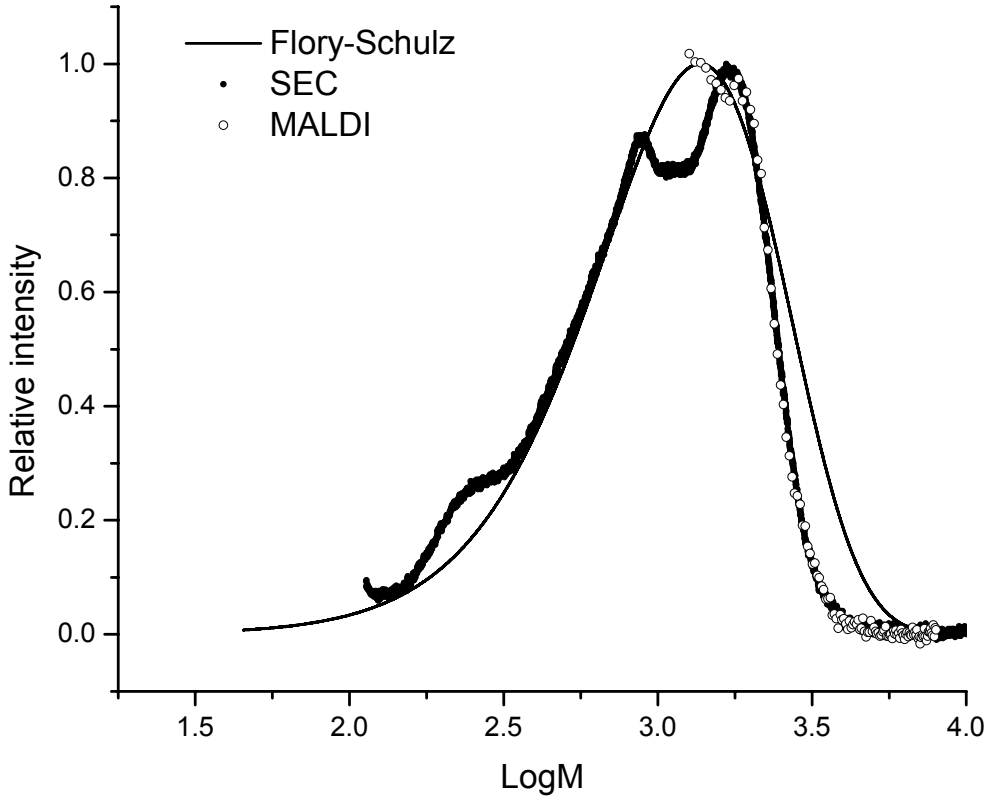

Figure 5-26 A SEC chromatogram of a polyketone. The MALDI trace seems to fit very well to the high-molar-mass tail of the distribution. The MMD is somewhat narrower than the theoretical Flory-Schulz distribution.

Reference List

1. a) Drent, E.; Budzelaar, P. H. M. *Chem. Rev.* **1996,** *96* (2), 663-681; b) A. Sen, *Catalytic Synthesis of Alkene-Carbon Monoxide Copolymers and Cooligomers*, Catalysis by Metal Complexes, Volume 27. Kluwer AP, Dordrecht, 2003, **16**, 1; c) P.W.N.M. van Leeuwen, *Homogeneous Catalysis*, Kluwer AP, Dordrecht, 2004, **12**, 239; d) Drent, E.; Budzelaar, P. H. M. *Chem. Rev.* **1996,** *96* (2), 663-681; e) C. Bianchini, A. Meli, W. Oberhauser, *Dalton Trans*., **2003**, 2627.

2. Wallace, W. E.; Guttman, C. M.; Antonucci, J. M. *American Society for Mass Spectrometry* **1999,** (10), 224-230.

3. Hawker, C. J.; Bosman, A. W.; Harth, E. *Chem. Rev.* **2001,** *101*, 3661-3688.

4. George, M. K.; Veregin, R. P. N.; Kazmaier, P. M.; Hamer, G. K. *Trends in Polymer Science* **1994,** *2*, 66-72.

5. Destarac, M.; Matyjaszewski, K.; Boutevin, B. *Macromol. Chem. Phys.* **2000,** *201*, 265-272.

6. Haddleton, D. M.; Jasieczeck, C. B.; Hannon, J. M.; Shooter, A. J. *Macromolecules* **1997,** *30*, 2190-2193.

7. Borman, C. D.; Jackson, A. T.; Bunn, A.; Cutter, A. L.; Irvine, D. J. *Polymer* **2000,** *41* (15), 6015-6020.

8. Haddleton, D. M.; Shooter, A. J.; Heming, A. M.; Crossman, M. C.; Duncalf, D. J.; Morsley, S. R. *In "Controlled Radical Polymerization"; Matyjaszewski, K. , Ed. ; ACS Symposium Series No. 685; AmericanChemical Society: Washington DC,* **1997,** 284.

9. Singha, N. K.; Rimmer, S.; Klumperman, L. *European Polymer Journal* **2004,** *40* (1), 159-163.

10. a) Dibowsky, H.; Schmidtchen, F. P. *Tetrahedron* **1995,** *51*, 2325-2330; b) M.T. Reetz, D. Moulin, A.Gosberg*, Organic Letters*, **2001**, 3(25), 4083; c) R.T. Boere', J.D. Masuda, Can.J.Chem., **2002**, 80, 1607; d) H.Dibowsky, F.P. Schmidtchen, *Tetrahedron*,**1995**,51(8), 2325-2330,; e) M Caporali,.; Müller, C.; Staal, B.B.P.; Tooke, D. M.; Spek, A. L.; van Leeuwen, P. W. N. M., manuscript in preparation.

11. a) Drent, E.; Van Broekhoven, J. A. M.; Doyle, M. J. *J. Organomet. Chem.* **1991,** *417*, 235-251; b)Wendt, N-F.K. Kaiser, L.I. Elding, *J.Chem.Soc.,Dalton Trans.,* **1997**, 4733-4737; c) K.Li, P.N. Horton, M.B. Hursthouse, K.K. Hii, *J.Organomet.Chem.,* **2003**, 665, 250.

12. Drent, E. *Chem. Abstr.* **1985,** *102*, 46423.

13. Chen, J.-T.; Sen, A. *J. Am. Chem. Soc.* **1984,** *106*, 1506.

14. Sen, A.; Chen, J.-T.; Vetter, W. M.; Whittle, R. R. *J. Am. Chem. Soc.* **1987,** *109*, 148.

Appendix 5A

Some of the possible structures regarding Table 13 are depicted below.

Structure A:

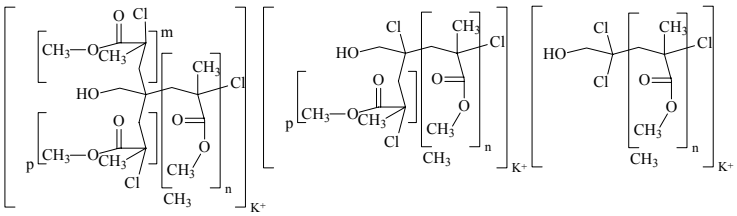

Structure B:

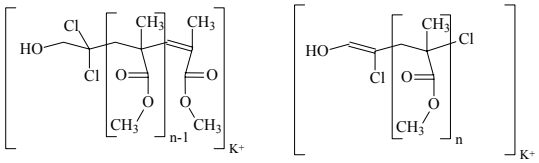

Structure C:

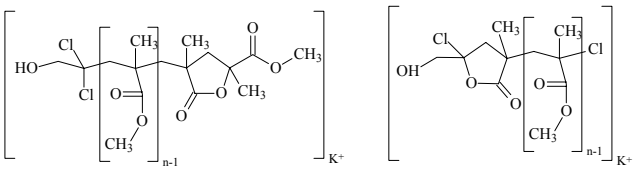

Structure D:

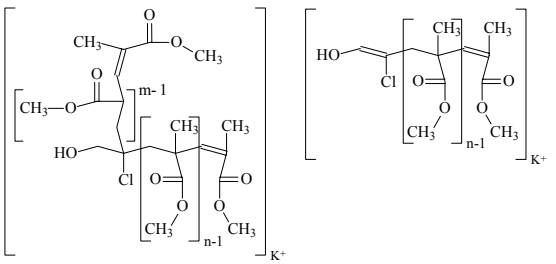

Structure E:

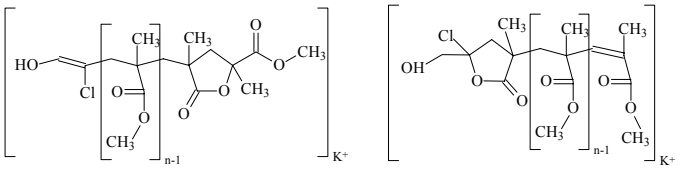

Structure F:

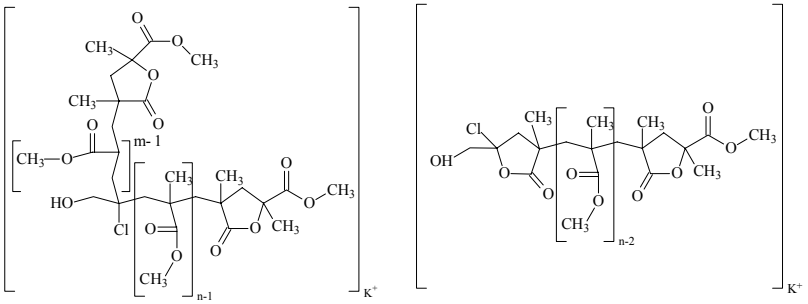

Structure G:

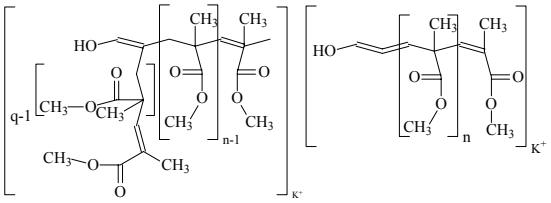

Structure H:

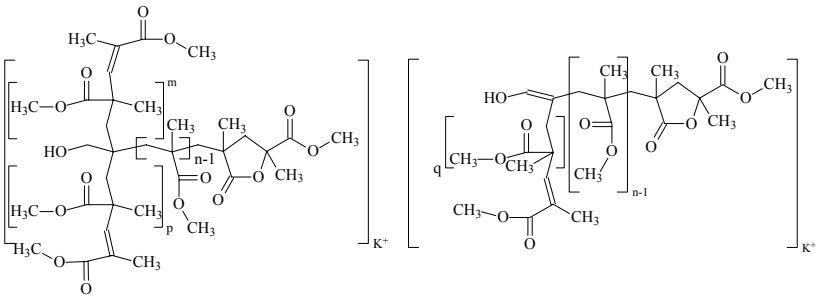

Structure I:

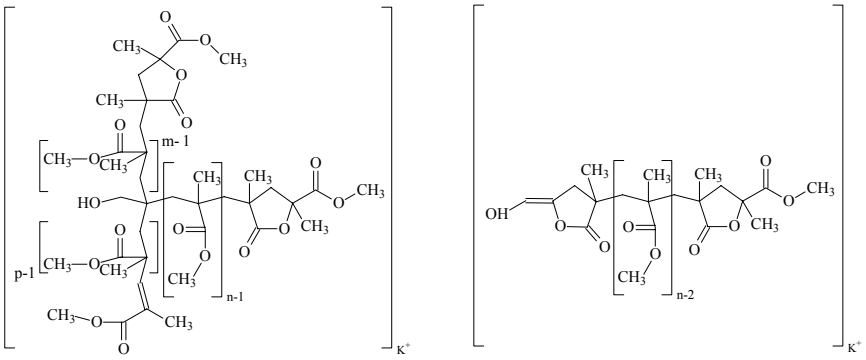

Structure J:

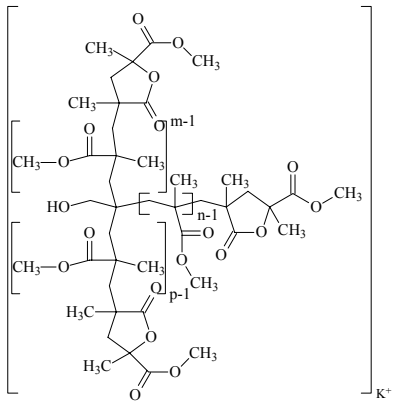
CH3
O
O
CH3
CH3
O
O
m-1
CH3—O
CH3
HO
CH3
CH3
n-1
O
O
CH3
O
O
CH3
O
O
CH3
p-1
H3C
O
H3C
CH3
O
O
K+

Chapter 6

MALDI of copolymers

6.1 *Introduction*

In the previous chapter it has been shown that, with a precise interpretation of the spectra, MALDI can reveal information about the molar-mass distribution (MMD) and the end-group masses of homopolymers. In this chapter the characterization of copolymers will be discussed. Although their spectra are more complex, with the correct interpretation not only the MMD and the end-group masses, but even the chemical composition, the topology (random, block or gradient), the block-length distributions, and the chain-length distributions of copolymers can be measured with MALDI-TOF-MS. Unfortunately, this information cannot be obtained as the direct outcome of the analysis. Hence, mathematical operations are needed. Based on the ideas described in this chapter we developed a program, to visualize the results of the calculations. With this program, within the limitations of mass spectrometry and the conditions of the developed methods, it is even possible to analyze copolymer samples for which no information about topology, end-group masses and type of monomers is available.

6.2 *Copolymer analysis*

The observed mass of a singly charged copolymer chain in MALDI-TOF-MS can be described by the following equation:

$$m_{obs} = m_A \cdot nr_A + m_B \cdot nr_B + m_{ion} + m_{end1} + m_{end2} \qquad \textbf{(6.1)}$$

Where m_{obs} is the observed mass from a peak in the MALDI-TOF-MS spectrum, m_A, m_B, m_{ion}, m_{end1}, and m_{end2} are the masses of the repeat units A and B, the adduct, and the end groups, respectively. nr_A and nr_B are the respective numbers of repeat units A and B.

The autocorrelation function (ACF) as discussed in section 5.2.3, can be applied to spectra of copolymers as well. The ACF helps to determine the possible types of monomers, which constitute the copolymer. The complexity of the copolymer obviously influences the accuracy of this method. In cases where the identification of the monomers is of great interest, other methods, such as, pyrolysis-gas chromatography mass-spectrometry are probably more reliable.

6.2.1 Copolymer topologies

Copolymers can be classified as random, block, gradient, grafted, or branched copolymers. These topologies cannot be identified based on only the mass of one polymeric chain, as obtained from a MALDI-TOF-MS spectrum. For example, the copolymers (random, block, alternating and gradient) shown in Figure 6-1, have the same molar mass, i.e. the same numbers of repeat units A and B, but the sequence differs completely. Fortunately, the relative abundance of the peaks in a spectrum is different for each topology. Therefore, by taking the pattern of all peaks within the entire molar-mass distribution into account, it is possible to distinguish between e.g. a gradient and a block copolymer.

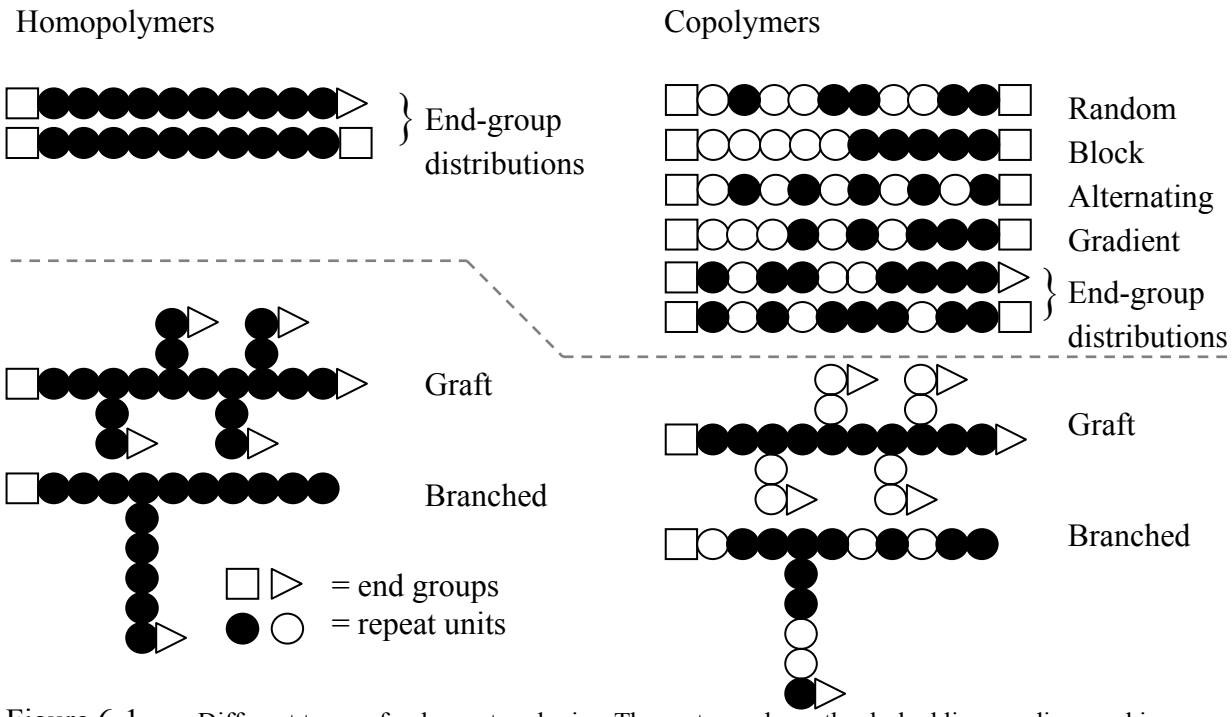

Figure 6-1 Different types of polymer topologies. The systems above the dashed line are discussed in this thesis.

The possible combinations to construct a copolymer out of different monomers are numerous. Only a few are depicted in Figure 6-1 and, hence, classification is needed. First of all, a distinction is made between homopolymers and copolymers. Secondly, a distinction is made between end-groups and chain structure, i.e. in what way the number of the different monomer units are incorporated in the polymer chain.

For a homopolymer, apart from the molar mass distribution, only end-group distributions can be observed. The only mass differences for different homopolymer topologies are the total end-group masses. Therefore, no distinction can be made between different topologies, except for grafted systems, where each molecule contains a different number of (the same) end groups.

For copolymers, the shape of a MALDI spectrum depends on the relative abundance of all individual chains, on the chain end-groups, and on the structure of the chains. Information on topology can be obtained from end-group analysis and from the chain structure. Since the latter gives the best indication of the possible topology, a method to obtain information on the chain structure from the copolymer spectrum will be discussed first. In section 6.5 the end-group determination will be discussed.

6.2.2 Copolymer structure

In a first attempt to reveal the chain structure of a copolymer, the relationship between nr_A and nr_B was investigated. For simplicity we assume the end-group mass to be known. The MALDI spectrum relates peak intensity $I(m)$ and mass. The mass of each peak can be assigned to a combination of nr_A and nr_B. The peak intensity can therefore be written as a function of nr_A and nr_B, $I(m) \rightarrow I(nr_A, nr_B)$, taking into account the following criterion:

$$\left| m_{obs} - m_{calc} \right| \leq \Delta m/2 \qquad \textbf{(6.2)}$$

$$m_{calc} = m_A \cdot nr_A + m_B \cdot nr_B + m_{ion} + m_{end1} + m_{end2} \qquad \textbf{(6.3)}$$

Where Δm is the mass accuracy, typically $\leq$ 0.5 amu and m_{calc} the calculated mass of the *most-abundant isotope* in the isotope distribution corresponding to a specific combination of nr_A and nr_B. The entire mass range of the spectrum can be subjected to the criterion of equation (6.2). In this way each combination of repeat units nr_A and nr_B can be related to the measured intensity of the spectrum, which is defined as the intensity matrix $I(nr_A, nr_B)$.

The intensities of the peaks in the spectrum are subject to peak-shape differences, overlapping isotopes, and isotope broadening. Before we can compute the intensity matrix, the observed intensities need to be corrected for these effects.

6.2.3 Peak-shape differences

The maximum peak intensity is sensitive to variations in resolution and in peak shape (i.e. tailing, ringing, and fronting; see section 2.3.1). In MALDI-TOF-MS it is impossible to have exactly the same resolution in the high- and low-mass regions within one measurement, due to variations in the initial velocity (see section 2.1.3). Errors due to peak-shape differences and resolution changes are minimized by summation across half an amu towards both sides of the peak maximum:

$$I_m = \sum_{m-0.5}^{m+0.5} I(m) \qquad \textbf{(6.4)}$$

Where $I(m)$ is the original peak intensity and I_m the intensity corrected for resolution differences. The value of 0.5 amu has not been chosen arbitrarily but represents half of the mass difference between two consecutive peaks in a well-resolved isotope pattern. Two well-resolved isotopes always differ by essentially one amu (the mass of a neutron is 1.00866497 amu).

Throughout the text two commonly used terms are *summation* and *integration*. As discussed in section 2.4, *summation* is performed in the mass domain, whereas *integration* is always performed in the time domain. Both results in the same values.
The reason not to sum the entire isotope patterns is that the isotope patterns of different polymer species overlap.

6.2.4 Overlapping isotopes

Overlap of isotopes is a typical problem of copolymer systems. Neighboring isotope peaks start to overlap, because of the great number of possible combinations of repeat-unit masses and their corresponding isotope distributions. Overlap of isotopes affects the areas of the most-abundant isotopes and, hence, a correction is needed to obtain the correct intensity matrix. This can be illustrated by an example of a copolymer of styrene and isoprene (Figure 6-2).

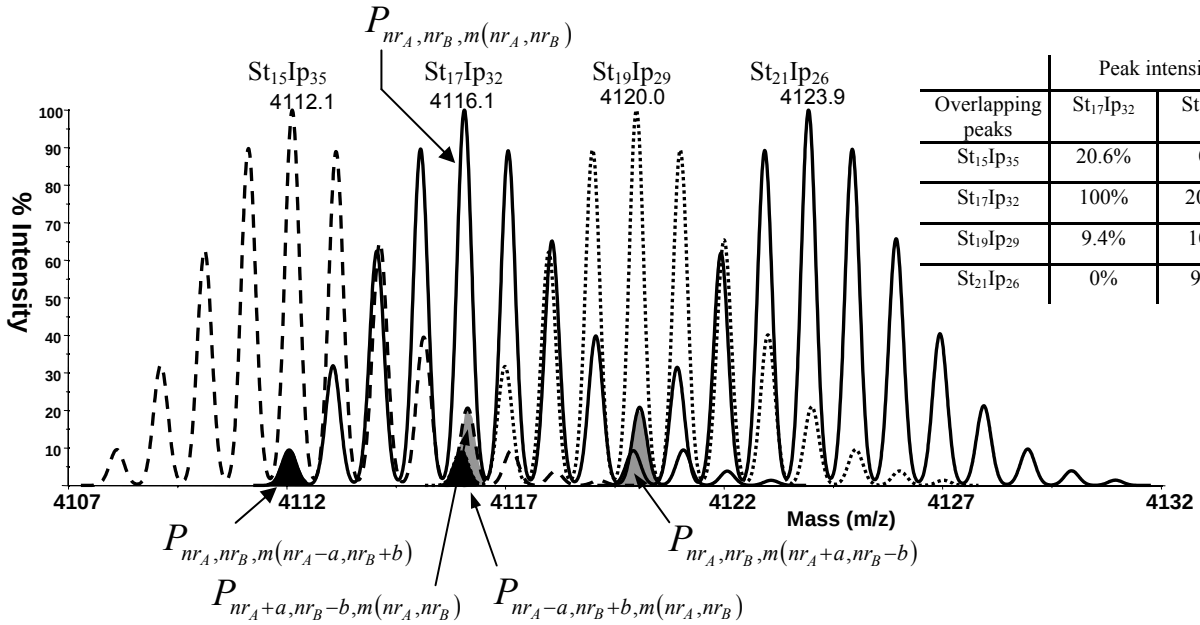

	Peak intensity	
Overlapping peaks	$St_{17}Ip_{32}$	$St_{19}Ip_{29}$
$St_{15}Ip_{35}$	20.6%	0%
$St_{17}Ip_{32}$	100%	20.8%
$St_{19}Ip_{29}$	9.4%	100%
$St_{21}Ip_{26}$	0%	9.3%

Figure 6-2 The simulated isotopic distribution of four polymer chains containing different numbers of repeat units styrene (St) and isoprene (Ip): end groups: *t*-butyl and H: charge Ag^+. The table shows the contribution of the overlapping peaks, in percentages at peak 4116.1 amu and at 4120.0 amu.

In order to correctly integrate the area of each isotope, the relative contributions of the overlapping isotopes should be known. Therefore, a secondary criterion is required to find all observed intensities which belong to the same isotope distribution in the spectrum.
To avoid the need for this secondary criterion, only the most-abundant-isotope peak is corrected for the contribution of the overlapping peaks. In the end, only the area under this peak is needed for further calculations.

The black/gray colored areas of peak $St_{19}Ip_{29}$ in Figure 6-2 show the contribution of overlapping isotopes. The table in Figure 6-2 shows the unbiased (i.e. without overlap) peak intensity of the most-abundant isotope for the distributions of $St_{17}Ip_{32}$ and $St_{19}Ip_{29}$ and the contribution of the neighboring isotope distributions to its observed intensity. These contributions of the neighboring isotope distributions are expressed relative to their most-abundant unbiased isotope. For example, the observed intensity of the most-abundant isotope of $St_{19}Ip_{29}$ can be expressed in terms of the unbiased intensity of the most-abundant isotopes of $St_{19}Ip_{29}$, $St_{17}Ip_{32}$ and $St_{21}Ip_{26}$:

Observed intensity of $St_{19}Ip_{29}$ = 100% of $St_{19}Ip_{29}$ + 20.8% of $St_{17}Ip_{32}$ + 9.3% of $St_{21}Ip_{26}$

Whether intensity or area is used is arbitrary. Since the correction for peak-shape differences (section 6.2.3) already provides the area of the most-abundant isotope, we will use the area instead of the intensity in further calculations. If in the following text, the peak of a given number of repeat units (e.g. I_{nr_A,nr_B}) is mentioned, it always refers to the most-abundant peak of the isotope distribution.

To correct a peak area, one needs to know the unbiased peak areas of the overlapping distributions. Those peak areas, on their turn, depend on the unbiased peak areas of their overlapping distributions, and so on. For practical reasons, we only take two consecutive neighboring isotope distributions into account. Furthermore, we assume the unbiased peak area of the second neighboring distribution to be equal to the unbiased peak area of the first neighboring distribution. We also assume both neighboring isotope distributions to be the same. For example, let Io be the area without overlap, to correct $Io_{19,29,m(19,29)}$ we assume (on the left side of the peak) $Io_{17,32,m(17,32)}$ and $Io_{15,35,m(15,35)}$ to have the same unbiased area and equal percentages ($P_{nr_A-2a,nr_B+2b,m(nr_A-a,nr_B+b)} = P_{nr_A-a,nr_B+b,m(nr_A,nr_B)}$). The same assumption can be made for the right side of the peak so that $Io_{21,26,m(21,26)}$ equals $Io_{23,23,m(23,23)}$ and $P_{nr_A+2a,nr_B-2b,m(nr_A+a,nr_B-b)} = P_{nr_A+a,nr_B-b,m(nr_A,nr_B)}$.

The total observed area can be written as the sum of the individual overlapping isotopes.

$$I_{nr_A,nr_B} = Io_{nr_A,nr_B,m(nr_A,nr_B)} + Io_{nr_A-a,nr_B+b,m(nr_A,nr_B)} \cdot P_{nr_A-a,nr_B+b,m(nr_A,nr_B)} + Io_{nr_A+a,nr_B-b,m(nr_A,nr_B)} \cdot P_{nr_A+a,nr_B-b,m(nr_A,nr_B)}$$

(6.5)

$$I_{nr_A-a,nr_B+b} = Io_{nr_A-a,nr_B+b,m(nr_A-a,nr_B+b)} + Io_{nr_A-2a,nr_B+2b,m(nr-2a_A,nr_B+2b)} \cdot P_{nr_A-2a,nr_B+2b,m(nr_A-a,nr_B+b)} + Io_{nr_A,nr_B,m(nr_A,nr_B)} \cdot P_{nr_A,nr_B,m(nr_A-a,nr_B+b)}$$

(6.6)

$$I_{nr_A+a,nr_B-b} = Io_{nr_A+a,nr_B-b,m(nr_A+a,nr_B-b)} + Io_{nr_A+2b,nr_B-2a,m(nr_A+2a,nr_B-2b)} \cdot P_{nr_A+2a,nr_B-2b,m(nr_A+a,nr_B-b)} + Io_{nr_A,nr_B,m(nr_A,nr_B)} \cdot P_{nr_A,nr_B,m(nr_A+a,nr_B-b)}$$

(6.7)

Where Io is the area without overlap or unbiased area, I the observed area in the spectrum at a given number of repeat units, and P the percentage relative to the most-abundant peak of the corresponding isotope distribution. The number of repeat units (nr_A, nr_B) indicates the isotopic distribution, whereas the mass $m(nr_A, nr_B)$ indicates the position of the most-abundant isotope peak used to calculate the percentage P. The percentage P is expressed as the percentage relative to the most-abundant isotope of the corresponding isotope distribution. The numbers a and b are integers, corresponding to the nearest neighboring isotopes relative to nr_A and nr_B. In order to compute the percentage P, the theoretical isotope distribution is used[1]. The outcome of the theoretical isotope distribution is a discrete set of probabilities corresponding to exact masses with a mass interval depending on the nature of the isotopes. Each peak mass of the isotope distribution corresponds to such an exact mass. In the simulation of the isotope pattern, shown in Figure 6-2, instrumental broadening is taken into account. The broadening can be assumed to be identical for the entire

isotope distribution. Therefore, the areas in Figure 6-2 are directly related to the outcome of the theoretical isotope distribution. As long as we express the intensities of isotopes relative to the most-abundant isotope, the outcome of the theoretical isotope calculations is already a percentage (*P)*.

After writing the *Io* 's explicitly the following equation is obtained:

$$Io_{nr_A,nr_B} = \frac{\left(-1-P1-P2-P2\cdot P1\right)\cdot I_{nr_A,nr_B} + \left(P2\cdot P1+P1\right)\cdot I_{nr_A-a,nr_B+b} + \left(P2\cdot P1+P2\right)\cdot I_{nr_A+a,nr_B-b}}{-1-P1+P1\cdot P3-P2-P2\cdot P1+P3\cdot P2\cdot P1+P2\cdot P4+P2\cdot P4\cdot P1} \quad \textbf{(6.8)}$$

Where:

$P1 = P_{nr_A-a,nr_B+b,m(nr_A,nr_B)}$, $P2 = P_{nr_A+a,nr_B-b,m(nr_A,nr_B)}$, $P3 = P_{nr_A,nr_B,m(nr_A-a,nr_B,nr_B+b)}$ and

$P4 = P_{nr_A,nr_B,m(nr_A-a,nr_B,nr_B+b)}$

Note, that the integration limits of the overlapping peaks (Figure 6-2) are not exactly the same, as can be seen from the position of the peak maximum (all peaks have exactly the same width, thus a change of the position of the peak maximum is related to a corresponding change of the integration limits). The peak $P_{nr_A-a,nr_B+b,m(nr_A,nr_B)}$ is slightly shifted to the left, whereas $P_{nr_A+a,nr_B-b,m(nr_A,nr_B)}$ is slightly shifted to the right. This shift is due to the exchange of hydrogen atoms with a carbon atom. The mass difference between one C_{12} and twelve H_1 atoms is smaller then 0.1 amu and, hence, the error of not taking the same integration limits around the individual isotopes can be neglected. The result for the corrections can be found in table 15.

Table 15 The isotope distributions of a given number of styrene units and isoprene units were summed according to a theoretical intensity distribution. After the summation, the observed intensities were corrected for the overlap of isotopes. The relative difference of the observed and theoretical intensities is shown.

Peak	Theoretical Intensity	Error[#] (%)	Error after correction (%)
$PS_{13}IP_{38}$	0.0073	1.8	0.3
$PS_{15}IP_{35}$	0.0184	1.2	1.2
$PS_{17}IP_{32}$	0.0312	2.0	1.5
$PS_{19}IP_{29}$	0.0358	0.0	1.6
$PS_{21}IP_{26}$	0.0276	5.2	0.9
$PS_{23}IP_{23}$	0.0144	14.3	1.8
$PS_{25}IP_{20}$	0.0051	27.1	7.8
Summed intensity	0.140	0.144	0.141

The observed intensity increases due to the overlap of isotopes. The intensity is normalized by peak height, whereas the intensity of the correction method is not normalized.

6.2.5 Isotope broadening

Isotope distributions become broader with increasing mass. The relative contribution of the most-abundant isotope, with respect to the total area of the isotope distribution, decreases with increasing mass. Therefore we introduce the isotope-broadening correction factor (IBC). The computation of the isotope distributions has been based on the work of Yergey[1].

$$IBC_{nr_A,nr_B} = \frac{\sum_{m_{abd}=-0.5}^{m_{abd}=+0.5} p_{nr_A,nr_B}(m)}{\sum_{nr_A=0}^{nr_{A\max}} \sum_{nr_B=0}^{nr_{B\max}} \sum_{m_{\min}}^{m_{\max}} p_{nr_A,nr_B}(m)} \qquad \textbf{(6.9)}$$

Where IBC_{nr_A,nr_B} is the normalized isotope-broadening correction factor, $p_{nr_A,nr_B}(m)$ is the theoretical isotope intensity at mass m, m_{abd} is the mass of the most-abundant isotope, and $m_{\min}$ and $m_{\max}$ are the lower and upper limit masses of the isotope distribution $p_{nr_A,nr_B}(m)$ respectively.

After correcting the intensity for peak-shape differences, overlapping isotopes, and isotope broadening we plot nr_A, nr_B and Ic_{nr_A,nr_B} as a quasi 3D plot[2-5] or as a two-dimensional contour plot[6]. The latter representation is easier to interpret and is called a "copolymer fingerprint"[7].

6.3 *Copolymer fingerprints*

Copolymer fingerprints are two-dimensional graphical representations of three dimensions (number of repeat units *A*, number of repeat units *B,* and the intensity). These graphical representations, so-called contour plots, directly reveal information on the polymer architecture, as will be discussed later.

The methods described in section 6.2.4 correct the observed intensity for isotope overlap and subsequently compute the intensity matrix. However, the method of isotope overlap requires prior knowledge on the position of the interfering isotope distributions. Equation (6.8) requires the integers *a* and *b*, i.e. the corresponding position of the nearest neighboring isotopes, to be known. The next section describes a method to predict these integers. With these predictions, the observed intensity can be corrected directly. Hence, the intensity matrix can be computed without the need of any prior knowledge on the position of the nearest neighboring isotopes.

6.3.1 Isotope overlap and isotope interference

In copolymer systems different combinations of repeat units *A* and *B* can result in nearly the same mass. Let us assume a copolymer system where the observed mass (m_{obs}) can be constructed (m_{calc}) from only two combinations of repeat units A and B. Both combinations, nr_{A1}, nr_{B1} and nr_{A2}, nr_{B2}, meet the criterion of $|m_{obs} - m_{calc}| \leq \Delta m$. The given mass interval, Δm, is determined by the instrument performance (normally, Δm <1.0 amu). The observed mass (m_{obs}) always refers to the *most-abundant isotope*. When two (or more) combinations of repeat units meet the criterion $|m_{obs} - m_{calc}| \leq \Delta m$, isotope interference occurs. *Isotope interference* can be defined as:

> Two (or more) combinations of repeat units with a corresponding most-abundant-isotope-mass difference smaller than Δm.

If the difference between the most abundant isotopes does not meet the criterion for isotope interference, but is within the range of the isotope width, other peaks may overlap with the most abundant isotope. If in this case the entire width of the isotope distribution is taken into account, combinations of nr_{A1}, nr_{B1} and nr_{A2}, nr_{B2} can be found that meet the criterion of $|m_{obs} - m_{calc}| \leq \Delta Im$, where ΔIm is the width of the isotope pattern. *Isotope overlap* can be defined as:

> Two (or more) combinations of repeat units resulting in isotope distributions where the most-abundant isotope of one distribution overlaps with a peak from the other distribution. The mass difference between the most-abundant peaks of the overlapping distributions is smaller than the width of the isotope pattern (ΔIm).

In principle, the problems of isotope interference and isotope overlap are related. Mathematically, isotope overlap is a simple form of isotope interference. Therefore, isotope overlap will be discussed first.

To illustrate the problem of isotope overlap we assume a situation as shown in Figure 6-3. We assume a narrow chemical-composition distribution the sample only consists of two polymer chains. The width of both isotope distributions equals 11 amu (ΔIm) and the mass difference of the polymer chains ($m(nr_A, nr_B) - m(nr_A - \Delta nr_A, nr_B + \Delta nr_B)$) is 2 amu.

In total six different combinations of repeat units nr_A and nr_B can be assigned that meet the criterion of isotope overlap. This multiple peak assignment leads to overlap of the

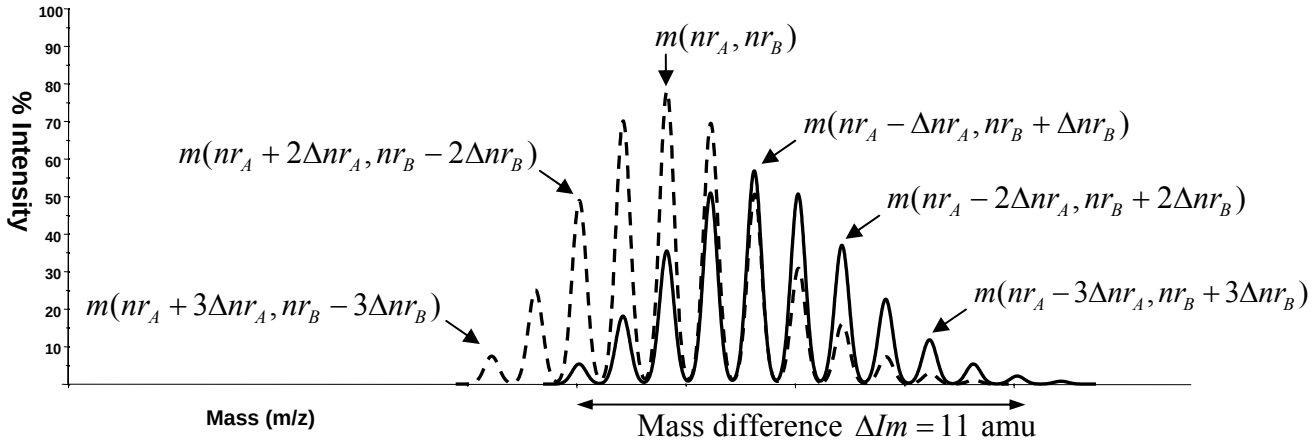

Figure 6-3 The simulated isotopic distribution of two polymer chains showing isotope interference. In total six different combinations of repeat units nr_A and nr_B could be assigned to the peaks of the two polymer chains. This multiple assignment leads to overlap of the contour plots.

contour plots (Figure 6-4). The method developed in section 6.2.4, to correct for overlapping isotopes, requires the values of Δnr_A and Δnr_B to be known. The following sections explain the complicated relation between Δnr_A and Δnr_B.

6.3.2 Calculation of Δnr_A and Δnr_B for isotope overlap

The problem of isotope overlap, also known as multiple peak assignment, has been addressed by Wilczek-Vera et al.[3] who proposed the following relationship:

$$\left|\frac{nr_{A1} - nr_{A2}}{nr_{B1} - nr_{B2}}\right| = \frac{m_B}{m_A} \text{ or } \left|\frac{\Delta nr_A}{\Delta nr_B}\right| = \frac{m_B}{m_A} \qquad \textbf{(6.10)}$$

Where m_A and m_B are the masses of the repeat units *A* and *B* respectively.

A graphical representation of isotope overlap is shown in Figure 6-4. The intensity matrix is depicted as small black spots on the left side of the figure. If a square around each black spot was filled with a color indicating its observed intensity, a contour plot is obtained. The solid line in this figure represents all solutions of nr_A and nr_B for a given m_{obs}, whereas the dashed lines represent the error intervals. The black spots represent the integer combinations of nr_A and nr_B. Figure 6-4 shows two data points within the error intervals, i.e. two combinations of nr_A, nr_B satisfy the criterion of $|m_{obs} - m_{calc}| \le \Delta Im$.

Strictly speaking, equation (6.10) is only valid when three out of the four variables $nr_{A1}, nr_{A2}, nr_{B1}, nr_{B2}$ are integers. If integer values are chosen for nr_{A1}, nr_{B1} and nr_{A2} then the value

of nr_{B2} cannot be an integer, as long as m_B/m_A is not an exact multiple (which is highly unlikely). In the following text non integers are marked with a capital *N*.

Equation (6.10) requires a given Δnr_A and Δnr_B. However, to minimize the number of input parameters, it would is attractive if Δnr_A and Δnr_B can be calculated out of any combination of repeat units *A* and *B* $\left(nr_A, nr_B\right)$. Starting from an arbitrary position in the contour plot of Figure 6-4, let nr_{A1}=0 and nr_{B1}=0. At a given nr_{A2} the corresponding Nr_{B2} follows from the equation of the solid line in Figure 6-4. The masses of both positions are exactly the same:

$$nr_{A1} \cdot m_A + nr_{B1} \cdot m_B = nr_{A2} \cdot m_A + Nr_{B2} \cdot m_B \qquad \textbf{(6.11)}$$

Taking the starting position into account (nr_{A1}=0 and nr_{B1}=0) the second index can be left out ($nr_{A2} = \Delta nr_A$, $Nr_{B2} = \Delta Nr_B$) and equation (6.11) can be rewritten as:

$$\Delta Nr_B = \frac{\Delta nr_A \cdot m_A}{-m_B} \qquad \textbf{(6.12)}$$

Equation (6.12) can be used to calculate the value of ΔNr_B, but it cannot be used to compute m_{calc} since m_{calc}, represents the mass of a polymer chain constructed from an integer number of repeat units. Figure 6-4 illustrates when the nearest integer value of ΔNr_B is within the criterion of $\left|m_{obs} - m_{calc}\right| \leq \Delta Im$.

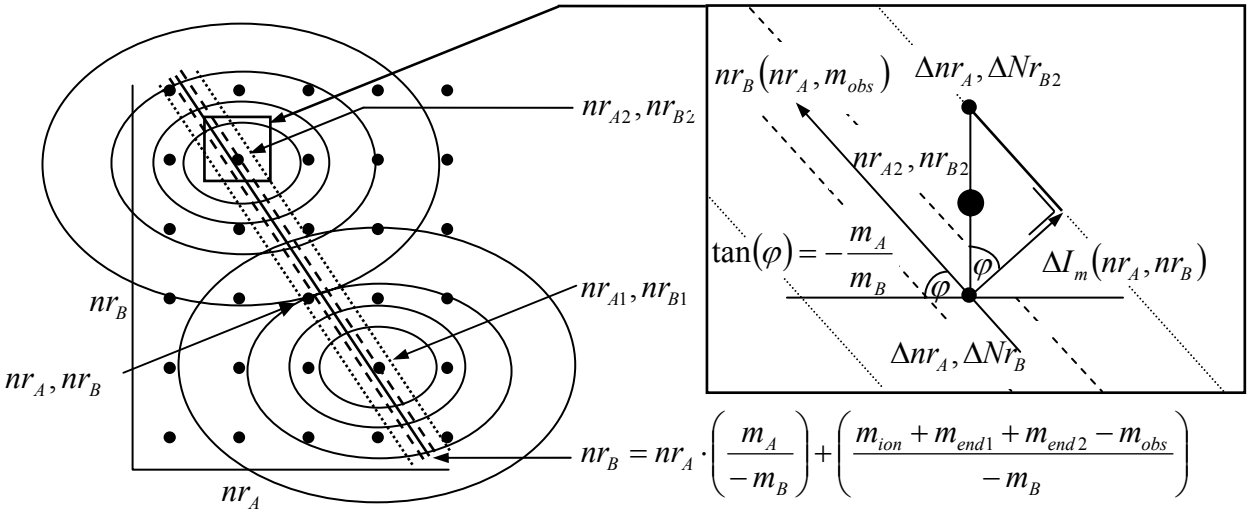

Figure 6-4 The solid line presents all possible solutions for nr_B as function of nr_A with a constant mass. The dashed lines present the upper and lower limits of a given mass interval. This 2D contour plot visualizes the *isotope interference* of the combinations of repeat units nr_{A1}, nr_{B1} and nr_{A2}, nr_{B2}. Although the two combinations have a completely different composition, their mass difference is less then Δm, thus one observed intensity is assigned to two positions of the intensity matrix. Since the ellipse connects all data points with equal intensities, the isotope interference leads to contour overlap as seen at the position of nr_A, nr_B. A smaller radius indicates a higher intensity. The dotted lines represent the upper and lower limits of the isotope width interval (ΔIm) indicating *isotope overlap*, i.e. the position of nr_{A1}, nr_{B1} and nr_A, nr_B will show isotope overlap.

The right side of Figure 6-4 shows an enlarged part of the intensity matrix. The big black spot represents the position of a combination of integer values (nr_{A2}, nr_{B2}). Two other (smaller) black spots are indicated as $\Delta nr_A, \Delta Nr_B$ and $\Delta nr_A, \Delta Nr_{B2}$ representing two non integer values, ΔNr_B and ΔNr_{B2}, for the same Δnr_A. The difference between ΔNr_B and ΔNr_{B2} depends on ΔIm. ΔIm represents the width of the isotopic pattern and is perpendicular to the line representing all solutions of nr_A and nr_B of a given observed mass $nr_B(nr_A, m_{obs})$. Note that ΔIm is expressed in mass (amu) whereas the arrow in Figure 6-4 is expressed in terms of nr_A and nr_B. Therefore ΔIm is written in terms of ΔNr_A and ΔNr_B:

$$\Delta I_m(\Delta Nr_A, \Delta Nr_B) = \sqrt{\frac{(\Delta Im)^2}{(m_A{}^2 + m_B{}^2)}} \qquad \textbf{(6.13)}$$

where ΔI_m is expressed in terms of ΔNr_A and ΔNr_B and no longer in mass units. The $\cos(\varphi)$ in the triangle shown in Figure 6-4 leads to the following relation for Nr_{B2}:

$$\Delta Nr_{B2} = \Delta Nr_B \pm \frac{\sqrt{\frac{(\Delta Im)^2}{\left(m_A{}^2 + m_B{}^2\right)}}}{\cos\left(a\tan\left(-m_A/m_B\right)\right)} \qquad \textbf{(6.14)}$$

Note that the difference between ΔNr_{B2} and ΔNr_B is constant. Substituting equation (6.12) into (6.14)gives:

$$\Delta Nr_{B2} = \Delta nr_A \cdot \left(\frac{m_A}{m_B}\right) \pm \frac{\sqrt{\frac{(\Delta Im)^2}{\left(m_A{}^2 + m_B{}^2\right)}}}{\cos\left(a\tan\left(-m_A/m_B\right)\right)} \qquad \textbf{(6.15)}$$

In Figure 6-4 the position of nr_{A2}, nr_{B2} is located above $\Delta nr_A, \Delta Nr_B$ but it can also be located below $\Delta nr_A, \Delta Nr_B$, indicated by the $\pm$ sign in equation (6.15).

The positions of ΔNr_B and ΔNr_{B2} can be calculated as a function of Δnr_A. If an integer exists within the range $\Delta Nr_B \pm \left(\Delta Nr_{B2} - \Delta Nr_B\right)$ for a given Δnr_A, then the number of repeat units that can be exchanged equals Δnr_A or, as can be seen in Figure 6-4, $nr_{A1} - nr_{A2} = \Delta nr_A$. To test whether an integer value is present in the range $\Delta Nr_B \pm \left(\Delta Nr_{B2} - \Delta Nr_B\right)$ the following inequality applies:

$$\frac{MOD\left(\left(\Delta nr_A \cdot \left(\frac{m_A}{m_B}\right) + \frac{\sqrt{\frac{(\Delta Im)^2}{\left(m_A{}^2 + m_B{}^2\right)}}}{\cos\left(a\tan\left(-m_A/m_B\right)\right)}\right),1\right) - MOD\left(\left(\Delta nr_A \cdot \left(\frac{m_A}{m_B}\right) - \frac{\sqrt{\frac{(\Delta Im)^2}{\left(m_A{}^2 + m_B{}^2\right)}}}{\cos\left(a\tan\left(-m_A/m_B\right)\right)}\right),1\right)}{2 \cdot \frac{\sqrt{\frac{(\Delta Im)^2}{\left(m_A{}^2 + m_B{}^2\right)}}}{\cos\left(a\tan\left(-m_A/m_B\right)\right)}} \neq 1 \qquad \textbf{(6.16)}$$

With $m_B > m_A$, $0 < \frac{\sqrt{\frac{(\Delta Im)^2}{\left(m_A{}^2 + m_B{}^2\right)}}}{\cos\left(a\tan\left(-m_A/m_B\right)\right)} < \frac{m_A}{m_B}$, where Δnr_A is a number of integer values of repeat units A and MOD the modulo. The integer value of Δnr_B for the given Δnr_A can be calculated from:

$$\Delta nr_B = INT\left(\left|\Delta nr_A \cdot \left(\frac{m_A}{m_B}\right)\right| + \frac{\sqrt{\frac{(\Delta Im)^2}{\left(m_A^{\,2} + m_B^{\,2}\right)}}}{\cos\left(a\tan\left(-m_A/m_B\right)\right)}\right) \qquad \textbf{(6.17)}$$

Finally, the width of Δnr_A depends on the ratio m_A/m_B and on the width of the isotope pattern (ΔIm). Under normal MALDI-TOF-MS conditions the accuracy of the acquired spectra is greater than the mass difference of two consecutive isotopes. Therefore, the isotope overlaps are the result of the existence of isotope distributions, as long as m_A/m_B is not an exact multiple. In systems where m_A/m_B is an exact multiple, Δnr_A is solely determined by the ratio m_A/m_B. This is due to the fact that the exchange of Δnr_A for Δnr_B with exactly the same mass is not affected by the accuracy of the measurement and, therefore, equation (6.14) is not valid.

To conclude, Δnr_A can be exchanged for a certain Δnr_B resulting in nearly the same m_{calc}. Hence, isotope overlap occurs. At such a value of m_{calc} the measured intensity equals the summed intensity of the two isotope distributions. With the use of equations (6.17) and (6.16) all solutions for Δnr_A and Δnr_B can be calculated in order to locate their overlapping masses. After obtaining the solutions for Δnr_A, the occurrence of isotope overlap can be verified, starting from the most abundant peak in the entire spectrum. In case no overlap of isotopes is observed, the chemical composition is either narrow enough to prevent overlap or one of the two combinations nr_A, nr_B is very weak in intensity.

6.3.3 Calculation of Δnr_A and Δnr_B for isotope interference

To calculate Δnr_A and Δnr_B for isotope interference the same method is used as for isotope overlap, except that ΔIm is replaced by Δm. The accuracy of Δm is set at a typical value of ± 0.5 amu. Normally, after calculating Δnr_A and Δnr_B, the areas of the most-abundant peak of the isotopic patterns can be used in equation (6.8) to correct for the isotope interference. Unfortunately there is a subtle difference between isotope overlap and isotope interference. As mentioned at the end of section 6.2.4, the difference between integration limits for the isotope overlap caused by the exchange of twelve hydrogen atoms for one carbon atom can be neglected. In case of isotope interference, the integration limits are different. For example, 17 units of styrene or 26 units of isoprene result in nearly the same mass (Figure 6-5) but the isotope distributions are shifted by approximately 0.5 amu, which complicates further calculations.

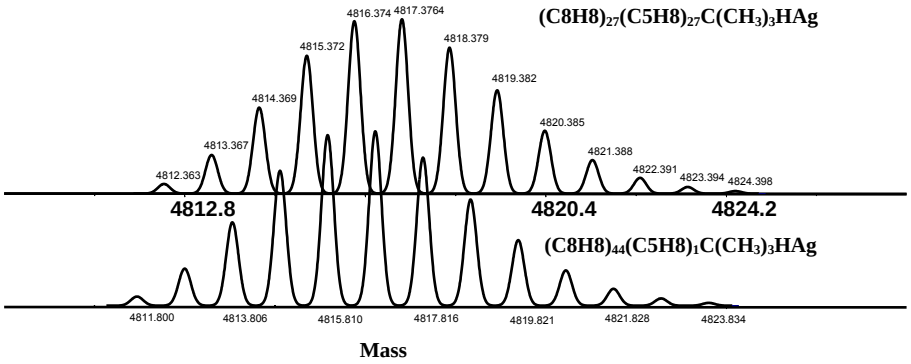

Figure 6-5 The figure above shows two simulated spectra of styrene and isoprene with only 0.5 amu mass difference.

Therefore, we developed a method to correct for this variation in integration limits. The shape of a single isotope peak can be described by a normal (Gaussian) distribution. If two isotope distributions interfere, the outcome of the MALDI-TOF-MS measurement will be the sum of the individual isotopic distributions. Therefore the observed intensity can be written, for any mass, as the sum of two Gaussian distributions.

$$I(m) = \frac{A}{\sqrt{2\cdot\pi}\cdot\sigma}\cdot\exp\left(-\frac{(\mu_1 - m)^2}{2\cdot\sigma^2}\right) + \frac{1}{\sqrt{2\cdot\pi}\cdot\sigma}\cdot\exp\left(-\frac{(\mu_2 - m)^2}{2\cdot\sigma^2}\right) \qquad \textbf{(6.18)}$$

Where A is the ratio of the two peaks, μ_1 and μ_2 are the corresponding masses of the most abundant isotopes, σ the standard deviation of the isotope peak, m the mass and I the observed intensity. The mass difference of $\mu_1 - \mu_2$ can be calculated from the mass difference (Δm) of the most abundant theoretical isotopic distributions:

$$\mu_1 = \mu_2 + \Delta m \qquad \textbf{(6.19)}$$

Although the exact masses of the mean values μ_1 and μ_2 can be predicted, there is always an error in the measurement. Moreover, the mass of the observed most-abundant isotope does not correspond exactly to μ_1 or μ_2, since it depends on the ratio of the two peaks of the isotope distributions. To overcome this problem we use the "least-squares" method to find the value of A. The observed (integrated) intensity is given by:

$$Ic(nr_A, nr_B) = \frac{I(nr_A, nr_B)}{1 + A} \qquad \textbf{(6.20)}$$

Where Ic is the corrected intensity of a system subject to isotope interference.

So far, ultimately, all described methods serve the same purpose: i.e. to obtain the corrected intensity matrix, $Ic(nr_A, nr_B)$. Normally the observed intensity corresponds to only one combination of repeat units and thus to only one position of the intensity matrix. However, an observed intensity is, after correction, still stored at all positions (combination of repeat units A and B) in the matrix that meet the criterion of equation (6.2). This results always in multiple contours of the contour plot, as depicted in Figure 6-4.

A criterion to determine which of these contours represent the "true" contours and which the so-called "ghost" contours, can be derived from the estimated chemical composition.

6.3.4 Estimating the chemical composition.

Although the "true" contours in the copolymer fingerprint have not been located yet, the shape already reveals whether the observed copolymer is block-like or more random. The procedure for estimating the chemical composition requires an initial assumption on whether the copolymer is block-like or random. Mathematics will verify retrospectively whether the correct initial assumption was made.

Random copolymers

The average composition of a random copolymer can be estimated using the top-to-top approach. This approach uses the most abundant peak in the intensity matrix as the starting position at $nr_A = 0$ and $nr_B = 0$ (Since the actual values are not relevant here, the starting positions of nr_A and nr_B, are set to zero). Figure 6-6 shows the graphical representation of the top-to-top approach. The black square in this figure is the starting position. A growing polymer chain at the starting position can either react with repeat unit A or with repeat unit B. Only the highest observed intensity at position $nr_A = +1$ or $nr_B = +1$ is added to the total intensity of A $\left(\sum I_A\right)$ or to the total intensity of B $\left(\sum I_B\right)$. The $nr_A = +1$ (and $nr_B = +0$) or $nr_B = +1$ (and $nr_B = +0$) forms the new starting position, from which the process is repeated. At the end of the matrix (the dimensions of the matrix corresponds with the outer limits of the spectra to avoid unnecessary adding noise to the matrix) the entire process is repeated towards the lower mass starting again from the zero position. Thus, in the top-to-top approach, the tops of the contour plot are used to calculate the estimated average composition $(comp_{est})$ based on numbers of repeat units.

$$comp_{est} = \frac{\sum I_A}{\sum I_A + \sum I_B} \qquad \textbf{(6.21)}$$

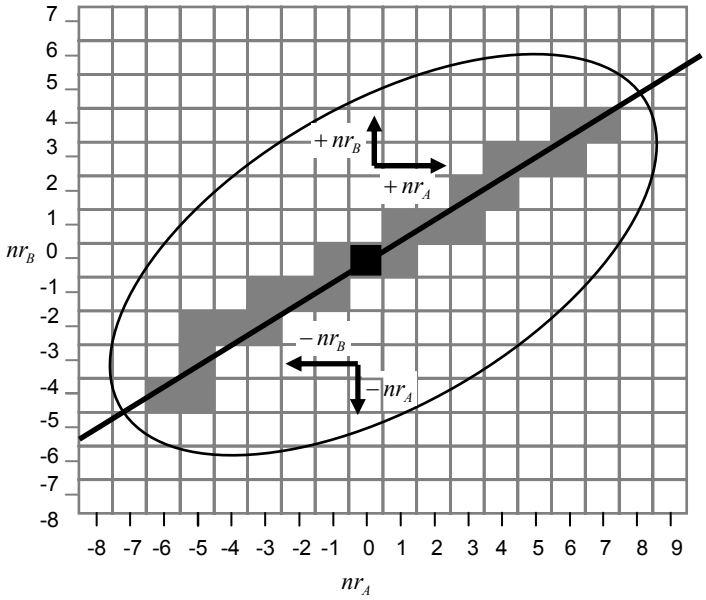

Figure 6-6 Schematic representation of only the most-abundant intensities (gray squares) of a contour plot. All combinations of nr_A and nr_B are contained within the ellipse. The slope of the solid line is related to the composition. "Walking" along the path of gray squares appears in the spectrum like "jumping" from top-to-top.

Although the obtained average chemical composition is not very precise, it is a good criterion to rule out the so-called "ghost" contour plots. The solid line in Figure 6-6 represents the ratio nr_B / nr_A, which is related to the chemical composition. In truly random copolymers the average chemical composition is constant throughout the polymerization if no composition drift occurs. In case composition drift does occur, broadening of the chemical-composition distribution will be observed. This, however, hardly affects the approximately linear relationship between nr_A and nr_B. Normally the estimated average chemical composition is accurate enough to reject the ghost contour plots.

If the average chemical composition is obtained, then the following line can be drawn in the contour plot.

$$nr_B = nr_A \left(\frac{1}{Comp_{est} + 1} \right) \qquad \textbf{(6.22)}$$

The contour which is best described by equation (6.22) is used for further calculations.

Block copolymers

The procedure to estimate the average composition for a block copolymer is similar to the one for a random copolymer. In contrast to a random copolymer, a growing polymer chain of a block copolymer can only add one kind of repeat unit. Starting again from the most-abundant peak in the intensity matrix, represented by the black square in Figure 6-7, two block lengths can be found.

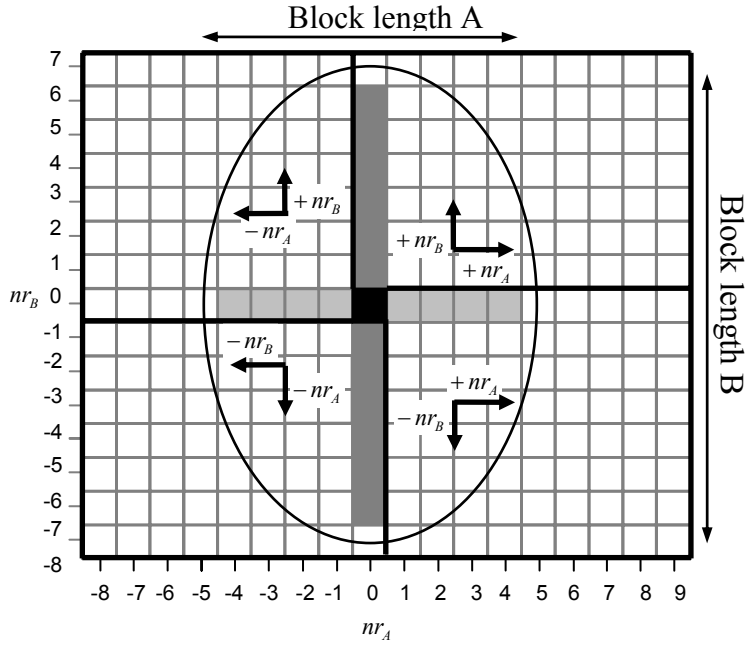

Figure 6-7 Schematic representation of only the most-abundant intensities (gray squares) of a contour plot of a block copolymer. All combinations of nr_A and nr_B are contained within the ellipse. The light-gray squares represents block A, the dark-gray squares represent block B.

In this case the summed intensities bear no relation with the chemical composition. In other words, the relationship between the repeat units *A* and *B* is not determined by kinetics or thermodynamics. Moreover, the block lengths are related to the chemical composition as shown in Figure 6-8 in the following manner. Imagine a homopolymer A with three different block lengths $\Delta A1$, $\Delta A2$ and $\Delta A3$. In the second step, block copolymers are obtained with different block lengths of $\Delta B1$, $\Delta B2$ and $\Delta B3$ and coupled to block A. In total nine combinations can be created. We assume that the relation between molar mass and chain length is comparable for both blocks. A higher molar mass, obviously, corresponds to a greater block length. A greater block length corresponds to a larger average number of repeat units. In this way, the block length can be related to the number of repeat units. Since the (average) ratio of repeat units *A* and *B* is related to the chemical composition, the relative block lengths are as well. Figure 6-8 shows different contour plots for blocks with different block lengths. The solid line presents the ratio of block lengths $(\Delta B/\Delta A)$. The slope is related to the chemical composition. The following relationship is proposed:

$$Comp_{est} = \frac{\Delta A}{\Delta A + \Delta B} \qquad \textbf{(6.23)}$$

Where ΔA, and ΔB are the (maximum) length of the blocks in term of repeat units and $Comp_{est}$ is the average chemical composition.

The methods developed so far, were used to estimate the average chemical composition for random and block copolymers. The two developed methods suffice to obtain a sufficiently reliable average chemical composition to rule out the ghost peaks in the contour plots. The other topologies, such as gradients, grafts, etc. can be classified in terms of "random-like" or more "blocky-like".

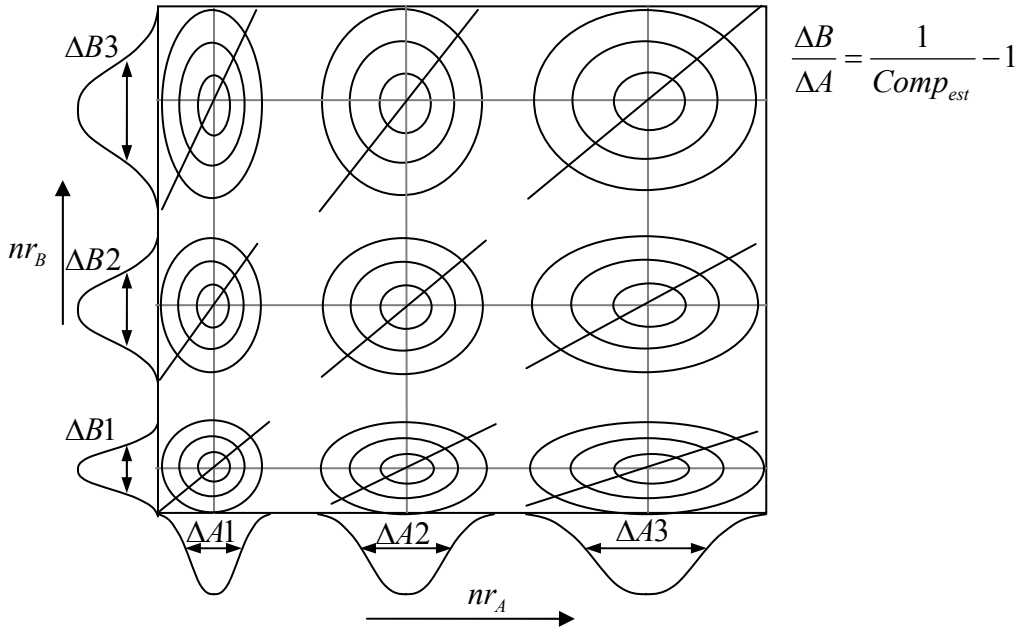

Figure 6-8 Schematic representation of the relationship between block length and chemical composition. The slope of the solid lines or the block-length ratio $(\Delta B/\Delta A)$ is directly related to the

After the "true" contour plot is obtained, the characteristics of the copolymer fingerprints will help us to obtain information on the polymer topology.

6.4 *characteristics of copolymer fingerprints*

Before discussing the characteristics of copolymer fingerprints, the characteristics of copolymers themselves should be understood, starting with a simple case, i.e. a block copolymer.

6.4.1 Block copolymers

A block copolymer can be characterized by the block lengths, which can be easily obtained from the contour plot. The individual block-length distributions are the projection on the nr_A-axis and nr_B-axis for blocks A and B, respectively.

$$BLD_A(nr_A) = \sum_{nr_B} Ic_{nr_A,nr_B} \text{ and } BLD_B(nr_B) = \sum_{nr_A} Ic_{nr_A,nr_B} \quad \textbf{(6.24)}$$

Where BLD is the block length distribution and Ic_{nr_A,nr_B} the corrected observed intensity.

If the random-coupling hypothesis holds, then the copolymer fingerprint can be interpreted as the product of the two block-length distributions. This criterion is used to distinguish between random and block copolymers and verifies whether the correct initial assumption was made to estimate the average composition. The correlation coefficient of a block, R_B, is defined as:

$$R_B{}^2 = \frac{\sum\left(\left(BLD_A(nr_A)\cdot BLD_B(nr_B) - \overline{BLD_A(nr_A)\cdot BLD_B(nr_B)}\right)\left(Ic_{nr_A,nr_B} - \overline{Ic}_{nr_A,nr_B}\right)\right)}{\sqrt{\sum\left(BLD_A(nr_A)\cdot BLD_B(nr_B) - \overline{BLD_A(nr_A)\cdot BLD_B(nr_B)}\right)^2 \sum\left(Ic_{nr_A,nr_B} - \overline{Ic}_{nr_A,nr_B}\right)^2}} \quad \textbf{(6.25)}$$

Where $R_B{}^2 = 1$ corresponds to a perfect block copolymer.

Even if the random-coupling hypothesis does not hold, the product of the two block-length distributions will still give a higher correlation coefficient (for a block copolymer) than the random copolymer test described below.

6.4.2 Random copolymers

As long as no composition drift occurs, a random copolymer can be characterized by a constant composition along the chain-length distribution. To plot the composition versus the chain length, a transformation of the intensity matrix is needed.

It is not correct to calculate the composition and chain length directly from the intensity matrix, because of the non-linear spacing of the composition curves versus the number of repeat units. The number of repeat-unit combinations having a composition between, for example, 50% ±0.5%, up to 100 repeat units equals 200, whereas for a composition of 35% ±0.5% this equals 92. The relationship between composition and the number of repeat-unit combinations is shown in Figure 6-9. A bin size of one (a finite element of given dimensions, in this example one percent by one repeat unit) does not contain equivalent number of combinations of the repeat units *A* and *B* at different compositions.

Figure 6-9 The counts present the number of repeat-units combinations that were found within the bin size of one percent with a maximum of 100 repeat units. The irregular relation between the composition and the number of counts makes the direct transformation not suitable. Note that this curve is perfectly symmetrical around the 50 % composition.

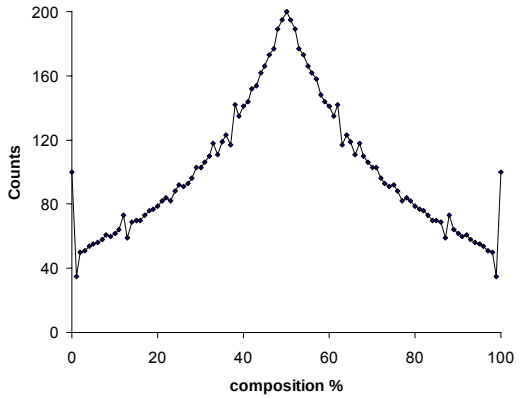

The correct transformation of the intensity matrix is obtained using the principle of latent variables. Given a set of *p* variables, s smaller number of new variables are constructed that describe as much of the information as possible (in statistical terms: as much variance as possible). New variables are constructed in such a way that each of them contains unique information. The result will be a set of uncorrelated or orthogonal variables. Note that for block copolymers the axes are already orthogonal and, hence, this transformation is not needed.

If the composition is chosen to be the new latent variable (C) , the second variable (D) must be oriented perpendicular to the composition axis to obtain an orthogonal system. The composition can be described as function of the number of repeat units (nr_A and nr_B) in the contour plot as:

$$nr_B = nr_A \cdot \gamma + C \qquad \textbf{(6.26)}$$

and the orthogonal axis becomes:

$$nr_B = \frac{-nr_A}{\gamma} + D \qquad \textbf{(6.27)}$$

where γ is the slope, which can be calculated from the average composition. In order to understand of the transformed intensity matrix, we recall the relationship between composition and chain length as given by the Stockmayer equation[8].

The Stockmayer equation describes the instantaneous relation between composition and chain length, with the assumption that the reactivity of radicals depends only on the nature of the reactive end, and with the kinetic effects of initiation and termination being neglected.

$$n(L,y)dLdy = \left(\exp\left(\frac{-L}{\lambda}\right)\cdot\frac{L}{\lambda}\cdot dL\right)\cdot\left(\sqrt{\frac{L}{2\cdot\pi\cdot\overline{C}_{ave}\cdot\left(1-\overline{C}_{ave}\right)\cdot\kappa}}\cdot\exp\left(\frac{-L\cdot y^2}{2\cdot\overline{C}_{ave}\cdot\left(1-\overline{C}_{ave}\right)\cdot\kappa}\right)\cdot dy\right) \quad \textbf{(6.28)}$$

$$\kappa = \sqrt{1-4\cdot\overline{C}_{ave}\cdot\left(1-\overline{C}_{ave}\right)\cdot\left(1-r_1\cdot r_2\right)} \quad \textbf{(6.29)}$$

$$y = \underline{C} - \overline{C}_{ave} \quad \textbf{(6.30)}$$

where $\overline{C}_{ave}$ is the average overall composition, λ the degree of polymerization, r_1 and r_2 are the reactivity ratios, y is the composition deviation, $\underline{C}$ the composition of an individual chain, and $w(L,y)$ the weight fraction of polymers of equal weight with lengths between L and $L+dL$ and composition deviations between y and $y+dy$. The chain length can be written as a function of C and D (see appendix 6A)

$$L = nr_A + nr_B = \frac{C - C\cdot\gamma + D\cdot\gamma + D\cdot\gamma^2}{1+\gamma^2} \quad \textbf{(6.31)}$$

Where C is the composition deviation expressed in terms of nr_A and nr_B and D is a chain length deviation expressed as the sum of nr_B and $\gamma\cdot nr_A$. Rewriting the composition in terms of C and D (see appendix 6A) we obtain:

$$y = \frac{C\cdot\left(1+\gamma^2\right)}{\left((1+\gamma)\cdot\left(-C+\gamma\cdot C-\gamma\cdot D-D\cdot\gamma^2\right)\right)} \quad \textbf{(6.32)}$$

Substitution of the expressions for *y* and *L* into equation (6.28) gives the instantaneous distribution of chain compositions and chain lengths as function of *C* and *D*. When C is plotted versus D the "flame" contour plot is obtained as seen in Figure 6-10.

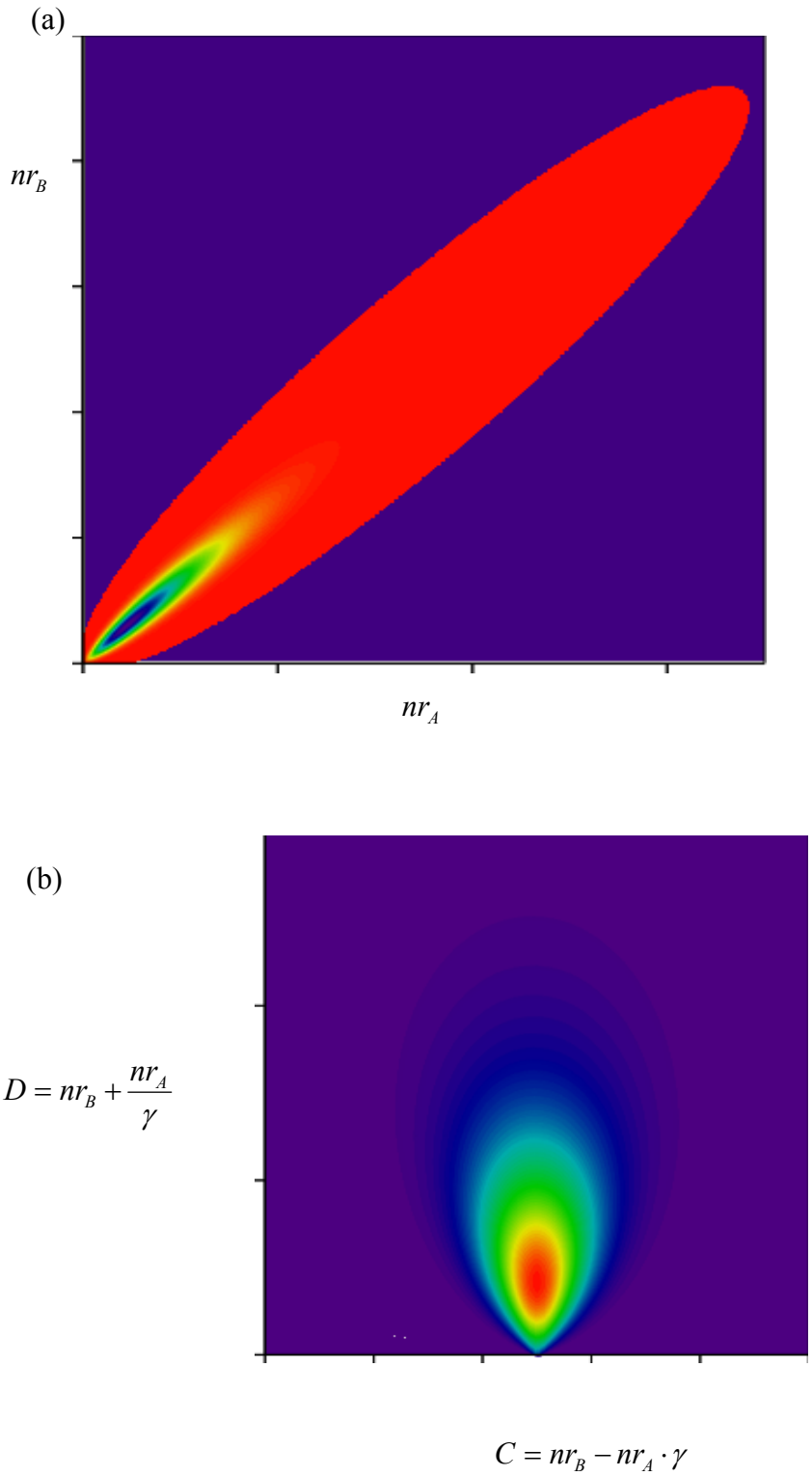

Figure 6-10 Figure (a) shows the conventional presentation of the contour plot. Picture (b) shows the "flame" contour plot with orthogonal axes. (r_1=0.8, r_2=1.1, $\overline{C}_{ave}$=0.6, λ=50)

We conclude from the graphs in Figure 6-10 that a fully random copolymer results in a perfectly symmetrical "flame" contour plot. The projection on the C-axis can be used to detect composition

drift. The projection of Figure 6-10b will result in a Gaussian distribution. Any asymmetry of this distribution can be directly related to composition drift. The asymmetry can be calculated from the second order moment of the distribution (appendix 6D). The projection on the C-axis represents the chemical-composition distribution and can be written in terms of nr_A and nr_B:

$$nr_A = \gamma \cdot \left(\frac{D_{\max} - C}{1+\gamma^2} \right) \text{ and } nr_B = \left(\frac{D_{\max} \cdot \gamma^2 + C}{1+\gamma^2} \right) \quad \textbf{(6.33)}$$

Where the highest intensity of both the projection on the C-axis and D-axis are denoted as $C_{\max}$ and $D_{\max}$ respectively.

The projection on the D-axis represents the chain length, which can be expressed in terms of nr_A and nr_B as well:

$$nr_A = \gamma \cdot \left(\frac{D - C_{\max}}{1+\gamma^2} \right) \text{ and } nr_B = \left(\frac{D \cdot \gamma^2 + C_{\max}}{1+\gamma^2} \right) \quad \textbf{(6.34)}$$

With the use of equations (6.33) and (6.34) the chemical-composition distribution (CCD) and the chain-length distribution (CLD) can be obtained by the following equations.

$$CCD(C) = \frac{nr_A}{nr_A + nr_B} = \frac{\gamma\left(D_{\max} - C\right)}{\gamma\left(D_{\max} - C\right) + \left(D_{\max} \cdot \gamma^2 + C\right)} \quad \textbf{(6.35)}$$

$$CLD(D) = nr_A + nr_B = \frac{\gamma\left(D - C_{\max}\right) + \gamma\left(D \cdot \gamma^2 + C_{\max}\right)}{1+\gamma^2} \quad \textbf{(6.36)}$$

The correlation coefficient of a random copolymer, R_R, is defined as:

$$R_{R^2} = \frac{\sum\left(\left(CCD(C) \cdot CLD(D) - \overline{CCD(C) \cdot CLD(D)}\right)\left(Ic_{C,D} - \overline{Ic}_{C,D}\right)\right)}{\sqrt{\sum\left(CCD(C) \cdot CLD(D) - \overline{CCD(C) \cdot CLD(D)}\right)^2 \sum\left(Ic_{C,D} - \overline{Ic}_{C,D}\right)^2}} \quad \textbf{(6.37)}$$

Where the $R_R{}^2 = 1$ corresponds to completely random.

In summary, various methods were discussed to correct the spectra to obtain the “true” contour plots, as well as ways in which the contour plots should be plotted (finger print, flame). In this way

a full CCD, CLD, or block-length distribution is the outcome of the developed program. The last item which will be discussed is end group determination.

6.5 *End-group analysis*

The entire data set cannot distinguish between end groups, as it results in complete overlap. To estimate the average composition, only the tops of the contour plot are used as described in section 6.3.4. This data set is very well suited for end-group determination. As discussed in section 5.1.2 the end-group-correlation function (ECF) is modified for copolymers and can be described by:

$$ECF(m_{end}) = \sum_{nr_{A_Min}}^{nr_{A_Max}} I\left(m_A \cdot nr_A + m_B \cdot nr_B + m_{ion} + m_{end}\right) \qquad \textbf{(6.38)}$$

The obtained spectrum for the ECF contains an acceptably low number of possible end-group masses, since the numbers of repeat units must meet the following criteria:

$$\left|Comp_{est} - Comp(nr_A, nr_B)\right| < \Delta Comp \qquad \textbf{(6.39)}$$

$$\left|m_{observed} - m_{calc}\left(nr_A, nr_B, m_{end}\right)\right| < \Delta m \qquad \textbf{(6.40)}$$

Where $\Delta Comp$ is the composition error of the estimate average composition (section 6.3.4), and Δm the accuracy, typically ± 0.5 amu.

For random copolymers, the entire set of the so-called “tops of the contour plot” can be used for the ECF. The ECF intensity is related to the probability of a particular end-group mass.

For block copolymers the “tops of the contour plot” exist of only one data point with a known estimated composition. This data point is located at the maximum intensity of block length A and block length B. Therefore all combinations of nr_A and nr_B that pass both criteria will result in the same ECF intensity or probability.

At this point the chemist has to reduce the remaining possible end-group masses. Note that once an end-group mass is assigned, end-group masses that differ by the mass of the repeated units cannot be distinguished from the previously assigned end-group mass.
After the end groups have been determined and the contour plots are made, the corresponding type of topology can be determined.

6.6 *Determining types of topology*

In this chapter the characteristics of the contour plots of block copolymers and random copolymers were discussed. The obtained contour plots have to meet the following criteria:

Random copolymer: The transformation of the contour plot into latent variables (C, D) results in results in a "flame" contour plot. The projection of the "flame" contour plot on the C and D axis is used to confirm the random-copolymer topology.

Block copolymers: For block copolymers, the relation between the number of repeat units and the composition is not known without any pre-knowledge. However depending on the relative lengths of the two blocks, a more circular or elliptical contour can be recognized in the contour plots. Projections of the contour plot on the number of repeat units *A* and *B*, is used to confirm the block topology.

Alternating copolymers: The chemical-composition distribution, obtained from the "flame" contour plot, is indicative for alternating copolymers, since an alternating copolymer has a very narrow chemical-composition distribution.

Gradient copolymer: A gradient copolymer can be characterized as the intermediate form of a random copolymer with a strong composition drift and a block copolymer. The asymmetry of the projections on the axis of the "flame" contour plot is used to confirm the gradient topology.

In conclusion, the methods described above help us to extract "hidden" information from complex spectra. Figure 6-11 shows the schematic overview of the followed procedure. Applications of these methods will be illustrated by the examples of copolymerization of styrene-isoprene and butadiene-styrene.

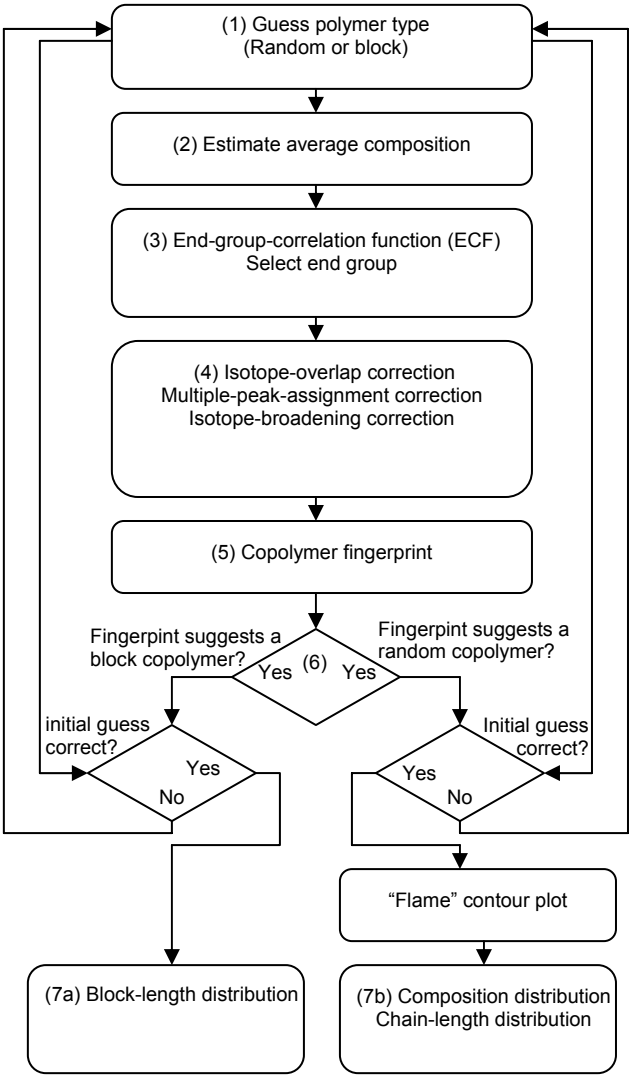

Figure 6-11 Schematic overview of all 7 steps to extract the information from the spectra.

6.7 *Polystyrene-co-isoprene*

Poly(styrene-*block*-polyisoprene) copolymer was prepared by anionic polymerization using *sec*-butyllithium as the initiator as described elsewhere[7]. Four samples were withdrawn from the reaction mixture after approximately 25, 50, 75, and 100% conversion of the isoprene monomer. The spectra can be found in appendix 6B.

The analysis will be discussed step by step as explained in Figure 6-11.

Step 1 As an initial guess a block copolymer was taken. In this case the type of polymer was already known.

Step 2 The initial compositions were calculated as described in section 6.3.4. The results are reported in appendix 6C.

Step 3 The next step is to decide which end-group mass is correct. All four samples were subjected to the ECF as can be seen in Table 18B (The results are listed in a table instead of a graph, since all peaks have the same intensity originating for the black square in Figure 6-7). Sample 2 shows the highest number of different end-group masses, due to the relative large composition error, as is shown in Table 18B. A larger error in composition allows more combinations of repeat units *A* and *B* to meet the criteria discussed in section 6.5.

Table 18A A list of all possible end-group-masses. Bold numbers correspond to the end-group-mass of 58 amu with zero, one or two units of styrene or isoprene (see table 4C).

Sample 2 Mass (amu)	Sample 3 Mass (amu)	Sample 4 Mass (amu)	Sample 5 Mass (amu)
1.5	**26**	**22**	18
2	30	**25.5**	**21.5**
25.5	**58**	**26**	**22**
26	**62**	**58**	**54**
29.5	66	**61.5**	**57.5**
30	**94**	**62**	**58**
33.5	98	**94**	**90**
34	102		122
37.5			
38			
58			
61.5			
62			
65.5			
66			
69.5			
70			
94			
97.5			
98			
101.5			
102			
105.5			
106			

Table 18B The error in the initial estimated average composition.

Sample number	2	3	4	5
Estimate average-composition (%)	41	45	51	55
Corrected composition	23	34	48	58
Error %	19	11	4	3

Table 18C Possible end-group masses due to the exchange of repeat mass units starting from 58 amu.

End-group masses (amu)	Exchange of number of Styrene units	Exchange of number of Isoprene units
58.08	0	0
94.08	1	-1
22.08	-1	1
26.02	1	-2
90.14	-1	2
62.03	2	-3
54.13	-2	3

In this case *sec*-butyllithium was used as initiator which corresponds to a mass of 58.08 amu. Table 18A shows all possible end-group masses for the different samples. Note that 58 amu is the only end-group mass which is found in each list of all samples. Some other frequently obtained end-group masses (printed in bold) can be explained by the end-group mass 58 amu with small changes in the chain composition (see Table 18C). Assuming that all end-group masses listed in Table 18C belong to the end-group mass of 58.08 amu (*sec*-butyllithium), the majority of the end-group masses can be explained.

Step 4 In order to see the effect of the corrections, different contour plots of sample 3 are shown in Figure 6-12.

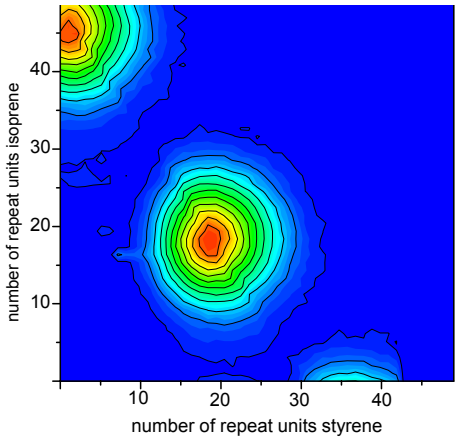

Figure 6-12a Contour plot without any correction.

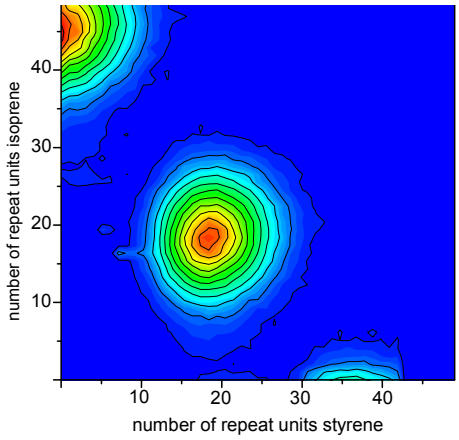

Figure 6-12b Contour plot after isotope-overlap correction.

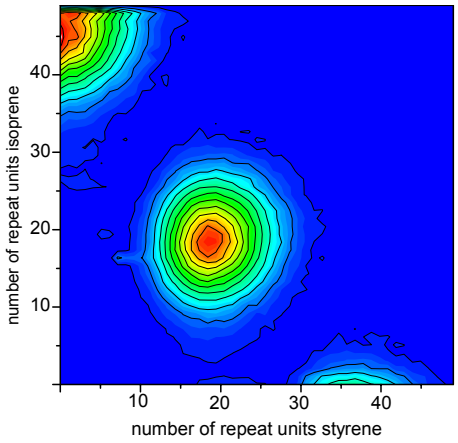

Figure 6-12c Contour plot after isotope-overlap and isotope-broadening correction.

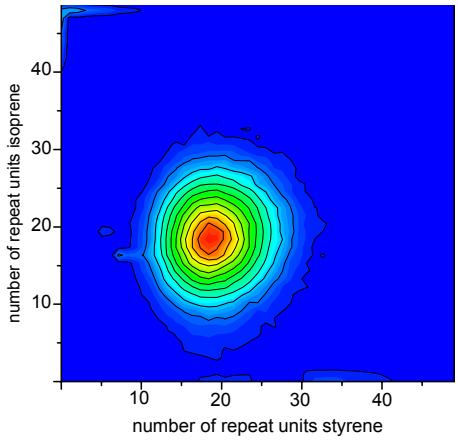

Figure 6-12d Contour plot after isotope-overlap, isotope-broadening and isotope-interference correction.

Besides the correction for isotope interference, hardly any difference could be noticed between the contour plots. However these small corrections make a significant difference in the projected distributions (not shown) and they are desirable to obtain the most-accurate computed outcome of the program.

Step 5 After selecting the end-group mass the copolymer fingerprints can be calculated. The results are shown in Figure 6-13a-d.

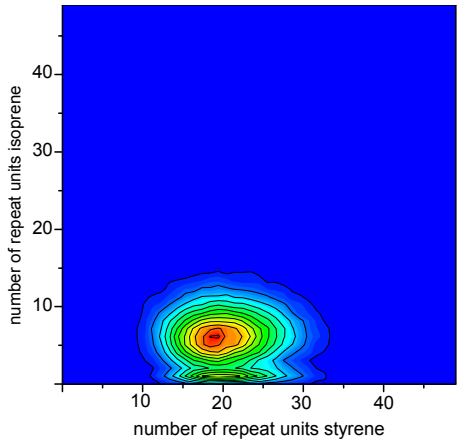

Figure 6-13a Sample 2, approximately 25% conversion of isoprene.

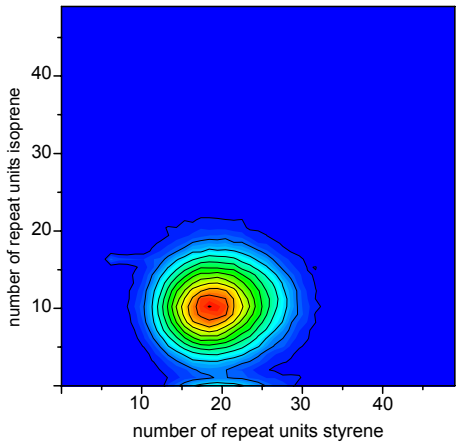

Figure 6-13b Sample 3, approximately 50% conversion of isoprene.

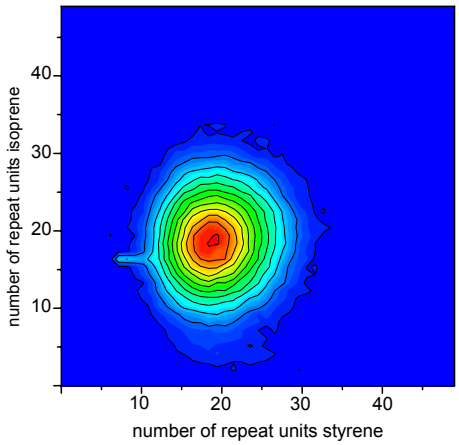

Figure 6-13c Sample 4, approximately 75% conversion of isoprene.

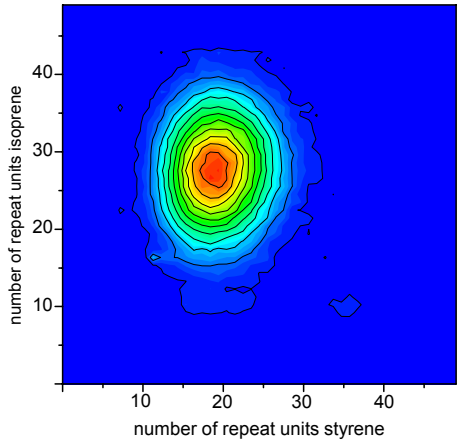

Figure 6-13d Sample 5, approximately 100% conversion of isoprene.

Step 6 and 7 The initial assumption of a block copolymer can be verified by reconstructing the contour plot of the block length distributions. The correlation between the original contour plot and the reconstructed contour plot is used to judge if the initial assumption was correct. The calculated block lengths are depicted in Figure 6-14. Correlation coefficients exceeding 0.998 where obtained for samples 1 through 4. In case of a correlation coefficient less then 0.975 (5% of unexplained variation) the entire cycle would be repeated to test the alternative topology (random copolymer).

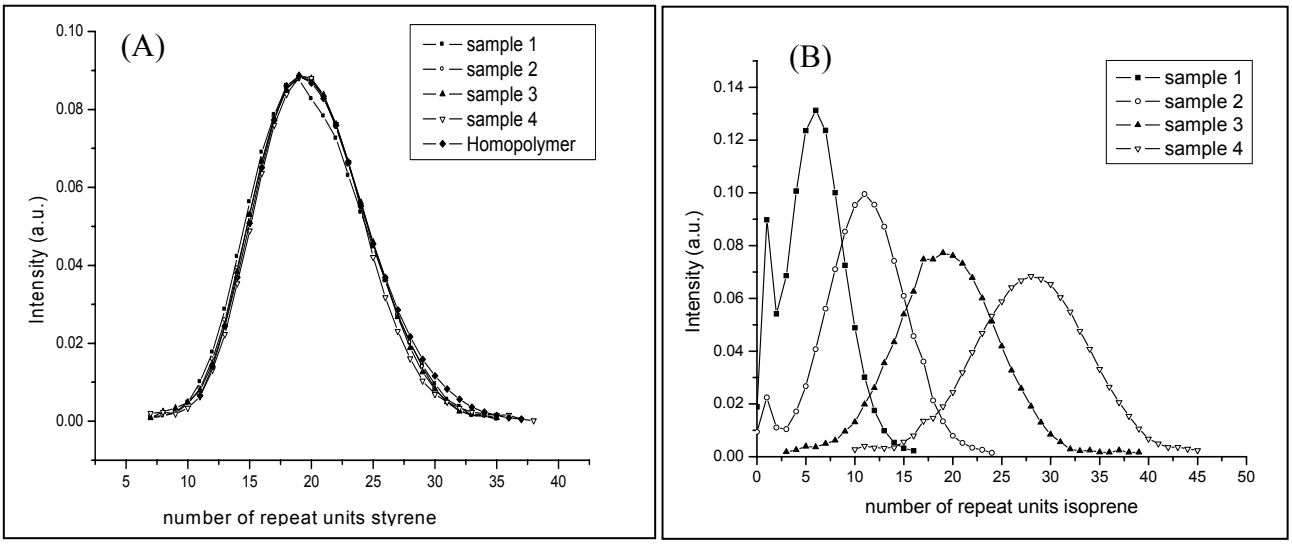

Figure 6-14 The block-length distribution of the polystyrene and polyisoprene.

Starting from a complex copolymer spectrum, the entire distribution has been reduced to only two simple graphs as depicted in Figure 6-14.

A completely different problem associated with MALDI-TOF-MS data is the need to apply a correct baseline subtraction (section 2.3.1). Extraction of the block-length distribution of the precursor block with increasing conversion of the second block, was used as a direct method to elucidate which baseline method resulted in the most consistent precursor block-length distributions. The results of both methods are shown in section 2.3.1. All spectra throughout this thesis were processed by the valley-to-valley method.

6.8 *Polystyrene-gradient-butadiene*

The program calculates the correlation coefficient for a block and a random copolymer. We can use these “extremes” to elucidate other topologies, for example a gradient copolymer.
A gradient copolymer was prepared by anionic polymerization of butadiene and styrene. Such a gradient copolymer can be obtained as long as the composition drift be can regulated to some extent during a living polymerization. Moreover, the system has to meet two criteria. First, the cross propagation in both directions should neither be too slow nor too fast. A too slow cross propagation leads to the formation of block structures. On the other hand, a too fast cross propagation leads to an alternating copolymer. Secondly, the two homopropagation rate constants should not differ orders of magnitude. The reactivity of the anions can be influenced by lewis bases, such as N,N,N',N'-tetramethylethylenediamine (TMEDA)[9,10], to meet the previously mentioned criteria.

6.8.1 Experimental section

The poly(styrene-*gradient*- butadiene) copolymer was prepared by anionic polymerization using *sec*-butyllithium (Acros, 1.3 M solution in cyclohexane/hexane (97.8/30.1 mL)) as the initiator. Reactions were carried out in a 2-L stainless-steel autoclave reactor under a nitrogen atmosphere using cyclohexane (VWR, high purity) as a solvent. Monomers and solvent were passed over an activated alumina column prior to polymerization. The autoclave reactor was loaded with 989 g of cyclohexane and heated to 40°C. A mixture of 50.2 g styrene (VWR, 99%), 26.2 g butadiene (Shell Chemicals, 99.5%), and 67.7 mL 0.028 M *sec*-butyllithium and 2.239 g of N,N,N',N'-tetramethylethylenediamine (TMEDA, VWR, 99%) solution in cyclohexane were added to the autoclave reactor. Within 15 minutes full conversion was achieved, since all samples drawn from the reaction mixture after 15 minutes showed 100% conversion. All samples were terminated by quenching in an excess of methanol.

6.8.2 MALDI-TOF-MS Analysis

Each step of the program is discussed in section 6.7, therefore only the outcome of the program is discussed here. A gradient copolymer can be seen as an “intermediate” between a block copolymer and a random copolymer and it will fail both tests to detect the random or block topology. Therefore the contour plots in both the block and random formats, are depicted.

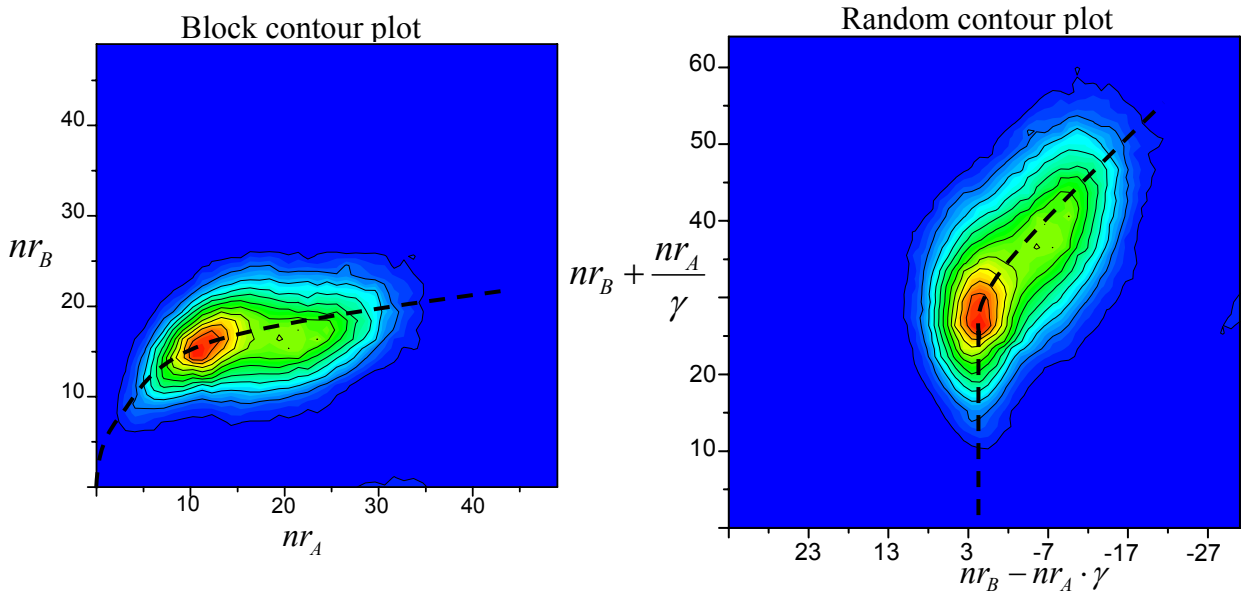

Figure 6-15 Contour plots of a poly(styrene-*gradient*-butadiene)polymer. The dashed line indicates "the path" of a gradient copolymer.

Although it is obvious that neither of these images obey the random or block copolymer topology, the projections on the axes were performed to confirm this mathematically.

Figure 6-16 and Figure 6-17 represent the projected distributions on the axes. The relatively low correlation coefficients and the relatively large skewness value of the composition distribution confirmed the gradient topology. Note that this gradient copolymer shows more resemblance with a random copolymer than with a block copolymer. Using the correlation coefficients, this copolymer can be characterized as a 33% block copolymer and a 67% random copolymer.

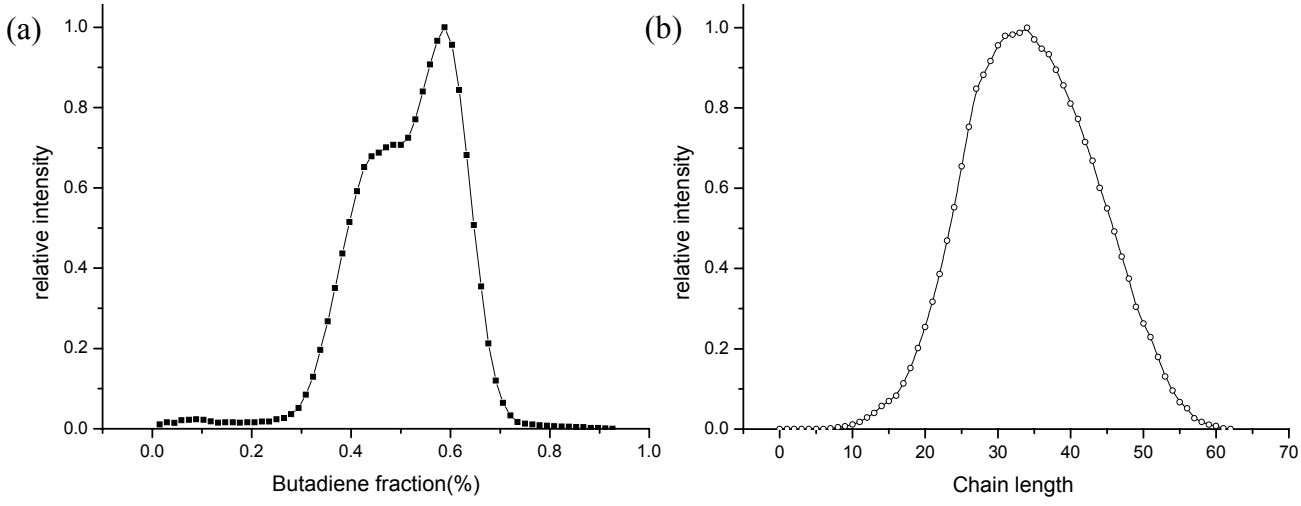

Figure 6-16 (a) The chemical-composition distribution and (b) the chain length distribution of the butadiene-*gradient*-styrene copolymer assuming a random copolymer structure. A correlation coefficient of 0.953 (10% unexplained variance) was obtained. τ_{CCD} = 20%.

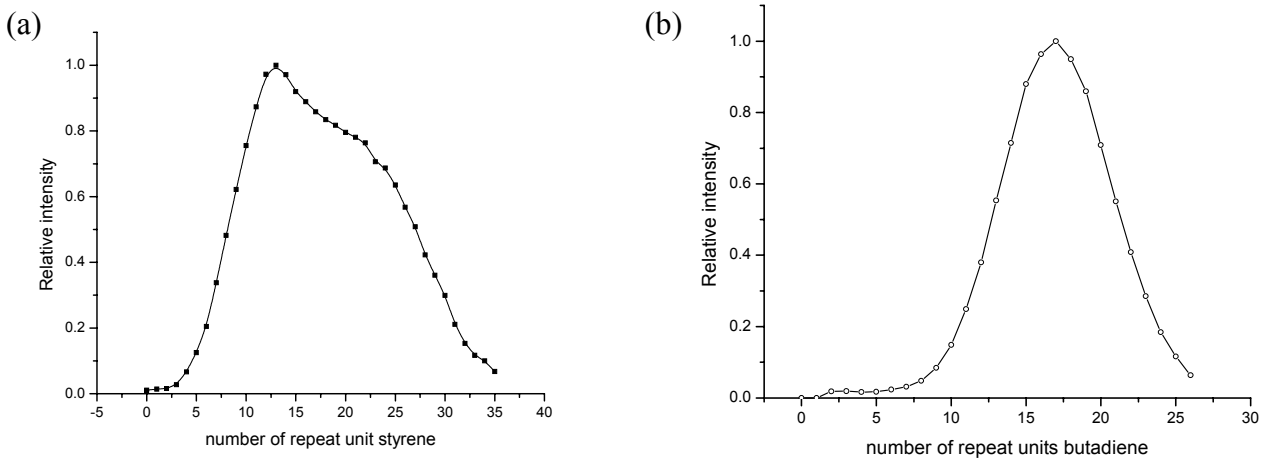

Figure 6-17 (a) The butadiene block-length distribution and (b) the styrene block-length distribution of the butadiene-*gradient*-styrene copolymer assuming a block-copolymer structure. A correlation coefficient of 0.903 (19% unexplained variance) was obtained.

6.9 *Conclusions*

The interpretation of copolymer spectra obtained by MALDI-TOF-MS is no longer laborious and time consuming with the help of our program. In essence, for a copolymer consisting of two monomers, the entire spectrum is "digitized" in a contour plot representation. This representation can elucidate, directly or indirectly, the relationship between the molar mass and the composition of the polymer chains expressed as the number of repeat units A and B. The criteria discussed in section 6.6 reveal the topology of the copolymer for a random, gradient, block, and alternating copolymer.

A long-lasting conflict concerning baseline subtractions in MALDI-TOF-MS is clarified. The so-called valley-to-valley method resulted in the most appropriate obtained values of the precursor block length distribution of a block copolymer, providing direct evidence of the correct baseline subtraction method.

To obtain the best contour plot, a number of corrections have to be made. These corrections are mainly mathematical in nature. These corrections allow elucidation of the most appropriate baseline-subtraction method. The corrections improve the quality of the program outcome significantly. Nevertheless, the differences are small and not always visually noticeable.

We hope that this work will contribute to a more systematic method for processing the MALDI-TOF-MS spectra of (co)polymer. The need for such standardized methods has been underlined by a round robin test[11] where a homopolymer end-group analysis is carried out. A round-robin test involving copolymers by MALDI-TOF-MS has not yet been carried out.

Reference List

1. Yergey, J. A. *Int. J. Mass Spectrom. Ion Phys* **1983,** *52*, 337-349.
2. Suddaby, K. G.; Hunt, K. H.; Haddleton, D. M. *Macromolecules* **1996,** *29*, 8642-8649.
3. Wilczek-Vera, G.; Yu, Y.; Waddell, K.; Danis, P. O.; Eisenberg, A. *Rapid commun. Mass Spectrom.* **1999,** *13* (9), 764-777.
4. Wilczek-Vera, G.; Danis, P. O.; Eisenberg, A. *Macromolecules* **1996,** *29* (11), 4036-4044.
5. Wilczek-Vera, G.; Yu, Y.; Waddell, K.; Danis, P. O.; Eisenberg, A. *Macromolecules* **1999,** *32* (7), 2180-2187.
6. van Rooij, G. J.; Duursma, M. C.; de Koster, C. G.; Heeren, R. M. A.; Boon, J. J.; Schuyl, P. J. W.; van der Hage, E. R. E. *Anal. Chem.* **1998,** *70* (5), 843-850.
7. Willemse, X. E.; Staal, B. B. P.; Donkers, E. H. D.; van Herk, A. M. *Macromolecules* **2004**.
8. Stockmayer, W. H. *The Journal of Chemical Physics* **2004,** *13* (6), 199-207.
9. Collum, D. B. *Acc. Chem. Res.* **1992,** *25*, 448-454.
10. Melenevskaya, Y. Y.; Zgonnik, V. N.; Denisov, V. M.; Dolinskaya, E. R.; Kalnin'sh, K. K. *Polymer Science U. S. S. R.* **1980,** *21*, 2215-2224.
11. Guttman, C. M.; Wetzel, J.W.; Wallace, W.E.; Blair, W.R.; Goldschmidt, R.M.; Vanderhart, D.L.; Fanconi, B.M.; . *Polym. Prepr.* **2000,** *41*, 678-679.

Appendix 6A

The instantaneous distribution of chain compositions and chain lengths can be described by the Stockmayer equation with the assumption that the reactivity of radicals depends only on the nature of its reactive end and the kinetic effects of initiation and termination are neglected.

$$n(L,y)dLdy = \left(\exp\left(\frac{-L}{\lambda}\right)\cdot\frac{L}{\lambda}\cdot dL\right)\cdot\left(\sqrt{\frac{L}{2\cdot\pi\cdot\overline{C}_{ave}\cdot\left(1-\overline{C}_{ave}\right)\cdot\kappa}}\cdot\exp\left(\frac{-L\cdot y^2}{2\cdot\overline{C}_{ave}\cdot\left(1-\overline{C}_{ave}\right)\cdot\kappa}\right)\cdot dy\right) \quad \textbf{(A6-1)}$$

$$\kappa = \sqrt{1-4\cdot\overline{C}_{ave}\cdot\left(1-\overline{C}_{ave}\right)\cdot\left(1-r_1\cdot r_2\right)} \quad \textbf{(A6-2)}$$

$$y = Comp - \overline{C}_{ave} \quad \textbf{(A6-3)}$$

where $\overline{C}_{ave}$ is the average overall composition, λ the degree of polymerization, r_1 and r_2 the reactivity ratios, y the composition deviation and C the composition of an individual chain and $n(L,y)$ the number fraction of polymers with lengths between L and $L+dL$ and composition-deviations between y and $y+dy$.
The direction of the new axis is chosen parallel to the slope of the contour plot (related to the average composition) and perpendicular to the latter axis to obtain a orthogonal axis.
The average composition can be described as function of nr_A and nr_B in the contour plot as:

$$nr_B = nr_A\cdot\gamma + C \quad \textbf{(A6-4)}$$

and the orthogonal axis becomes:

$$nr_B = \frac{-nr_A}{\gamma} + D \quad \textbf{(A6-5)}$$

where γ is the slope which can be calculated from the average composition $\overline{C}_{ave} = 1/(1+\gamma)$. The value C is the composition-deviation expressed in terms of repeat units A and B and D is a certain chain length expressed as the sum of nr_B plus $\gamma\cdot nr_A$.
Writing the repeat units A and B as function of C and D results in:

$$nr_B = \frac{D\cdot\gamma^2 + C}{1+\gamma^2} \quad \textbf{(A6-6)}$$

$$nr_A = \frac{\gamma\cdot(D-C)}{1+\gamma^2} \quad \textbf{(A6-7)}$$

Rewriting the chain length in terms of C and D:

$$L = nr_A + nr_B = \frac{C - C\cdot\gamma + D\cdot\gamma + D\cdot\gamma^2}{1+\gamma^2} \quad \textbf{(A6-8)}$$

Rewriting the composition in terms of C and D:

$$y = Comp - \overline{C}_{ave} = \frac{nr_A}{nr_A + nr_B} - \frac{1}{\gamma+1} \quad \textbf{(A6-9)}$$

$$y = \frac{C \cdot \left(1 + \gamma^2\right)}{\left(\left(1 + \gamma\right) \cdot \left(-C + \gamma \cdot C - \gamma \cdot D - D \cdot \gamma^2\right)\right)} \qquad \textbf{(A6-10)}$$

Substitute **A6-8** and **A6-10** into **A6-1** and the number fraction is obtained as function of C and D. Note that the molar mass can be written as a function of C and D:

$$M\left(C, D\right) = m_A \cdot \left(\frac{D \cdot \gamma^2 + C}{1 + \gamma^2}\right) + m_B \cdot \left(\frac{\gamma \cdot \left(D - C\right)}{1 + \gamma^2}\right) \qquad \textbf{(A6-11)}$$

After rearrangement:

$$D = C \cdot \left(\frac{m_B \cdot \gamma - m_A}{\gamma \cdot \left(m_A \cdot \gamma + m_B\right)}\right) + M \cdot \left(\frac{1 + \gamma^2}{\gamma \cdot \left(m_A \cdot \gamma + m_B\right)}\right) \qquad \textbf{(A6-12)}$$

It can be seen that the intercept is indicative for the molar mass in the contour plot of *C* versus *D*.

Appendix 6B

The spectra of the poly(styrene-*co*-isoprene) samples.

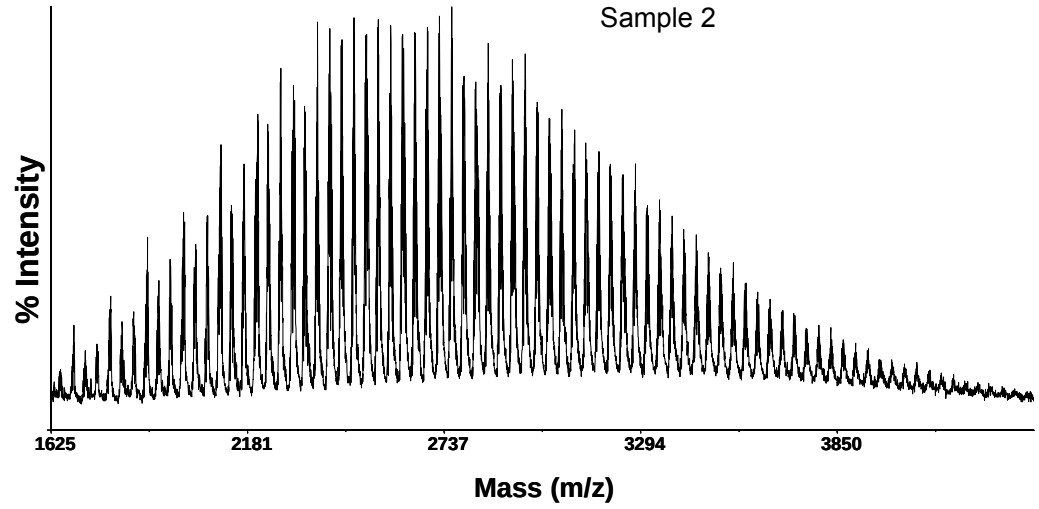

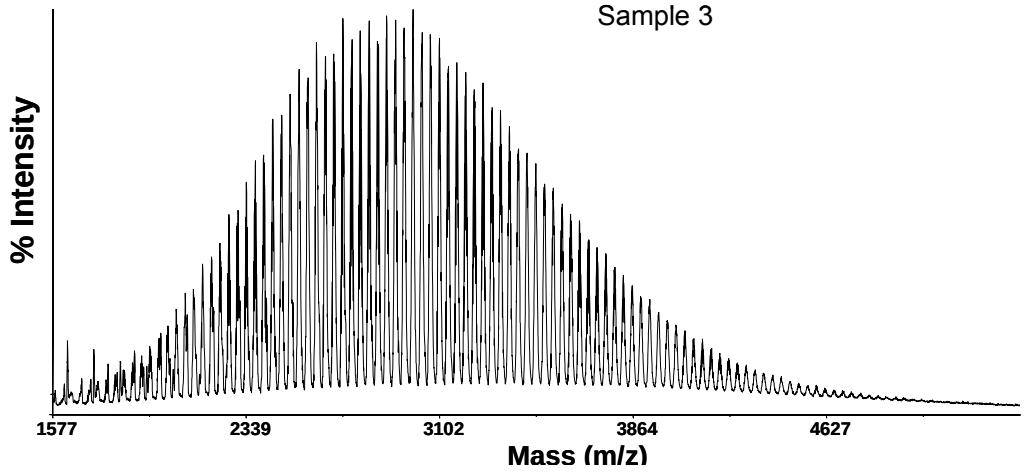

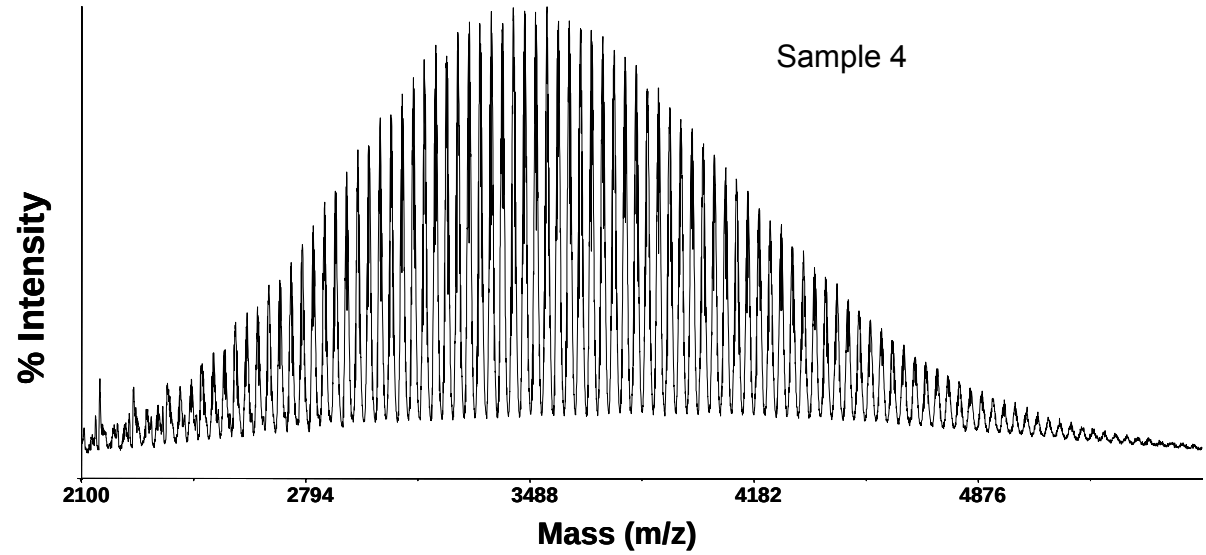

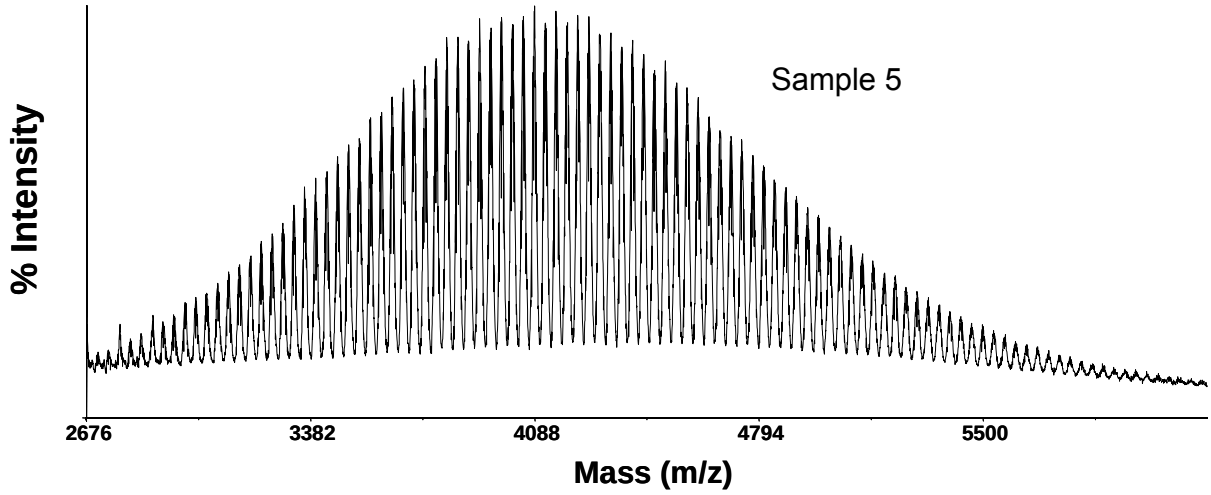

Appendix 6C

Table 19 The moments of poly(styrene-*co*-isoprene) were calculated after a baseline correction was applied.

	Isoprene		Styrene		Polystyrene-*co*-isoprene	
Sample nr.	$\overline{P}_n$	$\overline{P}_w$	$\overline{P}_n$	$\overline{P}_w$	$Comp_{est}$ Isoprene	$Comp_{calc}$ Isoprene
1	-	-	20.06	21.05	-	-
2	5.85	7.48	19.95	20.97	0.50	0.23
3	10.95	12.63	20.05	21.03	0.50	0.35
4	19.32	20.75	20.04	21.02	0.56	0.49
5	27.93	29.21	20.09	21.04	0.58	0.58

The $\overline{P}_n$, and $\overline{P}_w$ are calculated from the block length distributions (section 6.3.1).

$$\overline{P}_n = \sum_{nr_A} \frac{BLD_A(nr_A)\,nr_A}{BLD_A(nr_A)} \qquad \textbf{(C6-1)}$$

$$\overline{P}_w = \sum_{nr_A} \frac{BLD_A(nr_A)\,nr_A^{\,2}}{BLD_A(nr_A)\,nr_A} \qquad \textbf{(C6-2)}$$

Note, the rather large deviation of the estimated composition isoprene of sample 2 is related to the presence of the molar mass shoulder, see Figure 12a and Figure 13b. This should affect strongly the value of ΔB equation 6.23.

Appendix 6D

The asymmetry of any distribution can be calculated via the statistical moments.
The first moment of the distribution represents the mean value($\bar{n}$):

$$\bar{n} = \frac{\sum I}{\sum n} \qquad \textbf{(D6-1)}$$

Where I is the normalize distribution as function of n.
The second moment represents the standard deviation (σ):

$$\sigma^2 = \sum \left(n - \bar{n}\right)^2 I \qquad \textbf{(D6-2)}$$

The third moment is related to the skewness (τ):

$$\tau^3 = \frac{1}{\sigma^{3/2}} \sum \left(n - \bar{n}\right)^3 I \qquad \textbf{(D6-3)}$$

The skewness of a distribution is a measure of the composition drift. No composition drift leads a value of zero.

Chapter 7

Outlook and development

Matrix-Assisted Laser Desorption/Ionization Time-of-Flight Mass Spectrometry (MALDI-TOF-MS) of polymers is only a niche in the mass spectrometry market in comparison with clinical and biochemical applications. The main driving force of technological development in MALDI-TOF-MS is automation of high-throughput screenings. The benefits of these developments for polymer analysis are limited.

The more interesting areas for polymer analysis are related to sample preparation, new types of MALDI interfaces which allow hyphenation, and software development.

The development of new matrices is a continuous process as shown by some recent publications[1,2]. However, as long as there is no fundamental understanding of the role of the matrix in the MALDI process, the discovery of new matrices will proceed slowly. A new trend in sample preparation is solvent-free sample deposition. The sample and the matrix are mixed as powders and pasted on to the target. No fundamental difference was found in comparison with solvent based deposition.

Considerable progress has been made in the design of analyzers with the introduction of orthogonal acceleration (oa). The main advantage of the oa-analyzer is the possible hyphenation with liquid chromatography techniques. An additional advantage of oa-analyzers is the possibility to perform MS/MS experiments. Particularly successful are the hybrid Quadrupole Time-of-Flight (Q-TOF) mass spectrometers and the recently introduced MALDI-Q-TOF combination. A drastic mass-

resolution improvement can be expected from the coupling of MALDI with a Fourier Transform Ion Cyclotron Resonance Mass Spectrometer (FT-ICR-MS).

Fast online analysis and high-resolution measurements leave data interpretation as the limiting step in mass spectrometry. Not only fast computers are needed to process the data, also large capacities for data storage are needed. The use of "smart" software can help to extract only the essential information from acquired spectra. In case of end-group analysis of polymers, the end-group correlation function (ECF) can be seen as an end-group finger print of the entire spectrum. The same holds for copolymer systems, where the intensity matrix for a given total end-group mass contains all the information encrypted in the complex spectrum.

Despite all the promising techniques and developments, the main shortcomings of MALDI (the non-quantitative intensities and the mass discrimination in case of broad polymer distributions) will always necessitate the use of additional separation methods.

Reference List

1. Rajin, N. P.; Mirza, S. P.; Vairamni, M.; Ramulu, A. R.; Pard-Hasaradhi, M. *Rapid commun. Mass Spectrom.* **2001,** *15*, 1884.

2. Brown, T.; Cliptson, N. C.; Simjee, N.; Luftmann, H.; Hungerbühler, H.; Drewllo, T. *Int. J. Mass Spectrom.* **2001,** *210/211*, 249.

Glossary of Symbols and Abbreviations

η_{sp}	Specific viscosity
y	Composition deviation
TCE	functionality of 2,2,2-trichloroethanol
SEC	Size-Exclusion Chromatography
SEC	Size Exclusion Chromatography
RALS	Right-Angle Light Scattering
RAFT	Reversible Atom Fragmentation Transfer
p-TsCl	*p*-toluenesulphonyl chloride
PPI	*N*-*n*pentyl-2-pyridylmethanimine
PMDETA	*N,N,N′,N″,N″*-pentamethyldiethylenetriamine
PDI	Polydispersity index
PDA	Photodiode Array
NMP	Nitroxide Mediated Polymerization
MMD	Molar Mass Distribution
MMCCD	Molar-Mass-Chemical-Composition Distribution
MMA	Methylmethacrylate
MALDI-TOF-MS	Matrix-Assisted-Laser-Desorption Ionization Time-of-Flight Mass Spectrometry
L	Chain length
K	Mark-Houwink constant
IP	Pressure difference across the bridge
IBC	Isotope-broadening correction factor
FTIR	Fourier-Transform Infrared Spectroscopy
f	Correction factor for $n(M)$ to $w(\log M)$ distribution.
ESI	Electrospray ionization
ECF	End-group-correlation function
ECF	End-group Correlation Function
EBriB	Ethyl 2-bromoisobutyrate
DRI	Differential Refractive Index
DP	Viscosity signal
DP	Differential pressure within the bridge
DCTB	Trans-2-[3-(4-tert-butylphenyl)-2-methyl-2-propenylidene]malononitrile
CPR	Control Radical Polymerization
CLD	Chain-length distribution
CCD	Chemical-composition distribution
C, D	Latent variables to describe the chain length and chemical composition
b	Path length of the cell
ATRP	Atom-Transfer Radical Polymerization
amu	Atomeric mass units
ACF	Autocorrelation function
ACF	Auto Correlation Function
m_A, m_B	Molar mass of the monomers
nr_A, nr_B	Number of repeat units
m_{end1}, m_{end2}	Mass of one of the end groups of a polymer chain
$m_{\min}$, $m_{\max}$	Lower and upper limit masses of the isotope distribution
μ_1, μ_1	Corresponding masses of the most abundant isotopes
$(\sum I_A)$, $(\sum I_B)$	Total added intensity of repeat units A or B relative to the highest observed intensity
ΔA, ΔB	Block length in number of repeat units A or B

r_1 , r_2	Reactivity ratios
A_2 , A_3	Second-, and third-order virial coefficients
Δnr_A , Δnr_B	Number of repeat unit differences (integers)
ΔNr_A , ΔNr_B	Number of repeat unit differences (non integers)
z	Charge state
e	Charge of an electron
ΔV	Electric potential difference
m	Mass (amu)
v	Velocity of an ion
L	Length of the flight tube
t	Flight time
t_0	Time when the ablating laser pulse hits the target
Δt	Time difference across a peak at full-width-half-height
Δm	Mass difference expressed in amu
A	Integrated or summed area of a MALDI spectrum
$I(t)$	Observed intensity of the spectrum
V_{ex}	Exclusion volume
K_{SEC}	Distribution coefficient
V_p	Total pore volume
$\bar{M}_p$	Most probable molar mass
$\bar{M}_n$	Number averaged molar mass
$\bar{M}_w$	Weight averaged molar mass
$\bar{M}_z$	z-averaged molar mass
$R_{adj}^{\ 2}$	Adjusted correlation coefficient
(V_h)	hydrodynamic volume
$[\eta]$	Intrinsic viscosity
v	Retention volume
α	Mark-Houwink constant
k_{vis}	Calibration factors of the pressure transducers
η_0	Viscosity of the solvent
ϕ_{fr}	Flow-fraction correction factor
$\Delta R(\theta)$	Excess Rayleigh ratio
θ	Scattering angle
c	Concentration of the analyte in SEC
$P(\theta)$	Dissymmetry factor
K_{LS}	Light scattering constant
n_0	Refractive index of the eluent
λ_0	Wavelength in vacuum of the vertically polarized incident light
N_A	Avogadro number
(dn/dc)	Specific refractive-index increment
ε	Molar absorption coefficient
$y(v)$	Response of the DRI detector at an elution volume v
$y(v,\lambda)$	Response of the PDA detector at an elution volume v and a given wavelength (λ)

V_{inj}	Injection volume
k_{DRI}	DRI calibration factor
k_{PDA}	PDA calibration factor
σ	Dispersion constant
$G(v)$	Gaussian band-broadening function
$w(v^1)$	Unbiased true MMD
IDD_{DRI-LS}	Inter-detector delay of the DRI and the LS
IDD_{DRI-DP}	Inter-detector delay of the DRI and the DP
IDD_{DRI-UV}	Inter-detector delay of the DRI and the UV
$n(M)$	Number distribution
$w(M)$	Weight distribution
$w(\log M)$	Logarithmic weight distribution (SEC)
$R(v)$	Normalized concentration signal
σ	Dispersion constant, standard deviation
m_{obs}	Observed mass of a peak in the MALDI-TOF-MS spectrum
m_{ion}	Mass of the adduct
m_{end}	Mass of the total end group mass
nr_{A_Max}	Maximum number of repeat units
ECF_{HR}	High resolution End-group Correlation Function
m_{rep}	Mass step size
m_{calc}	Calculated mass of the most abundant isotope
$I(nr_A, nr_B)$	Intensity matrix
$I(m)$	Original peak intensity
I_m	Corrected peak intensity
$P_{nr_A,nr_B,m(nr_A,nr_B)}$	Percentage relative to the most abundant peak of the corresponding isotope distribution of a given number of repeat units at a given mass $m(nr_A, nr_B)$.
m_{abd}	Mass of the most abundant isotope
Δm	Mass interval expressed in amu
ΔIm	Mass interval of the isotope distribution expressed in amu
ΔI_m	Mass interval expressed in terms of ΔNr_A and ΔNr_B
$Ic(nr_A, nr_B)$	Corrected intensity matrix of a system subject to isotope interference
$comp_{est}$	Estimated average composition
BLD	Block length distribution
R_B	Correlation coefficient of a block
γ	Slope of a curve in a copolymer fingerprint
$\overline{C}_{ave}$	Average overall composition
λ	Degree of polymerization
$\underline{C}$	Composition of an individual chain
$w(L, y)$	Weight fraction of polymers of a given chain length and chemical composition deviation
R_R	Correlation coefficient of a random copolymer
$\overline{n}$	Mean value of a distribution
τ	Skewness of a distribution

Summary

Over the past decade, mass spectrometry (MS) has revolutionized the characterization of synthetic polymers. Moreover, with the introduction of matrix-assisted-laser-desorption ionization time-of-flight mass spectrometry (MALDI-TOF-MS), it has become possible to obtain the polymer characteristics (end groups, molar-mass distribution, topology etc.) However, the outcome of a single measurement, a MALDI spectrum, needs to be transformed to visualize the polymer characteristics since they are enclosed in the spectrum. The work described in this thesis, contains the development of methods to extract and visualize all polymer characteristics embedded in a spectrum.

One of the most well known characteristics of polymers is the molar-mass distribution. Traditionally, the MMD is determined by size exclusion chromatography (SEC). SEC is a relative method and is subject to column band-broadening. The effect of band broadening on the MMD can be diminished by the use of molar-mass dependent detectors, such as light scattering and viscometry. However, a setup with detectors connected parallel/serial requires accurate handling of the large number of parameters to obtain a reliable absolute MMD (Chapter 3).

The limiting factor to obtain the MMD with MALDI is the occurrence of mass discrimination. Polymers with a polydispersity index (PDI) larger than 1.2 show, in many cases, an underestimation of the MMD towards the high molar mass range. For (polystyrene) polymers with a PDI larger than 1.2 the use of a relatively new matrix, matrix trans-2-[3-(4-tert-Butylphenyl)-2-methyl-2-propenylidene]malononitrile (DCTB), significantly reduces mass discrimination in comparison with conventional matrices. An attractive method to avoid mass discrimination is the use of a SEC separation prior to MALDI measurement. This SEC separation supplies narrow molar-mass fractions (PDI<1.2), these fractions can be measured by MALDI without mass discrimination. Since MALDI-TOF-MS allows the determination of the mass of polymer chains with a high accuracy, this technique is very well suited for total end-group-mass analysis. Our method for end-group-mass analysis provides an end-group-mass spectrum where all end-group-masses within the sample are present. The end-group-mass spectrum can be used to e.g. reveal the initiator functionality or to distinguish between end-group-masses of nearly the same mass (Chapter 5).

The analysis and interpretation of MALDI spectra, in particular of copolymers, is a time consuming task. The in-house developed software based on the methods described in this thesis, digitizes a spectrum in terms of monomer repeat units. The representation of such a digitized spectrum is

called a copolymer fingerprint. The shape of a copolymer fingerprint reveals the copolymer topology (random, block, alternating or gradient) (Chapter 6).

The aim of this work is the development of a method to extract all (co)polymer characteristics enclosed from a MALDI spectrum, with absolute minimum prior knowledge. The use of the method we developed offers a powerful and fast tool to obtain detailed information about the (co)polymer characteristics.

Samenvatting

Sinds begin jaren negentig heeft massaspectrometrie (MS) zich een onmisbare positie verworven op het gebied van de synthetische polymeerkarakterisering. De kracht van de MS techniek zit vooral in de grote precisie waarmee de massa's van individuele polymeerketens kunnen worden bepaald. Een belangrijke plaats om verdelingen van polymeerketens te bepalen, wordt hedendaags ingenomen door Matrix Assisted Laser Desoption/Ionization (MALDI). Echter het resultaat van een meting is nog niet "vertaald" in de karakteristieken van het polymeer. Via het werk beschreven in dit proefschrift, is getracht een generieke methode te ontwikkelen om alle karakteristieken, opgeslagen in een MALDI spectrum, hanteerbaar en zichtbaar te maken.

Een van deze karakteristieken van polymeren is de molmassaverdeling. Traditioneel wordt deze veelal bepaald met Size Exclusion Chromatography (SEC). SEC is een relatieve methode en is o.a. onderhevig aan kolom verbreding wat kan worden ondervangen door het gebruik van molmassa afhankelijke detectoren, zoals licht verstrooiing en viscosimetrie. Echter, de moeilijkheid van het koppelen van detectoren in serie/parallel behelst een nauwkeurig inzicht in het grote aantal parameters om tot een zo absoluut mogelijke molmassaverdeling te komen (hoofdstuk 3).

Een beperkende factor in het gebruik van MALDI voor het bepalen van de molmassaverdeling, is de zogenoemde massadiscriminatie. Polymeren met een polydispersiteit index (PDI) groter dan 1.2 vertonen veelal een onderschatting van de hoogmoleculaire kant van de molmassa verdeling. De kwantificering van massadiscriminatie toont aan, dat het gebruik van de relatief nieuwe matrix DCTB een aanzienlijke verbetering vertoont voor het verkrijgen van de molmassaverdeling met een PDI groter dan 1.2.
Een zeer aantrekkelijk alternatief is de combinatie van MALDI en SEC. SEC levert een smalle molmassaverdeling die, zonder enige massadiscriminatie, gemeten kan worden met MALDI (hoofdstuk 4).
De grote precisie waarmee MALDI-TOF-MS de massa van polymeerketens bepaalt, leent zich voor de totale eindgroep massa analyse. De ontwikkelde procedures resulteren in een eindgroep spectrum waarin alle informatie van aanwezige eindgroepen wordt weergegeven. De verkregen informatie over de eindgroepen kan worden gebruikt om bijvoorbeeld de initiator functionaliteit te herleiden. Tussen eindgroepen met nagenoeg dezelfde massa kan, tot op zekere hoogte, het onderscheid worden gemaakt met behulp van een aangepaste procedure (hoofdstuk 5).

Het analyseren en interpreteren van MALDI spectra, in het bijzonder van copolymeren, is een lastige en tijd rovende puzzel. Met behulp van de in dit proefschrift ontwikkelde software wordt het spectrum gedigitaliseerd in termen van monomeer eenheden. De presentatie van een MALDI

spectra op deze manier wordt een copolymere vingerafdruk genoemd. De vorm van deze “vingerafdruk” is karakteristiek voor het type copolymeer (random, blok, altenerend of gradiënt) en daarmee kan het type copolymeer direct worden toegekend (hoofdstuk 6).

De doelstelling van dit werk is de ontwikkeling van een methode om alle (co)polymeer karakteristieken opgesloten in een MALDI spectrum er uit te extraheren met een minimale hoeveelheid voorkennis. Het gebruik van de door ons ontwikkelde methode, bied een krachtige en snelle manier om de (co)polymeer karakteristieken te verkrijgen.

Scientific papers

Bastiaan B. P. Staal[1]; Rajan Venkatesh[1]; Sreepadaraj Karanam; Bert Klumperman; *A study to reveal the initiator functionality of trichloroethanol in ATRP of PMMA by end-group analysis with MALDI-TOF-MS*, in preparation.

Willemse, Robin X. E.; Staal, Bastiaan B. P.; Donkers, Ellen H. D.; Van Herk, Alex M. *Copolymer Fingerprints of Polystyrene-block-polyisoprene by MALDI-ToF-MS;* Macromolecules, (2004), 37(15), 5717-5723

Willemse, Robin X. E.; Staal, Bastiaan B. P.; van Herk, Alex M.; Pierik, Sebastiaan C. J.; Klumperman, Bert. *Application of Matrix-Assisted Laser Desorption Ionization Time-of-Flight Mass Spectrometry in Pulsed Laser Polymerization;* Macromolecules, (2003), 36(26), 9797-9803

Venkatesh, Rajan; Staal, Bastiaan B. P.; Klumperman, Bert; Monteiro, Michael J. Characterization of 3 and 4-Arm Stars from Reactions of Poly(butyl acrylate) RAFT and ATRP Precursors. Macromolecules (2004), 37(21), 7906-7917

Willemse, Robin X. E.; Staal, Bastiaan B. P.; van Herk, Alex M.; Pierik, Sebastiaan C. J.; Klumperman, Bert. *Application of Matrix-Assisted Laser Desorption Ionization Time-of-Flight Mass Spectrometry in Pulsed Laser Polymerization. Chain-Length-Dependent Propagation Rate Coefficients at High Molecular Weight: An Artifact Caused by Band Broadening in Size Exclusion Chromatography?* Macromolecules (2003), 36(26), 9797-9803

Vander Heyden, Y.; Popovici, S.-T.; Staal, B. B. P.; Schoenmakers, P. J. *Contribution of the polymer standards' polydispersity to the observed band broadening in size-exclusion chromatography;* Journal of Chromatography, A (2003), 986(1), 1-15

Venkatesh Rajan; Staal Bastiaan B P; Klumperman Bert, *Olefin copolymerization via reversible addition-fragmentation chain transfer;* Chemical communications (Cambridge, England) (2004),13,1554-1555

F.Fitzpatrick, B.B.P. Staal , P.J. Schoenmakers, J. Chromatogr. A submitted.

L. Xue, U.S. Agarwal, M. Zhang, B.B.P. Staal, A.H.E. Müller, C.M.E. Bailly_ and P.J.Lemstra, *Synthesis and direct topology visualization of high molecular weight star*; Macromolecules submitted.

Acknowledgements

Het resultaat, zoals dat hier nu ligt, is nooit het werk van één enkel individu maar het resultaat van een geweldige samenwerking van tal van personen. Het is helaas onmogelijk om iedereen passend te bedanken, maar toch wil ik een poging wagen.

In de eerste plaats wil ik alle collega's en oud collega's van de vakgroep SPC bedanken voor jullie bijdrage aan discussies en gezelligheid van de afgelopen 3 jaar. In het bijzonder, het MALDI team, te weten Robin en Wouter. Zonder jullie was ik nooit zover gekomen met het kraken van complexe (co)polymeer vraag stukken en het betere programeer werk. Mijn bijzondere dank gaat ook uit aan diegene die geholpen hebben met het corrigeren van mijn proefschrift. Peter Schoenmakers. De snelheid, het enthousiasme en het korte tijdsbestek waarin jij mijn proefschrift hebt gecorrigeerd zal door weinig mensen worden geëvenaard. Bert Klumperman voor de vele nuttige suggesties en correcties, Alex van Herk en Chris de Koster voor het corrigeren en doorlezen van het manuscript. Maarten en Ellen, enorm bedankt voor de vele uurtjes die jullie hebben besteed aan het doorlezen van het manucript! Dear friends Rajan and Sreepad, I both own you more than a curry. Thanks for the brilliant time we have spend together and the useful corrections and suggestions.
De volgende mensen wil ik bedanken voor hun inzet om een positie beschikbaar te stellen aan de universiteit van Eindhoven om mijn promotie werk af te kunnen ronden, Alex van Herk, Bert Klumperman en Cor Koning.
Graag wil ik de overige leden van de commissie bedanken voor hun bereidheid om deel te nemen in de promotie commissie, Michel Nielen, Harry Philipsen, Thomas Hankemeier en Paul Cools.

Daarnaast zijn er nog een aantal mensen die indirect hebben mee geholpen aan dit proefschift. Paul Cools, de vele levendige discussies en je steun en toeverlaat zijn van onschatbare waarde. My special thanks to Maria Caporali, for your patience when I came with questions about your polymers. Raf Bussels voor de uiterst prettige samenwerking en het onvergetelijke vrijgezellen weekend. Vincent and Rajan for the introduction into the world of RAFT and ATRP. The colleagues and ex-colleagues of the Polymer-Analysis Group of the Universiteit of Amsterdam for their lively group meetings. Special thanks to Fiona Fitzpatrick, Simona Popovici, Gabriel Vivó, Maya Ziari, Kathalijne Oudhof and Wim Kok, for all discussions and good collaborations. De EGS voor de geweldige uitstapjes naar Claustal, Göttingen en Amsterdam. De gehele afdeling Verpakkingen & Sensortechnologie bij TNO, met in het bijzonder Richard Bas, Erwin Kaal en oud collega's Sander Kok, Paul Cools en Thomas Hankemeier. The people from SKA, more specific Lijing Xue, Merina Rajan and Irina Cotiugă (mulțumesc!!). Poul, bedankt voor de vele kopjes koffie en je interesse.

Mi mas profundo agradecimiento a todas mis amigos hispanos que he conocido a través estos años, Cristina, Rebeca, Hector, David y Juan, Jesús, Amaia (disfruté muchísimo las vacaciones con tus padres) y también Susana (por tu apoyo incondicional!).

Although I know that I could not mention everyone, be absolutely sure that your help was highly appreciated.

Als laatste zou ik graag Maarten, mijn ouders, Joost-Jan en de rest van mijn familie en vrienden willen bedanken voor de onvoorwaardelijke steun gedurende de laatste jaren van mijn onderzoek.

Curriculum vitae

Bastiaan Staal werd geboren op 19 augustus 1975 te Hoogerheide. Aan de scholengemeenschap “RSG ‘t Rijks” te Bergen op Zoom behaalde hij in 1993 zijn HAVO diploma, waarna vervolgens zijn opleiding aan de HTS te Breda in 1997 succesvol werd afgerond. In dat zelfde jaar begon hij aan de verkorte opleiding aan de Universiteit in Eindhoven waarbij het doctorale examen werd afgelegd op 31 augustus 1999.

In september 1999 werd de eerste basis voor dit promotie werk gelegd bij de Verpakkingen en Sensortechnologie afdeling van de Nederlandse Organisatie voor Toegepast Natuurwetenschappelijk Onderzoek (TNO) te Zeist. Dit geschiedde in nauwe samenwerking met de vakgroep Polymeer Analyse van de Universiteit onder begeleiding van prof. dr. ir. P.J. Schoenmakers (UVA), dr. T. Hankemeier (TNO) en dr. P.J.C.H. Cools (TNO). Na twee jaar is het onderzoek voortgezet aan de Technische Universiteit van Eindhoven de capaciteitgroep SPC onder begeleiding van Prof. dr. A.M. van Herk (TU/e) en prof. dr. ir. P.J. Schoenmakers (UVA).